Analysis, Numerical Methods, and Applications of Multiscale Problems

Alexandre L. Madureira

Laboratório Nacional de Computação Científica—LNCC, Brazil
URL: http://www.lncc.br/∼alm

July 19, 2004.
Not for dissemination.

Abstract. Multiscale Problems are omnipresent in real world applications, and present a challenge in terms of numerical approximations. Well-known examples include modeling of plates and shells, composites, flow in porous media, among other examples.

The PDEs that model these problems are characterized by either the presence of a small parameter in the equation (e.g., the viscosity of a turbulent flow), or in the domain itself (as in shell problems). These PDEs are commonly denominated *singular perturbed*.

In this course, I plan to discuss the modeling of some singular perturbed PDEs. Modeling here has two meanings. It can be in the sense of approximating the original PDE by another PDE that's easier to solve, as in plate and shell theory. It can also be in numerical approximation point of view, where the final goal is to develop a numerical scheme that is robust, i.e., that works well for a wide range of parameters.

The techniques involved will be introduced by means of examples. In all cases discussed, we shall derive modeling error estimates by means of asymptotic analysis. The problems I plan to describe are the Reaction–Diffusion Equation, Problem in domain with Rough Boundaries (think of a golf ball), and Plate problems. If time permits, I'll describe new techniques just developed to deal with PDEs with oscillating coefficients.

References: There's no single book I'll follow. Some basic references follow:

- *Numerical Methods Singularly Perturbed Differential Equations*, Roos, Stynes, Tobiska
- *An introduction to Homogenization*, Doina Cioranescu e Patrizia Donato
- *Asymptotic analysis of fields in multi-structures*, Vladimir Kozlov, Vladimir Maz'ya, Alexander Movchan.
- Mathematical elasticity Vol 2: theory of plates Ciarlet.
- Perturbation methods in applied mathematics, Kevorkian J., Cole J.D.

Also, some modern papers dealing with the topic will be refereed to whenever necessary.

Pre-requisites: I'll assume basic knowledge of analysis and Finite Element Methods. The main tools will be developed as the course goes.

Web Site: http://www.lncc.br/∼alm/cursos/multiescala04.html

Contents

CHAPTER 1

Notação e Material Introdutório

Neste texto assumimos que $\Omega \in \mathbb{R}^d$, onde $d \in \mathbb{N}$, é um aberto limitado cuja fronteira $\partial\Omega$ seja de Lipschitz. Dois exemplos típicos são no caso de domínios com fronteiras suaves ou poligonais. Domínios cujas fronteiras tenham formato de cúspide (mesmo localmente) não são de Lipschitz.

Definimos $L^2(\Omega)$ como o espaço das funções quadrado integráveis em Ω, no sentido de Lebesgue, e denotamos por $(\cdot,\cdot)_D$ o produto interno em $L^2(D)$ onde $D \subset \Omega$, i.e.,

$$(f,g)_D = \int_D f(x)g(x)dx \quad \text{para } f,g \in L^2(D).$$

Simplificamos a notação escrevendo $(\cdot,\cdot)$ quando $D = \Omega$.

Dado então Ω, o espaço de Sobolev $H^k(\Omega) \subset L^2(\Omega)$ é o conjunto de funções com k derivadas fracas em $L^2(\Omega)$. Neste espaço definimos a semi-norma e norma

$$|v|_{k,\Omega} = \left(\int_0^1 \left(\frac{\partial^k v}{\partial x^k}\right)^2 dx\right)^{1/2}, \qquad \|v\|_{k,\Omega} = \left(\sum_{i=0}^{k} |v|_{i,\Omega}^2\right)^{1/2}.$$

Definimos também $H_0^1(\Omega)$, o espaço de funções em $H^1(\Omega)$ que se anulam na fronteira $\partial\Omega$.

CHAPTER 2

One dimensional Singular Perturbed Problem

In this chapter, we introduce a singular perturbed problem and a numerical difficulty associate with its discretization.

2.1. Advection–Diffusion with constant coefficients

2.1.1. Problem description and a finite element discretization. Consider the following boundary value problem:

$$\begin{aligned} -\epsilon\frac{d^2u^\epsilon}{dx^2} + \frac{du^\epsilon}{dx} &= 0, \quad \text{in } (0,1), \\ u^\epsilon(0) = 1, &\quad u^\epsilon(1) = 0, \end{aligned} \tag{2.1.1}$$

where ϵ is a positive real number. It is convenient to assume that $\epsilon \leq 1$. The exact solution is simply

$$u^\epsilon(x) = 1 - \frac{e^{x/\epsilon} - 1}{e^{1/\epsilon} - 1}.$$

The function plots for $\epsilon = 1$, $\epsilon = 0.1$, and $\epsilon = 0.01$ follow in figures 1, 2, and 3. It is clear that when ϵ approaches zero, there is the onset of a boundary layer close to $x = 1$. This is also highlighted by the following fact:

$$\lim_{\substack{\epsilon\to 0 \\ x<1}} \lim_{\substack{x\to 1 \\ x<1}} u^\epsilon(x) = 0 \neq 1 = \lim_{\substack{x\to 1 \\ x<1}} \lim_{\substack{\epsilon\to 0}} u^\epsilon(x).$$

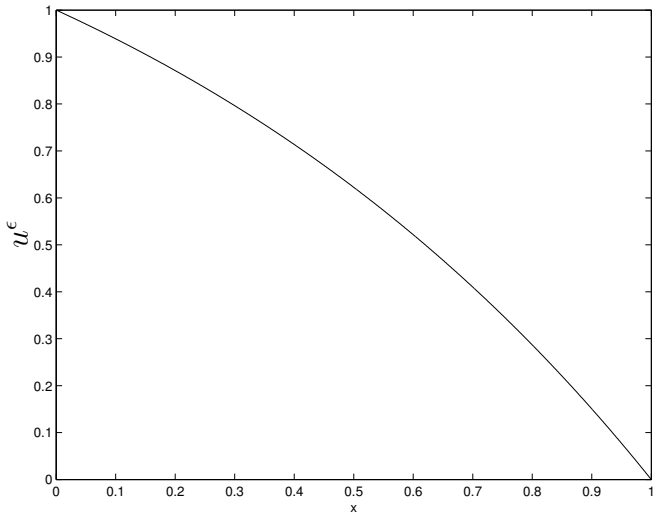

FIGURE 1. Exact solution for $\epsilon = 1$

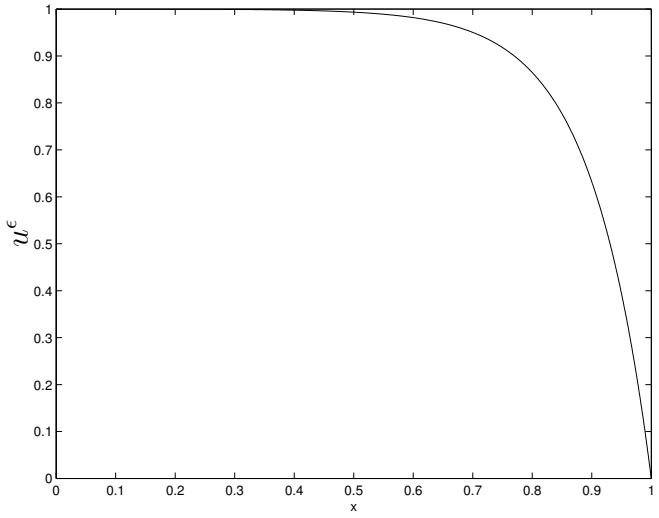

FIGURE 2. Exact solution for $\epsilon = 0.1$

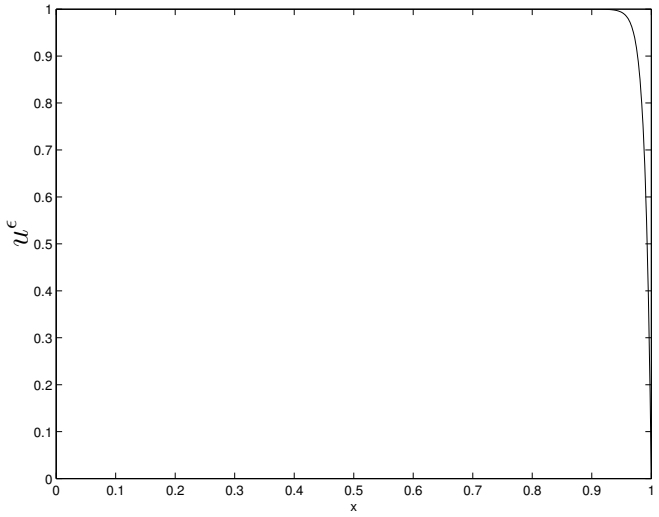

FIGURE 3. Exact solution for $\epsilon = 0.01$

Let's proceed with a straightforward Galerkin discretization of (2.1.1) using finite element method. We first rewrite (2.1.1) in a weak form, i.e, the exact solution

$$u^\epsilon \in V = \big\{ v \in H^1(0,1) \,:\, v(0) = 1 \text{ and } v(1) = 0 \big\},$$

satisfies

$$a(u^\epsilon, v) := \epsilon \int_0^1 \frac{du^\epsilon}{dx}\frac{dv}{dx}\,dx + \int_0^1 \frac{du^\epsilon}{dx} v\,dx = 0 \quad \text{for all } v \in H_0^1(0,1). \tag{2.1.2}$$

We introduce now a discretization of the domain $(0,1)$ into finite elements by defining the nodal points $0 = x_0 < x_1 < \cdots < x_{N+1} = 1$, where $x_j = j/(N+1)$. The mesh parameter $h = 1/(N+1)$. Next, we define the finite dimensional $V^h \subset V$, where

$$V^h = \big\{ v^h \in V \,:\, v^h \text{ is linear in } (x_{j-1}, x_j) \text{ for } j = 1, \ldots, N+1 \big\}.$$

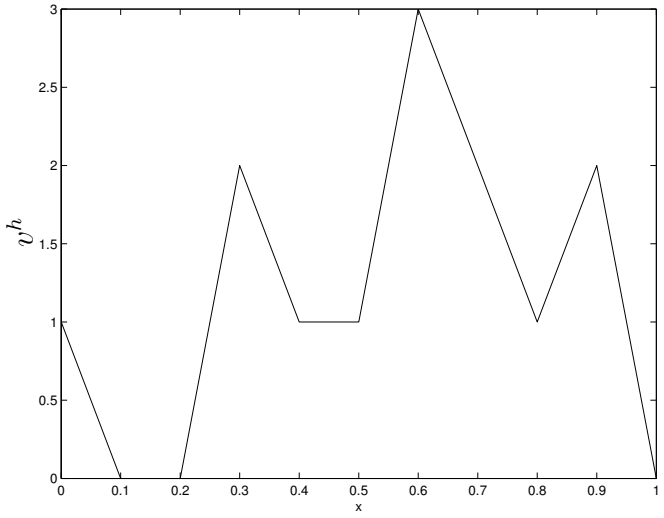

FIGURE 4. Typical piecewise linear function

We say that V^h is a space of piecewise linear functions. A typical function of V^h is depicted in figure 4. We finally define

$$V_0^h = \big\{ v^h \in H_0^1(0,1) \,:\, v^h \text{ is piecewise linear} \big\}.$$

The finite element approximation to u^ϵ is $u^h \in V^h$ such that

$$a(u^h, v) = 0 \quad \text{for all } v \in V_0^h. \tag{2.1.3}$$

OBSERVAÇÃO. Note that u^h depends on ϵ, although this is not explicitly indicated in the notation.

For a uniform mesh, as described above, with $h = 1/16$ the numerical solution for $\epsilon = 1$ is as in figure 5. On the other hand, with the same mesh, the numerical solution for $\epsilon = 0.01$ is as in figure 6. For a more refined mesh, $h = 1/32$, the numerical solution is less oscillatory, but still unsatisfactory, as in figure 7. Eventually, reducing even further the mesh size, the Galerkin approximation will look fine in the "picture norm."[1]

2.1.2. So, what goes wrong? To better understand, or, at least, have a feeling of what goes wrong, we develop an error analysis for this problem. We use the convenient convention that the constants that appear in our estimates are independent of the parameters ϵ and h, unless explicitly indicated. These constants are generally denoted by C.

We first investigate the "continuity" of the bilinear form $a(\cdot,\cdot)$. In fact, it follows from its definition that

$$a(u,v) \le C\|u\|_{1,(0,1)}\|v\|_{1,(0,1)} \quad \text{for all } u, v \in H_0^1(0,1). \tag{2.1.4}$$

[1]No, picture norm is not something one can define. What I mean is simply that the solution "looks" good.

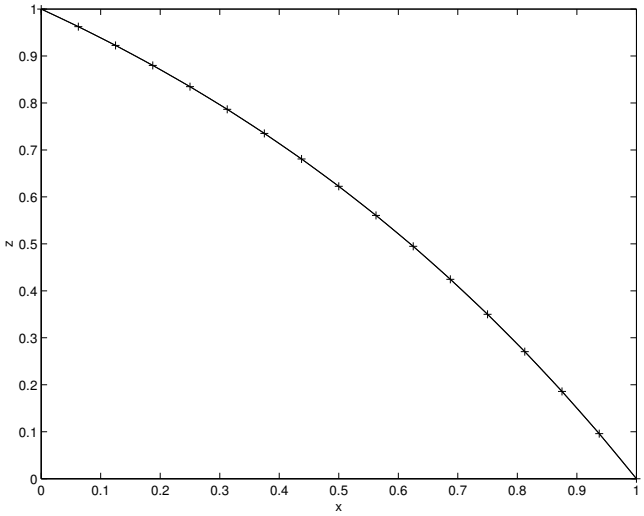

FIGURE 5. Galerkin approximation for $\epsilon = 1$ and $h = 1/16$

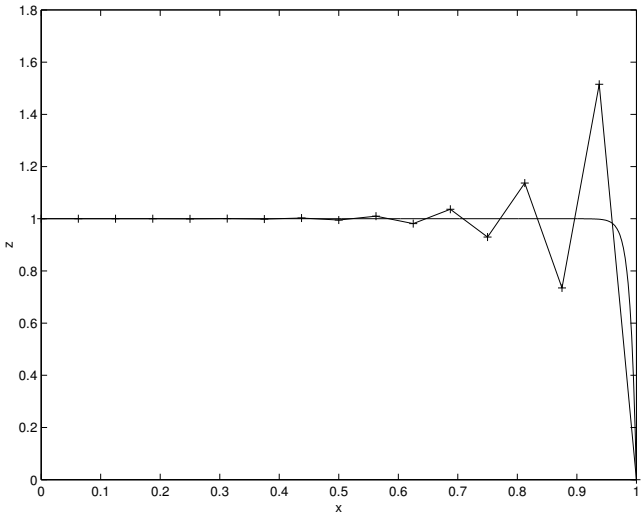

FIGURE 6. Galerkin approximation for $\epsilon = 0.01$ and $h = 1/16$

The problem starts when we try to derive the *coercivity estimate*:

$$a(v,v) = \epsilon \int_0^1 \left(\frac{dv}{dx}\right)^2 dx + \int_0^1 \frac{dv}{dx} v\, dx = \epsilon \int_0^1 \left(\frac{dv}{dx}\right)^2 dx \geq C\epsilon \|v\|^2_{1,(0,1)} \quad \text{for all } v \in H_0^1(0,1), \tag{2.1.5}$$

since integration by parts yields $\int_0^1 (dv/dx)v\, dx = 0$, for $v \in H_0^1(0,1)$. We also used Poincaré's inequality at the last step.

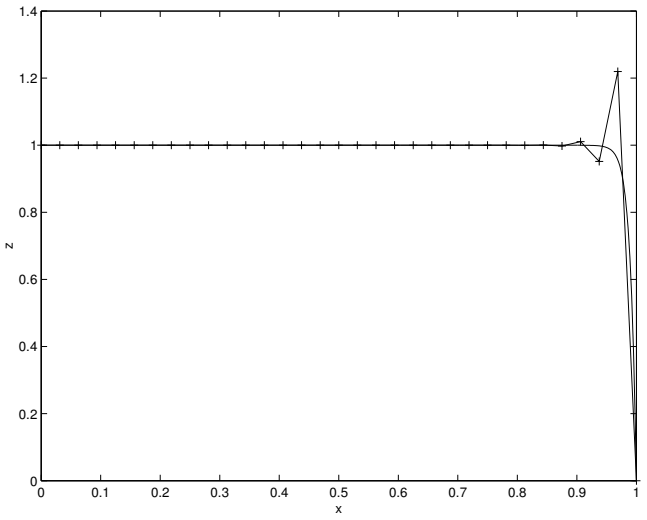

FIGURE 7. Galerkin approximation for $\epsilon = 0.01$ and $h = 1/32$

We are ready to derive error estimates. Using (2.1.5), and then (2.1.4), we gather that:

$$\|u^\epsilon - u^h\|^2_{1,(0,1)} \le C\epsilon^{-1} a(u^\epsilon - u^h, u^\epsilon - u^h) = C\epsilon^{-1} a(u^\epsilon - u^h, u^\epsilon - v^h) \le C\epsilon^{-1}\|u^\epsilon - u^h\|_{1,(0,1)}\|u^\epsilon - v^h\|_{1,(0,1)} \quad \text{for all } v^h \in V^h. \tag{2.1.6}$$

Using standard interpolation estimates, we have that

$$\|u^\epsilon - I^h u^\epsilon\|_{1,(0,1)} \le h|u^\epsilon|_{2,(0,1)},$$

where $I^h u^\epsilon$ is the interpolator of u^ϵ. Making $v^h = I^h u^\epsilon$ in (2.1.6), we conclude that

$$\|u^\epsilon - u^h\|_{1,(0,1)} \le C\epsilon^{-1} h|u^\epsilon|_{H^2(0,1)}. \tag{2.1.7}$$

We stop now to try interpret the error estimate we just obtained. First of all, *there is convergence in h*. Indeed, for a fixed ϵ, the error goes to zero as the mesh size goes to zero.

The problem is that the convergence in h is not uniform in ϵ. Hence, for ϵ small, unless the mesh size is very small, the $H^1(0,1)$ norm error estimate becomes large. The estimate is even worse than one can think at first glance, since $|u^\epsilon|_{2,(0,1)} = O(\epsilon^{-3/2})$. This makes (2.1.7) and the traditional Galerkin method almost useless.

Another way to look at this problem is by first noticing that we would like to have

$$\lim_{\epsilon\to 0} u^h = \lim_{\epsilon\to 0} u^\epsilon = 1.$$

After all, it would be just perfect to have a method that converges (with ϵ) to the correct solution *for a fixed mesh*. This is not happening. Indeed, looking at the matricial problem coming from (2.1.3), it is matter of computation to show that [**39**]

$$-\frac{\epsilon}{h^2}(u_{j+1} - 2u_j + u_{j-1}) + \frac{1}{2h}(u_{j+1} - u_{j-1}) = 0, \quad u_0 = 1,\ u_{N+1} = 0, \tag{2.1.8}$$

where $u_j = u^h(x_j)$. Assume N even. If $\epsilon \ll 1$, then $u_{j+1} \approx u_{j-1}$. This, and the boundary conditions originate the oscillatory behavior of the approximate solution. See figure 8.

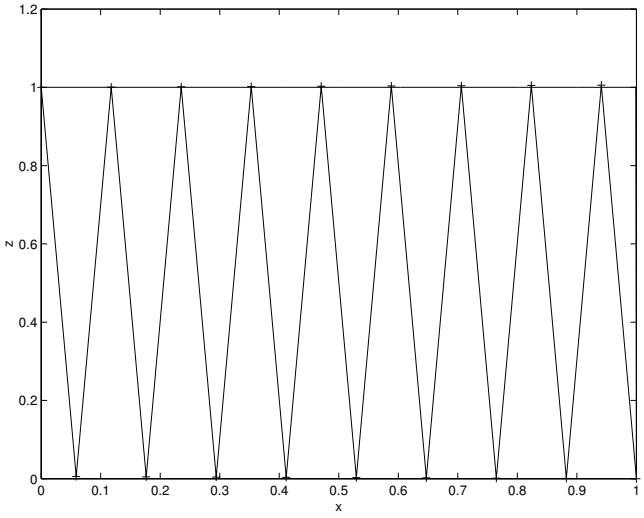

FIGURE 8. Numerical and exact solutions for $\epsilon = 10^{-5}$ and $N = 16$

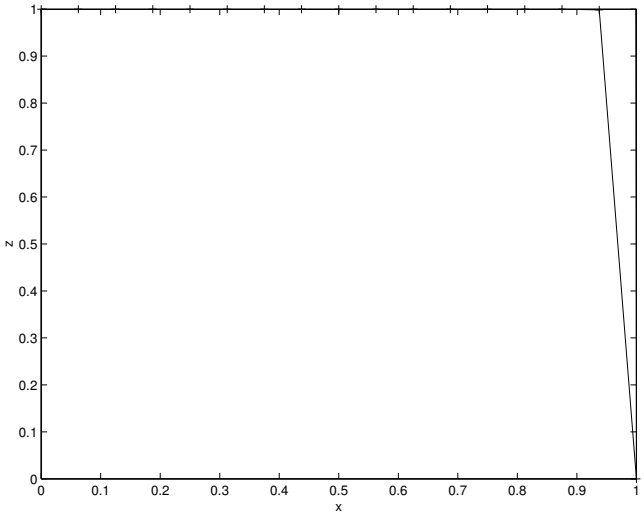

FIGURE 9. Finite difference approximation for $\epsilon = 0.0001$ and $h = 1/15$

OBSERVAÇÃO. Note that although we used a finite element scheme to derive (2.1.8), this scheme is also a finite difference scheme which uses a central difference approximation for the convective term du/dx. The more naive finite difference approximation

$$-\frac{\epsilon}{h^2}(u_{j+1} - 2u_j + u_{j-1}) + \frac{1}{h}(u_j - u_{j-1}) = 0, \quad u_0 = 1,\ u_{N+1} = 0,$$

yields in fact a better result. See figure (9). In fact, for this scheme, $u_j = u_{j-1}$, as ϵ goes to zero. Since $u_0 = 1$, it holds that $u_j = 1$ in the $\epsilon \to 0$ limit:

$$\lim_{\epsilon \to 0} u^h(x_j) = \lim_{\epsilon \to 0} u^\epsilon(x_j) = 1, \quad \text{for } j = 1, \ldots, N.$$

The behavior we described above is typical in singular perturbed PDEs, where the onset of boundary layers is a common phenomenon. But this is not all that can happen. For

instance, in plate models, in particular for the Reissner–Mindlin equation, as the plate thickness goes to zero (that is the small parameter in this case), numerical "locking" occurs, i.e., if a careless method is used, the computed solution goes to zero (a wrong limit). In due time we shall explain why this happens....

Several numerical methods try to somehow overcome these and other difficulties related to asymptotic limits. Some methods perform well for a certain asymptotic range, for instance by assuming $\epsilon \ll 1$. Some other methods try to be performing for a broader range of parameters. See for instance [**15**], [**26**], [**37**], [**51**].

Looking at these difficulties (and their corresponding solutions!) it becomes more clear that it is important to have a full understanding of the solution's behavior. This is useful not only to help designing new numerical methods, but also to analise and estimate old ones. A valuable analysis tool is the method of *matching asymptotics*, where the exact solution for a given singular perturbed PDE is expressed in terms of a (formal) power series with respect to a small parameter.

In the example we are considering in this section, the asymptotic expansion is trivial. Indeed the exact solution

$$u^\epsilon(x) = 1 - \frac{e^{x/\epsilon} - 1}{e^{1/\epsilon} - 1}$$

is the sum of a "regular function" (the unit function in this case), plus a "boundary layer" term. The regular part is independent of ϵ, and the boundary layer term, also called "boundary corrector", depends on ϵ only through x/ϵ, and becomes exponentially small in the interior of the domain. This is a typical behavior of singular perturbed problems.

We shall explain how an asymtotic expansion can be developed by looking at a simple, still one-dimensional, example.

2.2. A singular perturbed general second order ODE

Consider the differential operator

$$\mathcal{L}^\epsilon u^\epsilon = -\epsilon \frac{d^2 u^\epsilon}{dx^2} + b(x)\frac{du^\epsilon}{dx} + c(x)u^\epsilon,$$

and the problem

$$\mathcal{L}^\epsilon u^\epsilon = f \quad \text{in } (0,1), \tag{2.2.1}$$

$$u^\epsilon(0) = u^\epsilon(1) = 0. \tag{2.2.2}$$

We assume that b, c, and f are smooth functions, and that b is always positive.

In 2.2.1 we shall develop asymptotic expansion for u^ϵ, and in 2.2.2 we show error estimates. Then, in 2.2.3, we shall make some comments about what can happen if b vanishes at a particular point. This is the "turning point problem."

2.2.1. Formal development of the asymptotic expansion. In this subsection, we follow the outline of [**51**]. Consider the series

$$u^0 + \epsilon u^1 + \epsilon^2 u^2 + \dots \tag{2.2.3}$$

and formally substitute it in (2.2.1). Then

$$b(x)\frac{du^0}{dx} + c(x)u^0 + \epsilon\left(-\frac{d^2u^0}{dx^2} + b(x)\frac{du^1}{dx} + c(x)u^1\right) + \dots \\ + \epsilon^i\left(-\frac{d^2u^{i-1}}{dx^2} + b(x)\frac{du^i}{dx} + c(x)u^i\right) + \dots = f.$$

Comparing the different powers of ϵ, it is natural to require that

$$\mathcal{L}^0 u^0 = f, \quad \mathcal{L}^0 u^1 = \frac{d^2u^0}{dx^2}, \dots, \quad \mathcal{L}^0 u^i = \frac{d^2u^{i-1}}{dx^2}, \dots, \tag{2.2.4}$$

where $\mathcal{L}^0 v = b(x)dv/dx + c(x)v$.

From (2.2.2), it would be natural to impose $u^i(0) = u^i(1) = 0$. However, the equations in (2.2.4) are of first order, and only one boundary condition is to be imposed. We set then

$$u^i(0) = 0.$$

We correct this discrepancy by introducing the boundary corrector U. We would like to have

$$\mathcal{L}^\epsilon U = 0, \quad U(0) = 0, \quad U(1) = u^0(1) + \epsilon u^1(1) + \epsilon^2 u^2(1) + \dots$$

Note that if we make the change of coordinates $\hat{\rho} = \epsilon^{-1}(1-x)$, and set $\hat{U}(\hat{\rho}) = U(1-\epsilon\hat{\rho})$, then

$$-\frac{d^2\hat{U}}{d\hat{\rho}^2}(\hat{\rho}) - b(1-\epsilon\hat{\rho})\frac{d\hat{U}}{d\hat{\rho}}(\hat{\rho}) + \epsilon c(1-\epsilon\hat{\rho})\hat{U}(\hat{\rho}) = 0,$$
$$\hat{U}(0) = u^0(1) + \epsilon u^1(1) + \epsilon^2 u^2(1) + \dots$$

Going one step further, we develop the Taylor expansions

$$b(1-\epsilon\hat{\rho}) = b(1) - \epsilon\hat{\rho}\frac{db}{dx}(1) + \frac{\epsilon^2\hat{\rho}^2}{2}\frac{d^2b}{dx^2}(1) - \dots,$$
$$c(1-\epsilon\hat{\rho}) = c(1) - \epsilon\hat{\rho}\frac{dc}{dx}(1) + \frac{\epsilon^2\hat{\rho}^2}{2}\frac{d^2c}{dx^2}(1) - \dots.$$

Finally, assuming the asymptotic expansion

$$\hat{U} \sim \hat{U}^0 + \epsilon\hat{U}^1 + \epsilon^2\hat{U}^2 + \dots,$$

we gather that

$$-\frac{d^2\hat{U}^0}{d\hat{\rho}^2} - b(1)\frac{d\hat{U}^0}{d\hat{\rho}} = 0,$$
$$U^0(0) = u^0(1).$$

Noting that we need another boundary condition for $\hat{U}^0$, we try to ensure a "local behavior" for U^0 by imposing

$$\lim_{\hat{\rho}\to\infty} \hat{U}^0(\hat{\rho}) = 0.$$

Hence, $\hat{U}^0(\hat{\rho}) = u(1)\exp\bigl(-b(1)\hat{\rho}\bigr)$.

Similarly,

$$-\frac{d^2\hat{U}^1}{d\hat{\rho}^2} - b(1)\frac{d\hat{U}^1}{d\hat{\rho}} = -\hat{\rho}\frac{db}{dx}(1)\frac{d\hat{U}^0}{d\hat{\rho}} - c(1)\hat{U}^0,$$
$$U^1(0) = u^1(1), \qquad \lim_{\hat{\rho}\to\infty} U^1(\hat{\rho}) = 0,$$

etc.

So, putting everything together, we have that

(2.2.5)
$$u^\epsilon(x) \sim u^0(x)+\epsilon u^1(x)+\epsilon^2 u^2(x)+\cdots-\hat{U}^0(\epsilon^{-1}(1-x))-\epsilon\hat{U}^1(\epsilon^{-1}(1-x))-\epsilon^2\hat{U}^2(\epsilon^{-1}(1-x))-\ldots.$$

By construction, the above infinite power series *formally* solves the ODE (2.2.1). We did not make any comment regarding convergence of the above expansion. Actually, what we will prove is that a *truncated expansion* approximates well the exact solution.

Observaçãо. Note that each term u^i in the series (2.2.5) is independent of ϵ. Each boundary corrector terms $\hat{U}^i$ depends on ϵ but only up to a change of coordinates.

Observaçãо. Note that the U^i does not satisfy the boundary condition at $x = 0$, but for ϵ small enough, this error is exponentially small.

2.2.2. Truncation Error analysis. We start by developing here an analysis quite similar to that of Subsection 2.1.2. We assume that $b(x) > b_0 > 0$ and $2c - db/dx \geq 0$. Let

$$a(u,v) = \epsilon\int_0^1 \frac{du}{dx}\frac{dv}{dx}\,dx + \int_0^1 b\frac{du}{dx}v\,dx + \int_0^1 cuv\,dx$$

To obtain a coercivity estimate, first note that

$$a(v,v) = \epsilon\int_0^1 \left(\frac{dv}{dx}\right)^2 dx + \int_0^1 b\frac{dv}{dx}v\,dx + \int_0^1 c|v|^2\,dx$$

Integrating by parts yields

$$\int_0^1 b\frac{dv}{dx}v\,dx = -\frac{1}{2}\int_0^1 \frac{db}{dx}|v|^2\,dx \quad \text{for all } v \in H_0^1(0,1).$$

Thus,

$$a(v,v) = \epsilon\int_0^1 \left(\frac{dv}{dx}\right)^2 dx + \int_0^1 \left(c - \frac{1}{2}\frac{db}{dx}\right)|v|^2\,dx \geq \epsilon\int_0^1 \left(\frac{dv}{dx}\right)^2 dx \geq C\epsilon\|v\|^2_{1,(0,1)} \quad \text{for all } v \in H_0^1(0,1). \tag{2.2.6}$$

We again used Poincaré's inequality at the last estimate.

Lema 2.2.1. If $\mathcal{L}^\epsilon v = f$ weakly, and $v \in H_0^1(0,1)$, then

$$\|v\|_{1,(0,1)} \leq C\epsilon^{-1}\|f\|_{-1,(0,1)}.$$

Proof. From (2.2.6), we conclude that

$$\|v\|^2_{1,(0,1)} \leq C\epsilon^{-1}a(v,v) = C\epsilon^{-1}(f,v) \leq C\epsilon^{-1}\|f\|_{-1,(0,1)}\|v\|_{1,(0,1)},$$

where $(\cdot,\cdot)$ denotes the $L^2(0,1)$ inner product. □

COROLÁRIO 2.2.2. If $w \in H^1(0,1)$ is the weak solution of

$$\mathcal{L}^\epsilon w = f, \qquad w(0) = w_0, \quad w(1) = w_1,$$

then

$$\|w\|_{1,(0,1)} \leq C\epsilon^{-1}\big(\|f\|_{-1,(0,1)} + |w_0| + |w_1|\big).$$

PROOF. Let w_{bc} be such that $w_{bc}(0) = w_0$, and $w_{bc}(1) = w_1$, with $\|w_{bc}\|_{1,(0,1)} \leq C\big(|w_0| + |w_1|\big)$. Then Lemma 2.2.1 with $v = w - w_{bc}$ yields the result. □

With the aid of Corollary 2.2.2, we are ready to estimate how well the asymptotic expansion approximates the exact solution of (2.2.1)–(2.2.2). Let

$$e_N(x) = u^\epsilon(x) - \sum_{i=0}^{N} \epsilon^i u^i(x) + \sum_{i=0}^{N} \epsilon^i \hat{U}^i(\epsilon^{-1}(1-x)), \tag{2.2.7}$$

From its construction, $e_N \in H^1(0,1)$, and

$$\mathcal{L}^\epsilon e_N = \epsilon^{N+1}\frac{d^2u^N}{dx^2}, \qquad e_N(0) = \sum_{i=0}^{N} \epsilon^i U^i(\epsilon^{-1}), \quad e_N(1) = 0. \tag{2.2.8}$$

Note that by construction, for each integers i and k, there exist a constant C, also depending on arbitrarily high Sobolev norms of f but ϵ-independent, and another ϵ-independent positive constant α such that

$$\|u^i\|_{k,(0,1)} \leq C, \qquad U^i(\hat{\rho}) \leq C\exp(-\alpha\hat{\rho}). \tag{2.2.9}$$

Using now Corollary 2.2.2, equation (2.2.8), and estimate (2.2.9), we gather that there exists a constant C such that

$$\|e_N\|_{1,(0,1)} \leq C\epsilon^N.$$

This estimate is not sharp. We improve it by adding and subtracting the $(N+1)$th term of the expansion:

$$\|e_N\|_{1,(0,1)} \leq \|e_{N+1}\|_{1,(0,1)} + \|e_N - e_{N+1}\|_{1,(0,1)} \leq C\epsilon^{N+1/2}.$$

Estimates in other norms can be obtained in a similar fashion:

$$\|e_N\|_{0,(0,1)} \leq \|e_{N+1}\|_{1,(0,1)} + \|e_N - e_{N+1}\|_{0,(0,1)} \leq C\epsilon^{N+1}.$$

We obtained then the following important result.

TEOREMA 2.2.3. *Let u^ϵ be the solution of the ODE (2.2.1), and let e_N be as in (2.2.7). Then, for every nonnegative integer N, there exists a constant C such that*

$$\|e_N\|_{1,(0,1)} \leq C\epsilon^{N+1/2}. \qquad \|e_N\|_{0,(0,1)} \leq C\epsilon^{N+1}.$$

The constant C might depend on N, and on Sobolev norms of f, b, and c, but not on ϵ.

OBSERVAÇÃO. Theorem 2.2.3 does not imply convergence of the power series as N goes to infinity, since the constants that appear in the right hand side of the estimates depend on N. What the theorem provides is a convergence in ϵ, i.e., if ϵ is quite small, then the asymptotic expansion truncation error gets small.

To derive estimates in higher order norms, it is enough to gather from (2.2.8) and the definition of $\mathcal{L}^\epsilon$ that

$$\|e_N\|_{k,(0,1)} \leq \epsilon^{-1}\|e_N\|_{k-1,(0,1)}.$$

Hence, by induction we have that

$$\|e_N\|_{k,(0,1)} \leq C\epsilon^{N+1/2-k}.$$

OBSERVAÇÃO. The asymptotic *rule of the thumb* works quite well: the error estimates present in Theorem 2.2.3 are of the same order as the terms left out of the truncated asymptotic expansion.

2.2.3. Problems with "turning point". Here, we again follow the outline of [**51**]. Consider the problem

$$-\epsilon\frac{d^2u^\epsilon}{dx^2} + xb(x)\frac{du^\epsilon}{dx} + c(x)u^\epsilon = f \quad \text{in } (-1,1), \tag{2.2.10}$$

$$u^\epsilon(-1) = u^\epsilon(1) = 0. \tag{2.2.11}$$

We assume that $b(x) \neq 0$, $c(x) \geq 0$, and $c(0) \neq 0$.

From what we have seen, if $b(x)$ is positive, then $xb(x) < 0$ at $x = -1$, and $xb(x) > 0$ at $x = 1$. Hence we can expect boundary layers at -1 and 1. The reduced problem is

$$xb(x)\frac{du^0}{dx} + c(x)u^0 = f \quad \text{in } (-1,1),$$

no further boundary conditions are necessary. Indeed, since $c(0) \neq 0$, then $u^0(0) = f(0)/c(0)$. An example is given by

$$x\frac{du^0}{dx} + u^0 = 2x \quad \text{in } (-1,1).$$

The solution is simply $u^0 = x$.

If however b is negative, then the boundary layers occur at $x = 0$ only! In this case, the reduced problem splits in two:

$$xb(x)\frac{du^0}{dx} + c(x)u^0 = f \quad \text{in } (-1,0), \qquad u^0(-1) = 0,$$

$$xb(x)\frac{du^0}{dx} + c(x)u^0 = f \quad \text{in } (0,1), \qquad u^0(1) = 0.$$

Note from the above equations that u^0 is continuous, since we still have $u^0(0) = f(0)/c(0)$. An interesting example is given by the problem

$$xb\frac{du^0}{dx} + cu^0 = bx^k \quad \text{in } (-1,1), \tag{2.2.12}$$

where $b < 0$ and $c > 0$ are constants. The exact solution is

$$u^0(x) = \begin{cases} \frac{1}{k-\lambda}(|x|^k - |x|^\lambda) & \text{if } \lambda \neq k, \\ x^k \ln|x| & \text{otherwise,} \end{cases}$$

where $\lambda = -c/b$. See figures 10, 11.

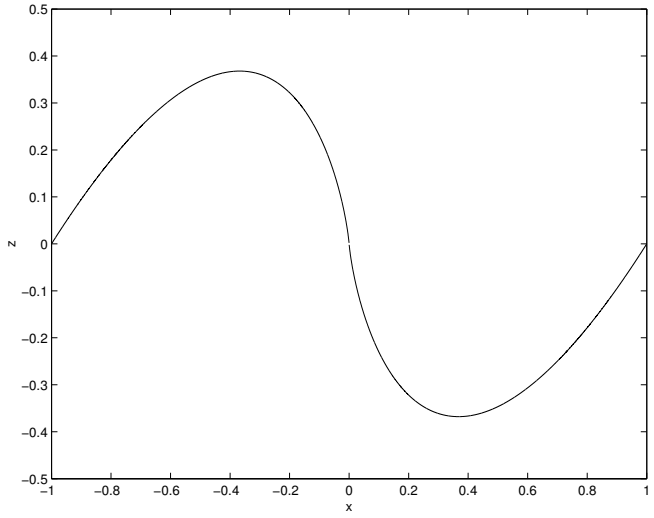

FIGURE 10. Exact solution of (2.2.12) for $k = \lambda = 1$

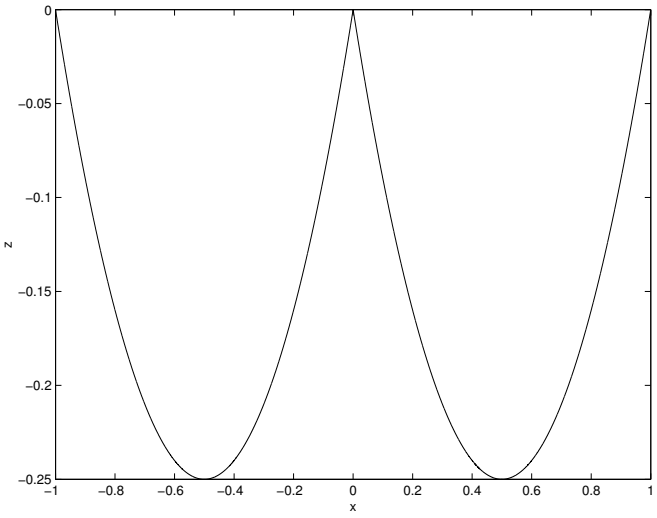

FIGURE 11. Exact solution of (2.2.12) for $k = 1$ and $\lambda = 2$

One last point for discussion is if $c(0) = 0$. Then u^0 might be discontinuous, and u^ϵ has an interior boundary layer. We are still assuming that b is non-negative. For instance,

$$x\frac{du^0}{dx} = x$$

with homogeneous boundary conditions has as solution

$$u^0(x) = \begin{cases} -1 - x & \text{for } x \in (-1, 0), \\ 1 - x & \text{for } x \in (0, 1). \end{cases}$$

CHAPTER 3

Asymptotic Analysis for Two Dimensional Reaction–Diffusion Equation

We now investigate two-dimensional domains, and consider a reaction–diffusion problem. We first develop an asymptotic expansion for the solution, and this time we show how to deal with the boundary layer in a two-dimensional problem. This will be important to devise efficient numerical methods.

3.1. Asymptotic Expansion

Consider the singuar perturbed Reaction–Diffusion problem

$$\begin{aligned} \mathcal{L}^\epsilon u := -\epsilon^2 \Delta u + u = f \quad \text{in } \Omega, \\ u = 0 \quad \text{on } \partial\Omega, \end{aligned} \tag{3.1.1}$$

where Ω is a smooth two-dimensional bounded domain, and ϵ is a positive constant. Also assume that f is smooth.

Consider the series

$$u^0 + \epsilon^2 u^2 + \epsilon^4 u^4 + \dots$$

and formally substitute it in (3.1.1). Then

$$u^0 + \epsilon^2\big(-\Delta u^0 + u^2\big) + \cdots + \epsilon^{2i}\big(-\Delta u^{2i-2} + u^{2i}\big) + \cdots = f.$$

By comparing the different powers of ϵ, it is natural to require that

$$u^0 = f, \quad u^2 = \Delta u^0, \dots, \quad u^{2i} = \Delta u^{2i-2}, \dots. \tag{3.1.2}$$

Since the u^i are already well-defined, we cannot impose the zero Dirichlet boundary condition. We again correct this by introducing boundary correctors. We would like to have

$$\mathcal{L}^\epsilon U = 0, \quad \text{in } \Omega, \qquad U = u^0 + \epsilon^2 u^2 + \epsilon^4 u^4 + \dots \quad \text{on } \partial\Omega, \tag{3.1.3}$$

and formally expand

$$U \sim U^0 + \epsilon U^1 + \epsilon^2 U^2 + \dots. \tag{3.1.4}$$

Motivated by the one-dimensional problem, we expect the boundary correctors to have only a "local" influence, and we introduce for that purpose boundary-fitted coordinates. We digress now to introduce these coordinates, following the notation of Chen [**16**]. Suppose that $\partial\Omega$ is arc-length parametrized by $\mathbf{z}(\theta) = (X(\theta), Y(\theta))$. Let $\mathbf{s} = (X', Y')$, $\mathbf{n} = (Y', -X')$ denote the tangent and the outward normal of $\partial\Omega$, and define the sub-domain $\Omega_b \subset \Omega$,

$$\Omega_b = \big\{\mathbf{z} - \rho\mathbf{n} \,:\, \mathbf{z} \in \partial\Omega,\, 0 < \rho < \rho_0\big\},$$

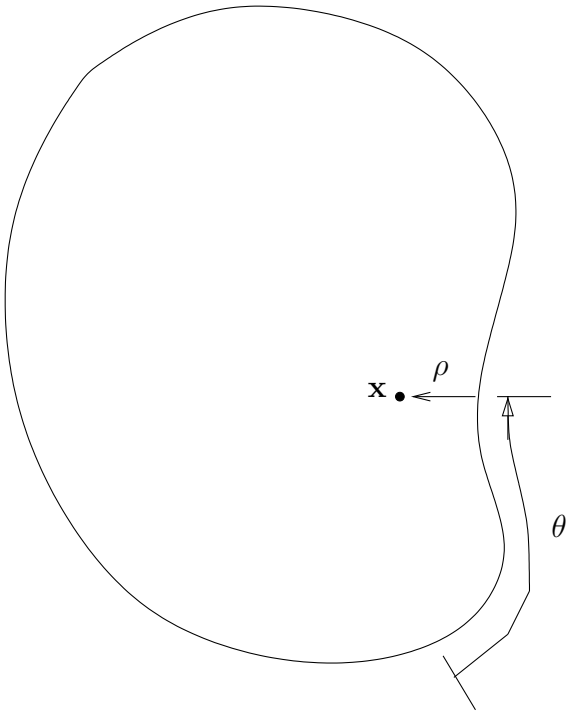

FIGURE 1. Boundary-fitted coordinates

where ρ_0 is a positive number smaller than the minimum radius of curvature of $\partial\Omega$. With L denoting the arc-length of $\partial\Omega$, then

$$\mathbf{x} : (0, \rho_0) \times \mathbb{R}/L \to \Omega_b,$$

where

$$\mathbf{x}(\rho, \theta) = \mathbf{z}(\theta) - \rho\mathbf{n}(\theta),$$

is a diffeomorphism. See figure 1 (based on a figure by Arnold and Falk [**4**]).

OBSERVAÇÃO. The smoothness of the domain is important here. In particular for a polygon, the transformation above is not a diffeomorphism.

By differentiating $|\mathbf{z}'| = 1$, it follows that $\mathbf{z}'$ is orthogonal to $\mathbf{z}''$. We define κ as the curvature of $\partial\Omega$ by the formula $\mathbf{z}'' = -\kappa\mathbf{n}$. We also gather the identity

$$\kappa(\theta) = -(\mathbf{z}'' \times \mathbf{z}') \cdot \mathbf{e_3} = -Y'X'' + X'Y''. \tag{3.1.5}$$

Note then that

$$D_{(\rho,\theta)}\mathbf{x} = \begin{pmatrix} \partial_\rho \mathbf{x} & \partial_\theta \mathbf{x} \end{pmatrix} = \begin{pmatrix} -\mathbf{n}(\theta) & \mathbf{z}'(\theta) - \rho\mathbf{n}(\theta) \end{pmatrix} = \begin{pmatrix} -Y' & X' - \rho Y'' \\ X' & Y' + \rho X'' \end{pmatrix},$$

and using (3.1.5), and $\rho < \rho_0$, we obtain that $\det D_{(\rho,\theta)}\mathbf{x} = 1 - \rho\kappa > 0$. Inverting the above matrix, we have that

$$D_{\mathbf{x}} \begin{pmatrix} \rho \\ \theta \end{pmatrix} = \begin{pmatrix} \nabla_{\mathbf{x}}^T \rho \\ \nabla_{\mathbf{x}}^T \theta \end{pmatrix} = \frac{1}{J} \begin{pmatrix} -Y' - \rho X'' & X' - \rho Y'' \\ X' & Y' \end{pmatrix},$$

where $J(\rho,\theta) = 1 - \rho\kappa(\theta)$. Hence,

$$\nabla_{\mathbf{x}}\,\rho = -\frac{1}{J}\mathbf{n} - \frac{\rho}{J}z'' = \frac{1}{J}(-1+\rho\kappa)\mathbf{n} = -\mathbf{n}.$$

Also,

$$\nabla_{\mathbf{x}}\,\theta = \frac{1}{J}\mathbf{s}.$$

Finally, the change of coordinates yields

$$\partial_\alpha f = \partial_\theta f \partial_\alpha \theta + \partial_\rho f \partial_\alpha \rho, \qquad \text{for } \alpha = 1,\, 2,$$

for an arbitrary function f.

The expression for the Laplacian in these new coordinates follows:

$$\begin{aligned}(3.1.6)\quad (\partial_{11}+\partial_{22})U &= \partial_{\rho\rho}U - \frac{\kappa}{J}\partial_\rho U + \frac{1}{J^2}\partial_{\theta\theta}U + \frac{\rho\kappa'}{J^3}\partial_\theta U \\ &= \partial_{\rho\rho}U + \sum_{j=0}^{\infty}\rho^j\left(a_1^j\partial_\rho U + a_2^j\partial_{\theta\theta}U + a_3^j\partial_\theta U\right),\end{aligned}$$

where we formally replace each coefficient with its respective Taylor expansion [**3**], and

$$a_1^j = -[\kappa(\theta)]^{j+1}, \quad a_2^j = (j+1)[\kappa(\theta)]^j, \quad a_3^j = \frac{j(j+1)}{2}[\kappa(\theta)]^{j-1}\kappa'(\theta).$$

Defining the new variable $\hat{\rho} = \epsilon^{-1}\rho$ and using the same name for functions different only up to this change of coordinates, we have from (3.1.6) that

$$(3.1.7)\qquad (\partial_{11}+\partial_{22})U = \epsilon^{-2}\partial_{\hat\rho\hat\rho}U + \sum_{j=0}^{\infty}(\epsilon\hat\rho)^j\left(a_1^j\epsilon^{-1}\partial_{\hat\rho}U + a_2^j\partial_{\theta\theta}U + a_3^j\partial_\theta U\right).$$

Aiming to solve (3.1.3) we formally use (3.1.4) and (3.1.7), collect together terms with same order of ϵ and for $k \geq 2$, pose the following sequence of problems parametrized by θ:

$$(3.1.8)\qquad \begin{aligned} -\partial_{\hat\rho\hat\rho}U^k + U^k &= F_k \qquad \text{in } \mathbb{R}^+, \\ U^k(0,\theta) &= u^k(0,\theta),\end{aligned}$$

with the convention that $u^k = 0$ for k odd, and

$$F_0 = 0, \qquad F_1 = a_1^0\partial_{\hat\rho}U^0,$$

$$F_k = \sum_{j=0}^{k-1}\hat\rho^j a_1^j\partial_{\hat\rho}U^{k-j-1} + \sum_{j=0}^{k-2}\hat\rho^j\left(a_2^j\partial_{\theta\theta}U^{k-j-2} + a_3^j\partial_\theta U^{k-j-2}\right), \quad \text{for } k \geq 2.$$

With the boundary layer terms defined, we gather that the asymptotic expansion is given by

$$\begin{aligned}(3.1.9)\quad u^\epsilon(\mathbf{x}) &\sim u^0(\mathbf{x}) + \epsilon^2 u^3(\mathbf{x}) + \epsilon^4 u^4(\mathbf{x}) + \dots \\ &\quad - \chi(\rho)\big[U^0(\epsilon^{-1}\rho,\theta) + \epsilon U^1(\epsilon^{-1}\rho,\theta) + \epsilon^2 U^2(\epsilon^{-1}\rho,\theta) + \dots\big],\end{aligned}$$

where χ is a smooth cutoff function identically one if $0 \leq \rho \leq \rho_0/3$ and identically zero if $\rho \geq 2\rho_0/3$.

OBSERVAÇÃO. The presence of a cutoff function is essential, since the boundary fitted coordinates are only defined in a neighborhood of $\partial\Omega$. Since the boundary correctors decay exponentially to zero, the cutoff functions will introduce only a exponentially small, thus negligible, error.

3.2. Error Estimates for the Asymptotic Expansion

Here we estimate how close a truncated asymptotic expansion approximates the exact solution. We shall assume that C is a constant that might depend on the domain, and the right hand side f.

We first estimate the boundary correctors. For every s and positive integer i, there exist ϵ-independent constants C and α such that

$$\|u^{2i}\|_{s,\Omega} \leq C, \quad |U^i(\hat{\rho})| + |\partial_{\hat{\rho}} U^i(\hat{\rho})| \leq C \exp(-\alpha\hat{\rho}). \tag{3.2.1}$$

Although (3.1.9) is a formal expansion, a rigorous error estimate shows that the difference between the exact solution and a truncated asymptotic expansion is of the same order of the first term omitted in the expansion. In fact, define

$$e_{2N}(\mathbf{x}) = u^\epsilon(\mathbf{x}) - \sum_{k=0}^{N} \epsilon^{2k} u^{2k}(\mathbf{x}) + \chi(\rho) \sum_{k=0}^{2N} \epsilon^k U^k(\epsilon^{-1}\rho, \theta). \tag{3.2.2}$$

In the theorem below we bound the $H^1(\Omega)$ norm of e_{2N}.

TEOREMA 3.2.1. *For any positive integer N, there exists a constant C such that the difference between the truncated asymptotic expansion and the original solution measured in the original domain is bounded as follows:*

$$\|e_{2N}\|_{1,\Omega} \leq C\epsilon^{2N+1/2}. \tag{3.2.3}$$

Before we prove Theorem 3.2.1, we develop some other estimates. For instance, in the $L^2(\Omega)$ norm, we have from the triangle inequality that

$$\|e_{2N}\|_{L^2(\Omega)} \leq \|e_{2N+2}\|_{1,\Omega} + \|e_{2N+2} - e_{2N}\|_{0,\Omega}.$$

Since

$$(e_{2N+2} - e_{2N})(\mathbf{x}) = -\epsilon^{2N+1}\chi(\rho)U^{2N+1}(\epsilon^{-1}\rho, \theta) + \epsilon^{2N+2}\big[u^{2N+2}(\mathbf{x}) - \chi(\rho)U^{2N+2}(\epsilon^{-1}\rho, \theta)\big], \tag{3.2.4}$$

we conclude that

$$\|e_{2N}\|_{0,\Omega} = O(\epsilon^{2N+3/2}),$$

for N nonnegative.

Using similar arguments, it is possible to compute *interior estimates*, which achieve better convergence in regions "far away" from the lateral boundary of the plate. The reason for the improvement in such subdomains is that the influence of the boundary layer is negligible. The table below presents these interior and various other error estimates. We assume that f is a sufficiently smooth function and we show only the order of the norms with respect to ϵ. "BL" stands for "Boundary Layer" and the "Relative Error" column presents the norm of e_{2N} divided by the norm of u^ϵ. In parentheses are the interior estimates, when these are better than the global estimates.

The remainder of this section contains a proof of Theorem 3.2.1.

TABLE 1. Order with respect to ϵ of the exact solution, the first term of the boundary layer expansion, and the difference between the solution and a truncated asymptotic expansion in various norms.

norm	u^ϵ	BL	e_{2N}, $N \geq 0$	Relative Error
$\|\cdot\|_{0,\Omega}$	1	$\epsilon^{1/2}$	$\epsilon^{2N+3/2}(\epsilon^{2N+2})$	$\epsilon^{2N+3/2}(\epsilon^{2N+2})$
$\|\partial_\rho \cdot\|_{0,\Omega}$	$\epsilon^{-1/2}(1)$	$\epsilon^{-1/2}$	$\epsilon^{2N+1/2}(\epsilon^{2N+2})$	$\epsilon^{2N+1}(\epsilon^{2N+2})$
$\|\partial_\theta \cdot\|_{0,\Omega}$	1	$\epsilon^{1/2}$	$\epsilon^{2N+3/2}(\epsilon^{2N+2})$	$\epsilon^{2N+3/2}(\epsilon^{2N+2})$
$\|\cdot\|_{1,\Omega}$	$\epsilon^{-1/2}(1)$	$\epsilon^{-1/2}$	$\epsilon^{2N+1/2}(\epsilon^{2N+2})$	$\epsilon^{2N+1}(\epsilon^{2N+2})$

DEFINIÇÃO 3.2.2. *Set*

$$u_{2N}(\mathbf{x}) = \sum_{k=0}^{N} \epsilon^{2k} u^{2k}(\mathbf{x}), \quad U_{2N}(\mathbf{x}) = \sum_{k=0}^{2N} \epsilon^k U^k(\epsilon^{-1}\rho, \theta).$$

Some results regarding the boundary layer terms are collected below.

LEMA 3.2.3. For any positive integer N, there exists positive constants C and α such that

$$\epsilon^{-1/2}\|\chi' U_{2N}\|_{0,\Omega} + \epsilon^{1/2}\|\chi' \nabla U_{2N}\|_{0,\Omega} \leq C\exp(-\alpha\epsilon^{-1}). \tag{3.2.5}$$

Also, for all $v \in H_0^1(\Omega)$,

$$\left| \int_\Omega \epsilon^2 \nabla U_{2N} \cdot \nabla(\chi v) + U_{2N}\chi v \, d\mathbf{x} \right| \leq C\epsilon^{2N}\|v\|_{1,\Omega}. \tag{3.2.6}$$

PROOF. Changing to (ρ, θ) coordinates, we gather that

$$\begin{aligned}\|\chi' U_{2N}\|_{0,\Omega}^2 = \int_{\Omega_b} (\chi' U_{2N})^2 \, d\mathbf{x} &= \int_0^L \int_0^{\rho_0} (\chi' U_{2N})^2 |J| \, d\rho \, d\theta \\ &\leq C \int_0^L \int_{\rho_0/3}^{2\rho_0/3} [U_{2N}(\rho,\theta)]^2 \, d\rho \, d\theta \leq C\epsilon\exp(-\alpha\epsilon^{-1}),\end{aligned}$$

where we also used the definition of χ, and (3.2.1). The other inequality in (3.2.5) follow from similar arguments. To see that (3.2.6) holds, first rewrite (3.1.6) as a finite series, using Taylor expansion with remainders. Then the result follows from the definition of U_{2N}, (3.1.8), and (3.2.1). □

PROOF (OF THEOREM 3.2.1). Let $v \in H_0^1(\Omega)$. If we define

$$E(2N, v) = \int_\Omega \epsilon^2 \nabla(u^\epsilon - u_{2N}) \cdot \nabla v + (u^\epsilon - u_{2N}) v \, d\mathbf{x},$$

then, by construction of the asymptotic expansion, we have

$$E(2N, v) = \int_\Omega f v \, d\mathbf{x} - \sum_{k=0}^{N} \epsilon^{2k} \int_\Omega \left(\epsilon^2 \nabla u^{2k} \cdot \nabla v + u^{2k} v\right) d\mathbf{x} = -\epsilon^{2N+2} \int_\Omega \nabla u^{2N} \cdot \nabla v \, d\mathbf{x},$$

and we conclude that

$$|E(2N, v)| \leq C\epsilon^{2N+2}\|v\|_{1,\Omega}. \tag{3.2.7}$$

We also have

$$\left|\int_\Omega \nabla(\chi U_{2N}) \cdot \nabla v - \nabla U_{2N} \cdot \nabla(\chi v)\, d\mathbf{x}\right| \leq \big(\|\chi' U_{2N}\|_{0,\Omega} + \|\chi' \nabla U_{2N}\|_{0,\Omega}\big)\|v\|_{1,\Omega}.$$

Hence, by Lemma 3.2.3

$$\left|\int_\Omega \big[\epsilon^2 \nabla(\chi U_{2N}) \cdot \nabla v + \chi U_{2N} v\big]\, d\mathbf{x}\right| \leq C\epsilon^{2N}\|v\|_{1,\Omega}. \tag{3.2.8}$$

Finally, since e_{2N} vanishes on $\partial\Omega$,

$$\begin{aligned}\epsilon^2\|e_{2N}\|^2_{1,\Omega} &= \epsilon^2 \int_\Omega |\nabla e_{2N}|^2 + (e_{2N})^2\, d\mathbf{x} \\ &\leq E(2N, e_{2N}) + \int_\Omega \big[\epsilon^2 \nabla(\chi U_{2N}) \cdot \nabla e_{2N} + \chi U_{2N} e_{2N}\big]\, d\mathbf{x} \leq C\epsilon^{2N}\|e_{2N}\|_{1,\Omega},\end{aligned} \tag{3.2.9}$$

from (3.2.7) and (3.2.8). The estimate (3.2.9) is not sharp yet, so we use the triangle inequality:

$$\|e^\epsilon_{2N}\|_{1,\Omega} \leq \|e_{2N+2} - e_{2N}\|_{1,\Omega} + O(\epsilon^{2N+2}),$$

and then the result follows from (3.2.4). □

3.3. Estimates for Non Smooth Domain

We consider now estimates for problem (3.1.1) when the domain Ω is not necessarily smooth, for example, if Ω is polygonal.

We shall need the following interpolation inequality:

$$\|g\|^u_{s+v,\Omega} \leq \|g\|^{u-v}_{s,\Omega}\|g\|^v_{s+u,\Omega}, \quad s \geq 0,\ u \geq v \geq 0. \tag{3.3.1}$$

Furthermore, for $g \in L^2(\Omega)$, let $\Delta^{-1} g$ be the unique function in $H^2(\Omega) \cap \mathring{H}^1(\Omega)$ whose Laplacian is equal to g. Then

$$C^{-1}\|\Delta^{-1} g\|_{s+2,\Omega} \leq \|g\|_{s,\Omega} \leq C\|\Delta^{-1} g\|_{s+2,\Omega}, \quad s \geq 0. \tag{3.3.2}$$

See [**3**] for further details.

From [**2**], we have the following result. We reproduce here the proof, in some detail.

LEMA 3.3.1. Let $f \in H^1(\Omega)$, and u be the solution of (3.1.1). Then there exists a constant that might depend on Ω such that

$$\epsilon^2\|\nabla u\|^2_{0,\Omega} + \|u - f\|^2_{0,\Omega} \leq C\big(\epsilon\|f\|^2_{0,\partial\Omega} + \epsilon^2\|f\|^2_{1,\Omega}\big).$$

PROOF. Multiplying the differential equation by $-\Delta u$, and integrating by parts yields

$$\epsilon^2\|\Delta u\|^2_{0,\Omega} + \|\nabla u\|^2_{0,\Omega} = \int_\Omega \nabla f \cdot \nabla u\, d\mathbf{x} - \int_{\partial\Omega} f \frac{\partial u}{\partial n}\, ds.$$

Note that using the trace inequality, and (3.3.1) with $u = 1$, $v = 1/2$, and $s = 1$, we find that

$$\|\frac{\partial u}{\partial n}\|_{0,\partial\Omega} \leq \|u\|_{3/2,\Omega} \leq \|u\|^{1/2}_{1,\Omega}\|u\|^{1/2}_{2,\Omega}.$$

Hence,

$$\|\frac{\partial u}{\partial n}\|^2_{0,\partial\Omega} \leq C\big(\epsilon^{-1}\|u\|^2_{1,\Omega} + \epsilon\|u\|^2_{2,\Omega}\big).$$

So, for any $\delta_1 > 0$,

$$\left|\int_{\partial\Omega} f\frac{\partial u}{\partial n}\,ds\right| \leq \|f\|_{0,\partial\Omega}\|\frac{\partial u}{\partial n}\|_{0,\partial\Omega} \leq C_{\delta_1}\epsilon^{-1}\|f\|^2_{0,\partial\Omega} + \delta_1\epsilon\|\frac{\partial u}{\partial n}\|^2_{0,\partial\Omega}$$
$$\leq C_{\delta_1}\epsilon^{-1}\|f\|^2_{0,\partial\Omega} + C\delta_1\big(\|u\|^2_{1,\Omega} + \epsilon^2\|u\|^2_{2,\Omega}\big) \leq C_{\delta_1}\epsilon^{-1}\|f\|^2_{0,\partial\Omega} + C\delta_1\big(\|u\|^2_{1,\Omega} + \epsilon^2\|\Delta u\|^2_{0,\Omega}\big),$$

where the norm equivalence (3.3.2) was used in the last inequality above. Similarly, for any $\delta_2 > 0$,

$$\left|\int_\Omega \nabla f\cdot\nabla u\,d\mathbf{x}\right| \leq \|f\|_{1,\Omega}\|u\|_{1,\Omega} \leq C_{\delta_2}\|f\|^2_{1,\Omega} + \delta_2\|u\|^2_{1,\Omega}.$$

It follows from these estimates, and careful choices of δ_1 and δ_2 that

$$\epsilon^2\|\Delta u\|^2_{0,\Omega} + \|\nabla u\|^2_{0,\Omega} \leq C(\epsilon^{-1}\|f\|^2_{0,\partial\Omega} + \|f\|^2_{1,\Omega}).$$

We finally multiply the above inequality by ϵ^2, and use that

$$\epsilon^2\Delta u = u - f$$

to conclude the proof. □

Hence, if $f \in H^1(\Omega)$, the solution u converges to f in $L^2(\Omega)$ as $\epsilon \to 0$.

CHAPTER 4

Finite Element Approximations for Reaction–Diffusion Equation

Apresentamos aqui um método de *elementos finitos multiescala* recentemente proposto para tratar problemas do tipo reação-difusão singularmente perturbados [**27**]. O espaço usual de elementos finitos de funções polinomiais por partes é enriquecido com *funções multiescala*, soluções locais do problema original, como no método *Residual Free Bubble* (RFB), mas não há mais a exigência que estas funções se anulem no bordo de cada elemento, uma mudança em relação ao RFB. Há aqui forte semelhança com enriquecimento via funções bolha como no RFB, mas aqui as funções de enriquecimento não são bolhas. Estas funções multiescala são calculadas analiticamente para triangulos e quadrados. Bubbles are the choice for the test functions allowing static condensation, thus the method is of Petrov–Galerkin type. We perform several numerical validations which confirm the good performance of the method.

O método é derivado formalmente, e a performance do método é ilustrada por testes numéricos. In Section 4.2, we propose a new scheme that performs well for all range as the small parameter of the problem approaches zero.

In Section 3 approximations of the solution for the trial enrichment at the element level are discussed, and next, in Section 4, we perform numerical tests.

4.1. Introduction

Como vimos no caso unidimensional do Capítulo, 2, métodos numéricos podem apresentar sérias limitações para aproximar de forma adequada problemas singularmente perturbados. Considere por exemplo a equação de reação-difusão singularmente perturbada dada por

$$\begin{aligned} \mathcal{L}^\epsilon u &= f \quad \text{in } \Omega, \\ u &= 0 \quad \text{on } \partial\Omega, \end{aligned} \tag{4.1.1}$$

onde

$$\mathcal{L}^\epsilon u = -\epsilon^2 \Delta u + u$$

e Ω is a two-dimensional bounded, Lipschitz domain, ϵ is a positive constant, and $f \in L^2(\Omega)$.

The usual weak formulation of problem (4.1.1) consists on finding $u \in H_0^1(\Omega)$ such that

$$a(u, v) = (f, v), \quad \text{for all } v \text{ in } H_0^1(\Omega), \tag{4.1.2}$$

where the bilinear form $a : H_0^1(\Omega) \times H_0^1(\Omega) \to \mathbb{R}$ is given by

$$a(u, v) = \epsilon(\nabla u, \nabla v) + (u, v). \tag{4.1.3}$$

The weak problem (4.1.2) is well-posed thanks to the coercivity of the bounded bilinear form $a(\cdot, \cdot)$ over $H_0^1(\Omega)$ and the Lax–Milgram Theorem.

In what follows, we consider a partition $\mathcal{T}_h = \{K_j\}$ of Ω into elementos triangulares ou quadrangulares. Some usual restrictions apply:

$$K_i \cap K_j = \emptyset \quad \text{if } i \neq j, \qquad \cup_{k \in \mathcal{T}_h} \bar{K}_j = \bar{\Omega},$$

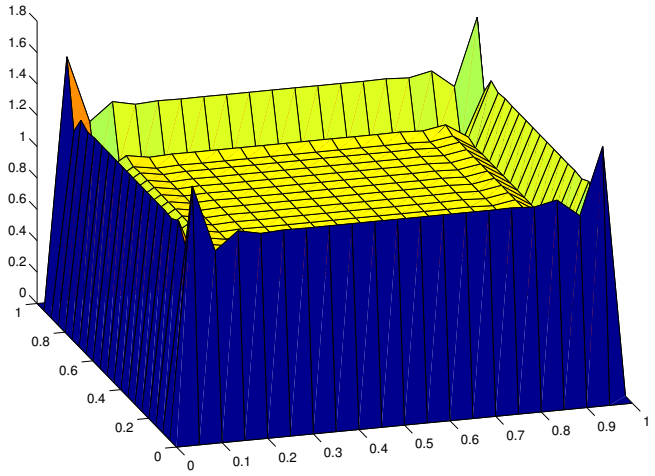

FIGURE 1. Galerkin Solution for $\epsilon^2 = 10^{-6}$

and for $i \neq j$, the intersection $\partial K_i \cap \partial K_j$ is either a common edge or a vertex. We denote by h_K the diameter of $K \in \mathcal{T}_h$, and we set $h = \max_{K \in \mathcal{T}_h}\{h_K\}$. Finally, let $P^1(\Omega)$, be the space of continuous functions in Ω that are bilinear polynomials in each quadrilateral, and define $P_0^1(\Omega) = P^1(\Omega) \cap H_0^1(\Omega)$.

We briefly describe a Galerkin approximation for (4.1.1), and show a numerical result displaying its limitations. Basically, the same phenomena that we described in Section 2.1 occurs. Since the error analysis is also similar, with the same shortcomings, we do not repeat it here.

In the Galerkin formulation, we seek $u^h \in P_0^1(\Omega)$, such that

$$a(u^h, v^h) = (f, v^h) \quad \text{for all } v^h \in P_0^1(\Omega).$$

We include an example to show how the Galerkin method fails to approximate boundary layer, em malhas não refinadas. Consider $\Omega = (0,1) \times (0,1)$, $f = 1$ with $u = 0$ on $\partial\Omega$. The Galerkin approximation for $\epsilon^2 = 10^{-6}$ is depicted in figure 1, e é notável a presença de oscilações espúrias na vizinhança da fronteira.

4.2. Toward Multiscale Functions: Enriching Finite Element Spaces

In this section we describe the work developed in [**27**]. The goal is to find a finite element discretization for (4.1.1) that is stable and coarse mesh accurate for all ϵ. We use the approach of enriching the finite element space. The idea is to add special functions to the usual polynomial spaces to stabilize and improve accuracy of the Galerkin method. This goes along the philosophy of the Residual Free Bubbles (RFB) method [**10**] (see also [**13, 29, 30, 31**]), and actually extends it.

This method is based upon a Petrov–Galerkin formulation, i.e., the space of test functions differs from the trial space. The space of test functions has piecewise polynomials plus bubbles, but trial space is quite different.

Consider

$$U^h = P_0^1(\Omega) \oplus E^*(\Omega),$$

as the trial space, where $E^*(\Omega)$ is yet to be defined. As the test space, we set

$$P_0^1(\Omega) \oplus V^B,$$

onde

$$V^B = \{v \in h_o^1(\Omega) \,:\, v_{|_K} \in H_0^1(K)\}.$$

In our Petrov–Galerkin formulation, we seek $u^h = u^1 + u^* \in U^h$, where $u^1 \in P_0^1(\Omega)$ and $u^* \in E^*(\Omega)$, and

$$a(u^h, v^h) = (f, v^h) \quad \text{for all } v^h \in P_0^1(\Omega), \tag{4.2.1}$$

$$a(u^h, v) = (f, v) \quad \text{for all } v \in H_0^1(K) \text{ and all } K \in \mathcal{T}. \tag{4.2.2}$$

Integrating by parts in (4.2.2), we conclude that for every K,

$$\mathcal{L}^\epsilon\, u^* = f - \mathcal{L}\, u^1 \quad \text{in } K. \tag{4.2.3}$$

The usual residual-free bubble formulation subjects u^* to a homogeneous Dirichlet element boundary condition, i.e., $u^* = 0$ on ∂K, for all elements K. Herein, we replace this condition by a more sophisticated choice, based on ideas by Hou and Wu [**34**].

To determine u^* uniquely, we impose the boundary conditions

$$\mathcal{L}_{\partial K}\, u^* = \mathcal{R}(f - \mathcal{L}\, u^1) \quad \text{on } \partial K, \text{ if } \partial K \not\subset \partial\Omega,$$
$$u^* = 0 \quad \text{on all vertices of } K,$$

where $\mathcal{R}$ is the trace operator, and we choose

$$\mathcal{L}_{\partial K}\, v = -\epsilon^2 \partial_{ss} v + \overline{\sigma} v, \tag{4.2.4}$$

where s denotes a variable that parametrizes ∂K by arc-length. Note that the restriction of f to K must be regular enough so that its trace on ∂K makes sense. Henceforth, we assume that $f \in P^1(\Omega)$.

The choice of (4.2.4) is ad hoc, and by no means unique. But it can be justified under the light of asymptotic analysis. Indeed this is the equation satisfied by the boundary correctors, *in the direction of the boundary layers*, see (3.1.8). Hence, we are enriching the space of polynomials with functions that have the same behavior as the correctors. In some sense, the polynomial part of the approximation (u^1 in our case) "captures" the smooth behavior of the exact solution. The local, "multiscale behavior" is seen by the enrichment functions (u^* in our case), that adds its contribution to the final formulation, without making the method expensive. In other words, it is possible to describe the multiscale characteristics of a solution for a singular perturbed PDE, without having to resolve all the fine scales with a refined mesh.

We can formally write the solution of (4.2.3)–(4.2.4) as

$$u^* = \mathcal{L}_*^{-1}(f - \mathcal{L}_{\mathcal{T}}\, u^1) \in L^2(\Omega), \quad \text{where } \mathcal{L}_{\mathcal{T}} = \sum_{K \in \mathcal{T}} \chi_K\, \mathcal{L}, \tag{4.2.5}$$

and χ_K is the characteristic function of K. We finally set $E^*(\Omega) = \mathcal{L}_*^{-1}\, P^1(\Omega)$.

Substituting (4.2.5) in (4.2.1), we gather that

$$a((I - \mathcal{L}_*^{-1}\, \mathcal{L}_{\mathcal{T}})u^1, v^h) = (f, v^h) - a(\mathcal{L}_*^{-1}\, f, v^h) \quad \text{for all } v^h \in P_0^1(\Omega). \tag{4.2.6}$$

Finally, $u^h = (I - \mathcal{L}_*^{-1}\,\mathcal{L}_{\mathcal{T}})u^1 + \mathcal{L}_*^{-1}\,f$. Note nevertheless that, because of (4.2), $u^h = u^1$ at the nodal points, as in the usual polynomial Galerkin formulation.

OBSERVAÇÃO. Note that our particular choice of test space allowed the *static condensation* procedure, i.e., we were able to write u^* with respect to u^1 and f, as in (4.2.5).

The matrix formulation can be obtained as follows. Under the assumption that $f \in P^1(\Omega)$, we write

$$f = \sum_{j\in J} f_j\psi_j, \quad u^1 = \sum_{j\in J_0} u_j^1\psi_j$$

where J and J_0 are the set of indexes of total and interior nodal points, $\{\psi_j\}_{j\in J}$ form a basis of $P^1(\Omega)$, and $\{\psi_j\}_{j\in J_0}$ form a basis of $P_0^1(\Omega)$. Substituting in (4.2.5), we have that

$$u^* = \sum_{j\in J} f_j\,\mathcal{L}_*^{-1}\,\mathcal{L}_{\mathcal{T}}\,\psi_j - \sum_{j\in J_0} u_j^l\,\mathcal{L}_*^{-1}\,\mathcal{L}_{\mathcal{T}}\,\psi_j, \tag{4.2.7}$$

where we used that

$$\mathcal{L}_{\mathcal{T}}\,\psi_j = \psi_j. \tag{4.2.8}$$

To write the variational formulation in an explicit form, it is convenient to define $\lambda_j = (I - \mathcal{L}_*^{-1}\,\mathcal{L}_{\mathcal{T}})\psi_j$. Hence, (4.2.6) reads as

$$\sum_{j\in J_0} a(\lambda_j,\psi_i)u_j^1 = \sum_{j\in J}\big[(\psi_j,\psi_i) - a(\mathcal{L}_*^{-1}\,\psi_j,\psi_i)\big]f_j \quad \text{for all } i\in J_0. \tag{4.2.9}$$

Using the definition of the bilinear form $a(\cdot,\cdot)$, and (4.2.8), yields

$$\sum_{j\in J_0} a(\lambda_j,\psi_i)u_j^1 = \sum_{j\in J}\big[(\lambda_j,\psi_i) - \epsilon^2(\nabla\,\psi_j,\nabla\,\psi_i) + \epsilon^2(\nabla\,\lambda_j,\nabla\,\psi_i)\big]f_j \quad \text{for all } i\in J_0. \tag{4.2.10}$$

Concrete computations of the matrix formulation follows.

4.3. Solving Local Problems

A core and troublesome issue in the present method is solving the local problems. From its definition, λ_j solves

$$\begin{gathered}\mathcal{L}\,\lambda_j = 0 \quad \text{in } K,\\ \mathcal{L}_{\partial K}\,\lambda_j = 0 \quad \text{on } \partial K, \qquad \lambda_j = \begin{cases}1 & \text{on the jth vertice of } \mathcal{T},\\ 0 & \text{on the other vertices of } \mathcal{T},\end{cases}\end{gathered} \tag{4.3.1}$$

OBSERVAÇÃO. In fact, we have that $\mathcal{L}_{\partial K}\,\lambda_j = \mathcal{L}_{\partial K}\,\psi_j - \mathcal{L}\,\psi_j$ on ∂K. Since we are assuming that ψ_j is bilinear over a rectangular mesh, we have that ψ_j is still linear *over* ∂K. Hence, $\mathcal{L}_{\partial K}\,\psi_j = \psi_j$.

If we take a particular node $I \in J_0$, and look at all elements connected to this node, then the equation (4.3.1) can be used to illustrate the nodal shape functions λ_I. We obtain for $\epsilon = 1,\ 10^{-1},\ 10^{-3}$, the shape functions λ_I, depicted in figures 2 and 3. Note that as ϵ approaches zero, the usual pyramid is squeezed in its domain of influence in the neighborhood around the node I. The functions plotted below were computed using the formulas described in subsection 4.3.1.

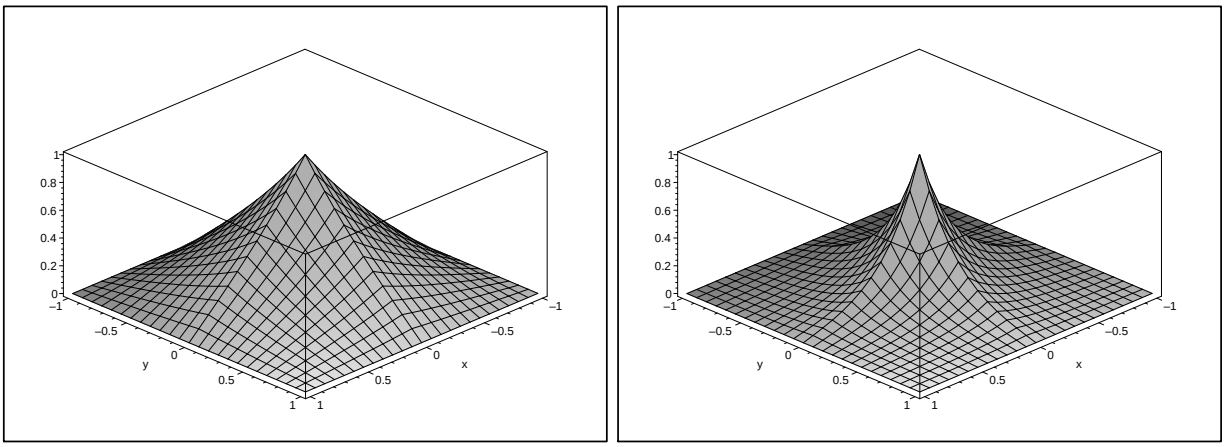

FIGURE 2. The function λ for $\epsilon = 1,\ 10^{-1}$

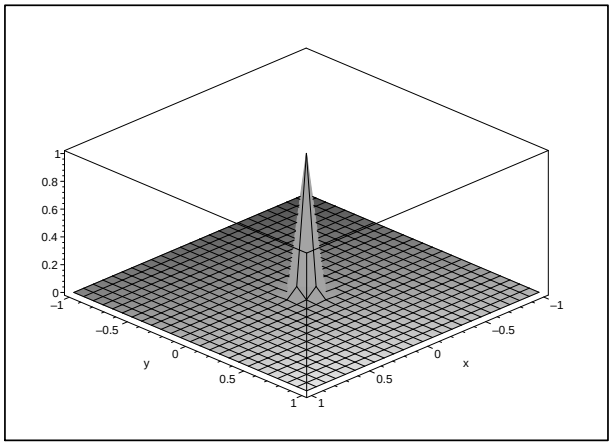

FIGURE 3. The function λ for 10^{-3}

Actually, the functions used to enrich the finite element space, i.e., the functions in $E^*(\Omega)$ are as in Figures 4 and 5.

4.3.1. Rectangles. Consider now a rectangular straight mesh. Our goal is to find λ_j. Without loss of generality, consider a rectangle K with vertices $1, \cdots, 4$ at $(0,0)$, $(h_x, 0)$, (h_x, h_y), and $(0, h_y)$. So, again without loss of generalization, we want to find λ_1. We have that

$$-\epsilon^2 \Delta \lambda_1 + \lambda_1 = 0 \quad \text{in } K. \tag{4.3.2}$$

On the side $y = 0$, we have that

$$-\epsilon^2 \partial_{xx} \lambda_1 + \lambda_1 = 0 \quad \text{for } x \text{ in } (0,1),$$
$$\lambda_1(0,0) = 1, \quad \lambda_1(h_x, 0) = 0.$$

Hence,

$$\lambda_1(x,0) = \mu_x(x) := -\frac{\sinh\big(\epsilon^{-1}(x - h_x)\big)}{\sinh\big(\epsilon^{-1} h_x\big)}. \tag{4.3.3}$$

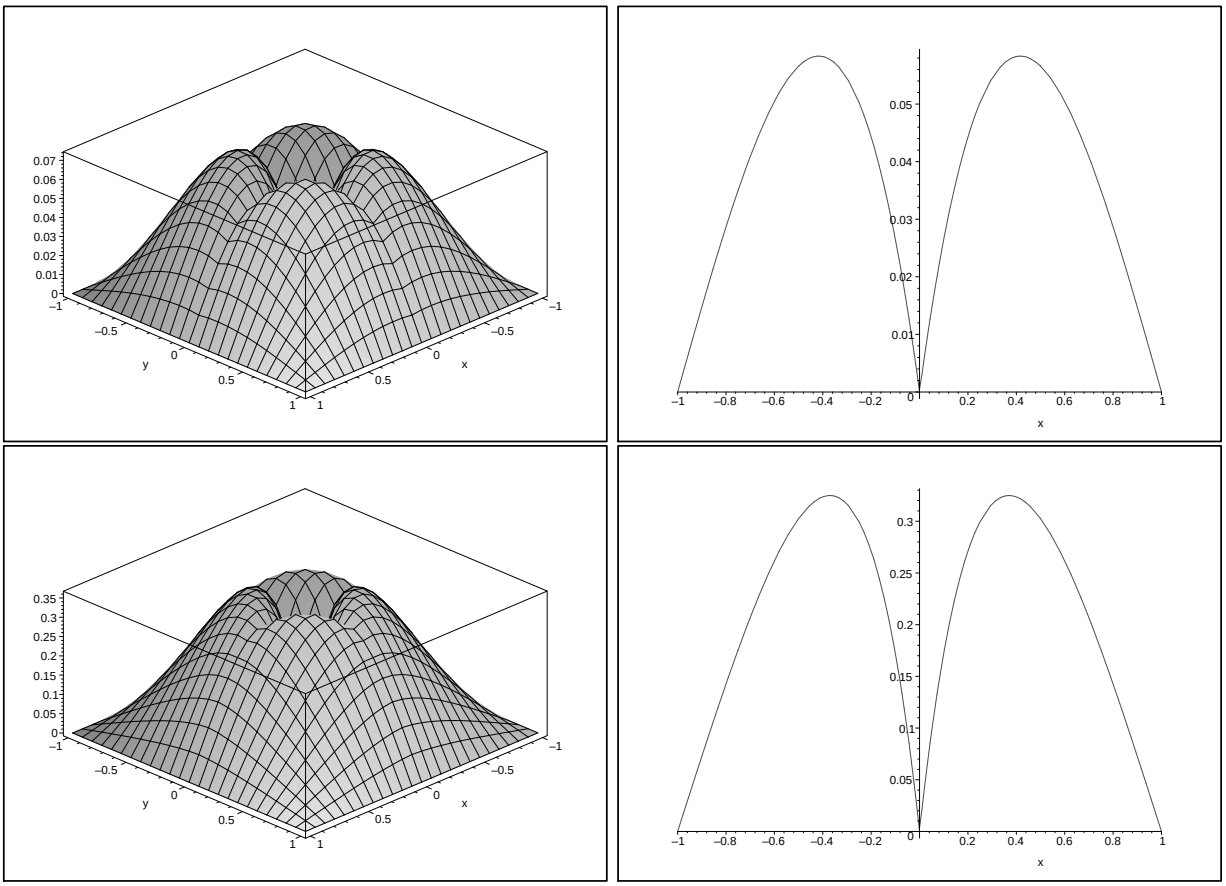

FIGURE 4. Enriching functions for $\epsilon = 1$ and $\epsilon^2 = 0.1$.

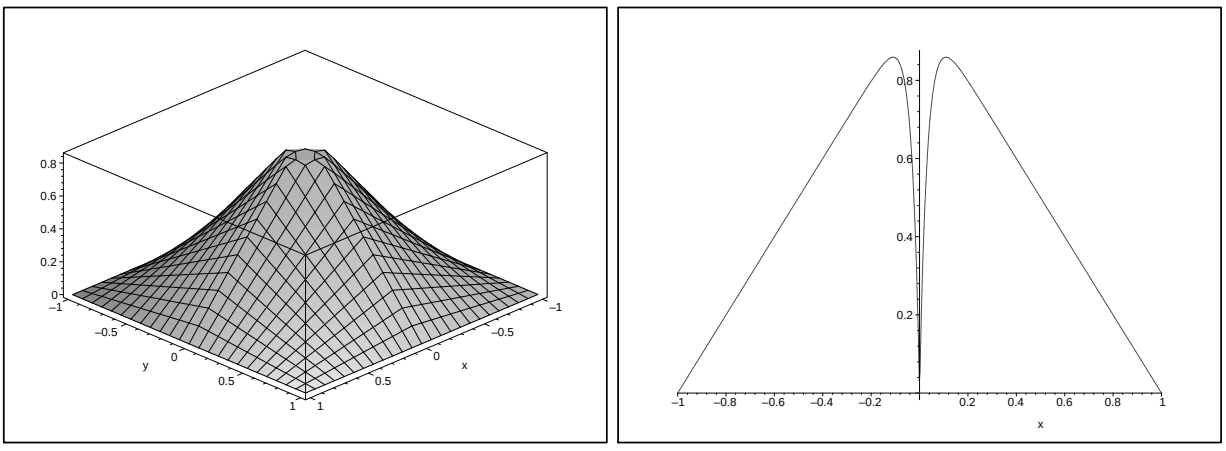

FIGURE 5. Enriching functions for $\epsilon^2 = 10^{-3}$.

Similarly,

$$\lambda_1(0,y) = \mu_y(y) := -\frac{\sinh\bigl(\epsilon^{-1}(y-h_y)\bigr)}{\sinh\bigl(\epsilon^{-1}h_y\bigr)}, \qquad \lambda_1(h_x,y) = \lambda_1(x,h_y) = 0. \tag{4.3.4}$$

We propose two simple closed forms for λ_1, none of which satisfy (4.3.2)–(4.3.4) exactly. If we set $\lambda_1(x,y) = \mu_x(x)\mu_y(y)$, then (4.3.3)–(4.3.4) holds, but

$$-\epsilon^2\,\Delta\,\lambda_1 + 2\lambda_1 = 0 \quad \text{in } K,$$

thus (4.3.2) is *not* satisfied.

If we let

$$\lambda_1(x,y) = \frac{\sinh\big(\epsilon^{-1}\sqrt{\tfrac{1}{2}}(x-h_x)\big)\sinh\big(\epsilon^{-1}\sqrt{\tfrac{1}{2}}(y-h_y)\big)}{\sinh\big(\epsilon^{-1}\sqrt{\tfrac{1}{2}}h_x\big)\sinh\big(\epsilon^{-1}\sqrt{\tfrac{1}{2}}h_y\big)},$$

then (4.3.2) holds, but the boundary conditions at the edges $x = 0$ and $y = 0$ do not hold.

4.3.2. Triangles. Consider now a triangular mesh. Let K be an element of the triangulation $\mathcal{T}_h$, and Z an edge of its boundary ∂K. We explicit the dependence of coefficients $\overline{\sigma}$ in terms of the shape of elements K by setting

$$\overline{\sigma} = \frac{1}{(\gamma_K^i|Z|)^2} \quad \text{for all } i \in I, \tag{4.3.5}$$

where the positive constant γ_K^i is defined by

$$\gamma_K^i = \sqrt{\left(\frac{\partial\psi_i}{\partial x}|_K\right)^2 + \left(\frac{\partial\psi_i}{\partial y}|_K\right)^2} \quad \text{for all } i \in I. \tag{4.3.6}$$

Observaçãо. We can identify the constant introduce in (4.3.6) in terms of the shape of K by $2\gamma_K^i = |\overline{Z}|/|K|$, where $\overline{Z}$ denotes the corresponding edge of K opposed to the node i. We note that γ_K^i is of order h_K^{-1} for all $i \in I$ and $K \in \mathcal{T}_h$.

Thanks to (4.3.5) and (4.3.6) we are able to compute the analytical solution of (4.3.1). Indeed, it is straightforward to check that

$$\lambda_i(x,y) = \frac{\sinh\left(\frac{1}{\epsilon\gamma_K^i}\psi_i(x,y)\right)}{\sinh\left(\frac{1}{\epsilon\gamma_K^i}\right)} \quad \text{for all } i \in I, \tag{4.3.7}$$

satisfies the boundary value problem (4.3.1).

Observaçãо. The enriched basis functions (4.3.7) are discontinuous across element edges since γ_K^i varies *a priori* in each $K \in \mathcal{T}_h$. Therefore, the method is nonconforming in general, but we can recover the continuity and the conformity in the case of the value of γ_K^i is the same for all $K \in \mathcal{T}_h$.

4.4. Outros Comentários

Previous works, as [**24**], tried to find more stable and accurate formulations based on stabilized methods, which are based on piecewise polynomials employed on modified variational formulations. These modifications are additional perturbation terms involving stability parameters and are functions of residuals of the governing differential equation.

Partial justification of these ideas were made possible by relating them to the Galerkin method using piecewise polynomials enriched with "bubble" functions [**8, 11, 12**]. For

the sake of simplicity, consider at this point bubble functions as continuous within each element and with zero value on the elements boundaries. The relation between these enriched Galerkin methods to stabilized ones is based on eliminating the bubble functions at the element level (a.k.a. static condensation), made possible due to the assumption of the zero value on the element boundary. This produces a stabilized-like formulation, in which the stability parameter is given by the shape of the bubble function, i.e., there is no *ad hoc* procedure to establish these parameters, other than selecting bubble functions.

To systematically treat various singularly perturbed problems, residual-free bubbles were introduced in [**14, 25, 28, 29, 30, 31**]. These bubbles are produced by solving, exactly or not, differential equations at the element level, involving the differential operator of the problem. The right hand sides of these local problems are the residuals due to the polynomial part of the solution. The other ingredient is the requirement that the bubble part vanishes on element boundaries for second order problems.

It turns out that this construction for the reaction diffusion problem yields a poor approximation. Assuming the bubble part of the trial solution to be zero introduces inaccuracies across element edges. We wish to explore a possible avenue that builds on former ideas, without the zero boundary value restriction on elements, as follows:

(1) We let the test space to be enriched with residual-free bubble functions;
(2) We let the trial space to be derived from the previous construction with boundary values determined by local restriction of the governing differential operator.

Therefore we start out with a Petrov-Galerkin setting.

We keep the restriction of zero value on element boundary for the test space bubble functions, so that we can still use the static condensation argument. In this manner we are allowed to integrate by parts and get a differential equation for the trial enrichment, as before. Even more importantly, we keep the modification computable at the element level.

Now, we are in principle free to set the boundary condition for the trial enrichment. Towards this end, we use the restriction of the differential operator on the element edges and get ordinary differential equations that can be solved *a priori*. A related idea was proposed by Hou and Wu [**34, 35**] for some multiscale examples. A numerical analysis for the present method is performed in [**26**].

4.5. Numerical Results

4.5.1. A Numerical Test: Source Problem. As in the beginning of this chapter, consider the unit source problem ($f = 1$) defined on the unit square $\Omega = (0,1) \times (0,1)$, subject to a homogeneous Dirichlet boundary condition. For small ϵ, boundary layers appear close to the domain boundary. Figure 6 shows, for $\epsilon^2 = 10^{-6}$, the solutions of three different methods, Galerkin, Residual Free Bubble, and the present enriched method. It is clear that the current method performs better than the other two methods. Examining the solutions profiles, see Figure 7, it becomes clear that the current method is superior to other methods. For $\epsilon^2 = 10^{-3}$ and $\epsilon = 1$, all methods have comparable performance, see Figures 8, 9 .

4.5.2. Boundary layer problem using refined mesh. Here we consider a rectangular domain with nontrivial boundary conditions, as depicted in Figure 10. We assume that $f = 0$, and the domain is discretized using a refined mesh in part of the domain. Again for this problem we have the onset of boundary layers that causes spurious oscillations in the

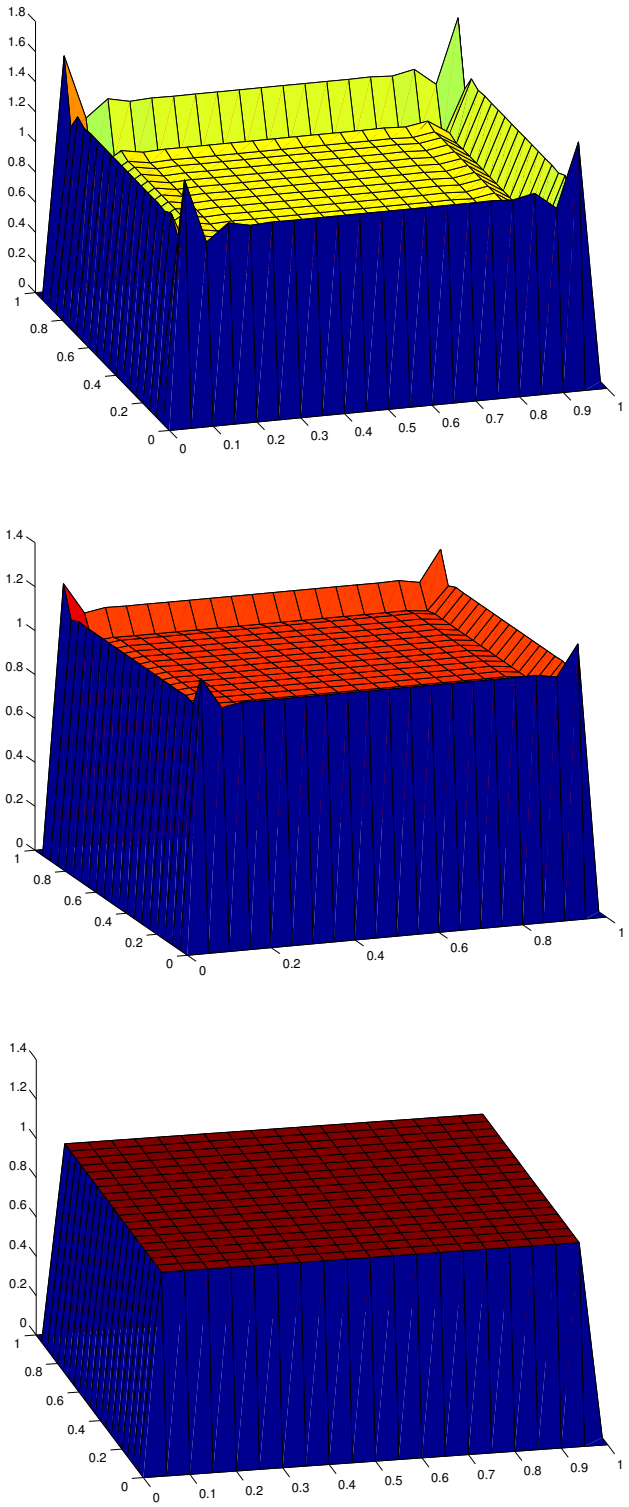

FIGURE 6. Comparison among Galerkin, Residual Free Bubble, and the enriched methos for $\epsilon^2 = 10^{-6}$.

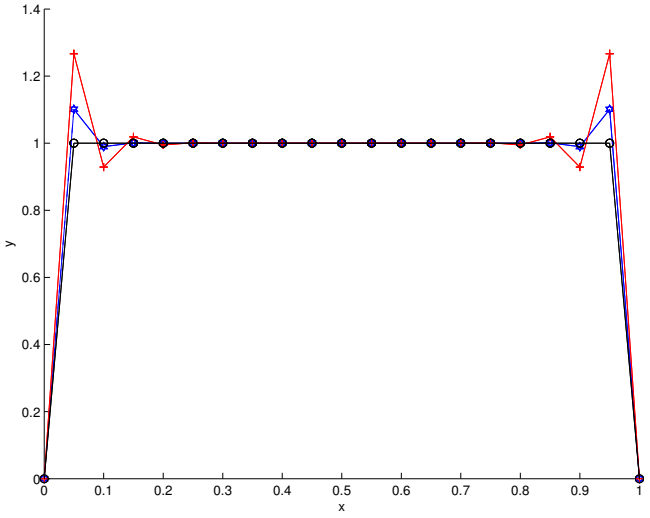

FIGURE 7. Profile of solutions at $x = 0.5$ ($\epsilon^2 = 10^{-6}$).

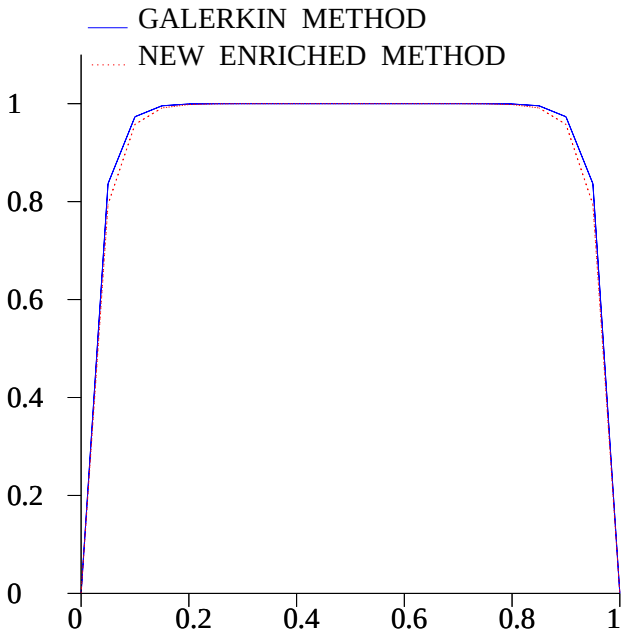

FIGURE 8. Profile of solutions at $x = 0.5$ ($\epsilon^2 = 10^{-3}$).

numerical solutions. We computed the solution with different methods for $\epsilon = 10^{-6}$. Figures 11, 12, 13 show the good performance of the current method, while all other methods suffer from spurious oscillations. Finally, Figure 14 illustrate that for large ϵ, we recover the usual Galerkin method.

4.5.3. NACA problem. Here we illustrate the good performance of the present method even for unstructured meshes. We consider the domain Ω and its discretization as depicted

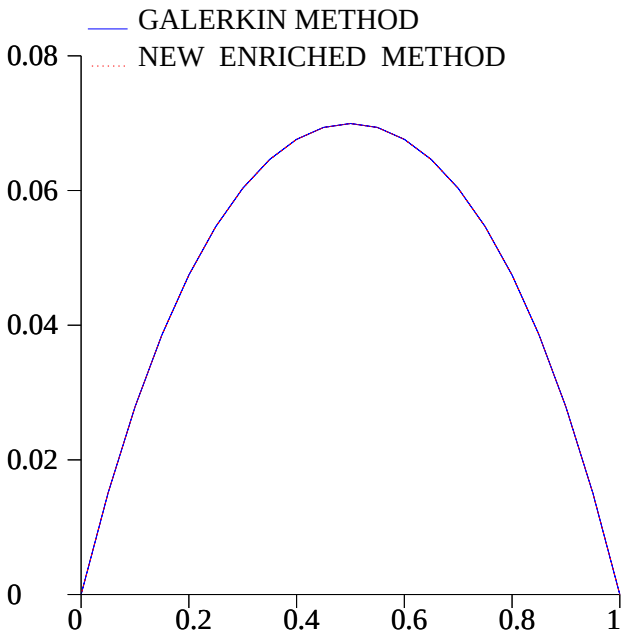

FIGURE 9. Profile of solutions at $x = 0.5$ ($\epsilon^2 = 10^{-3}$).

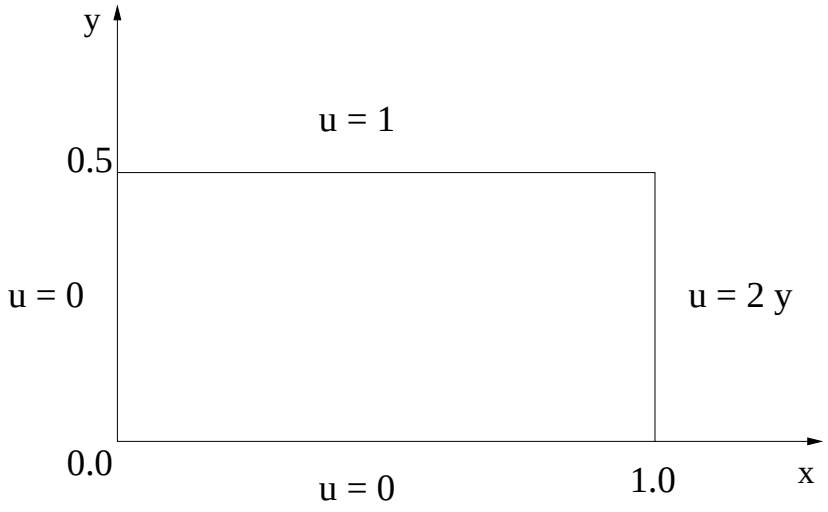

FIGURE 10. Problem statement.

in Figure 15. We assume $f = 0$ and homogeneous boundary Dirichlet conditions at the outer boundary. On the inner boundary we impose $u = 1$. In figure 16 we show that for moderate ϵ, both Galerkin and the present method perform well. As expected, for small ϵ, the Galerkin method presents spurious oscillations. It is remarkable here that even the unusual method is oscillatory, as shown in Figures 16, 18. As we show in Figure 17, the present method captures the boundary layer without any oscillatory behavior.

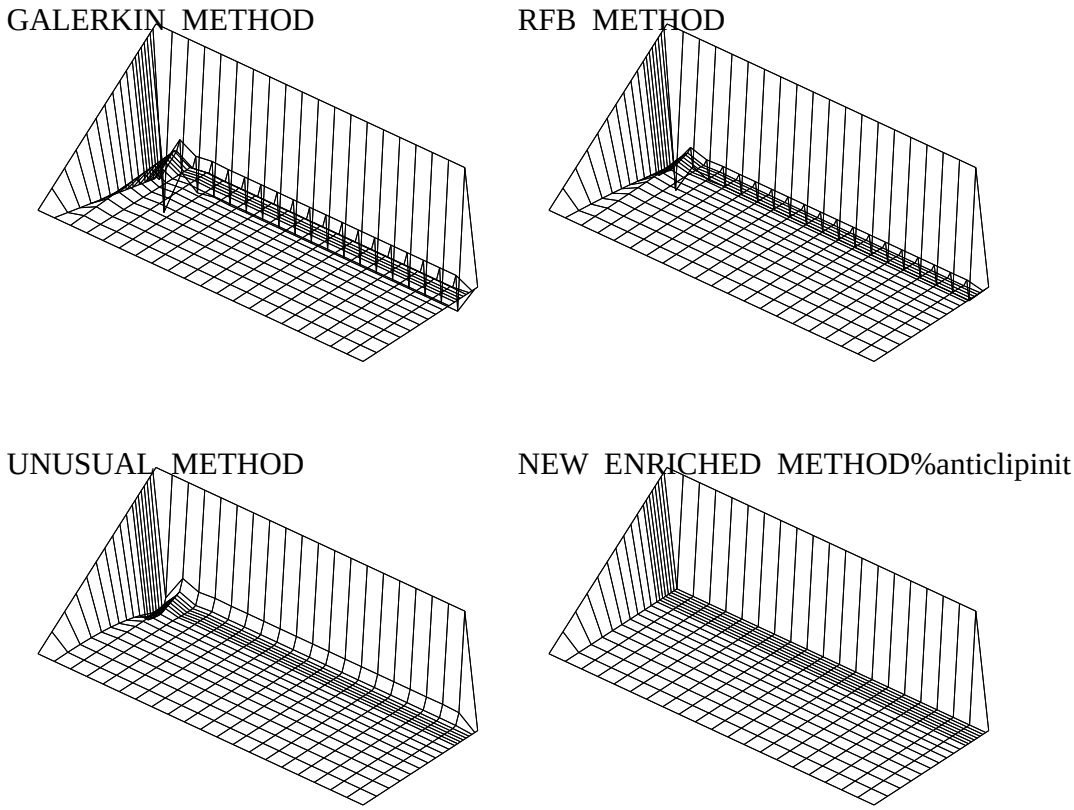

FIGURE 11. Comparison between solutions obtained by different methods ($\epsilon = 10^{-6}$).

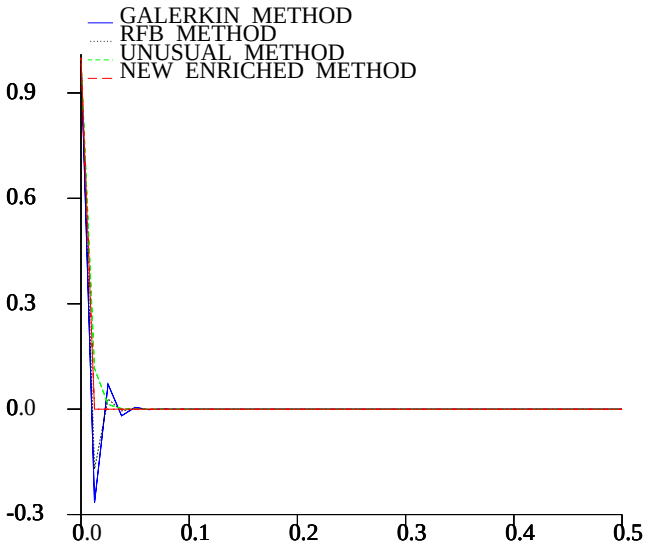

FIGURE 12. Profile of solutions at $x = 0.5$ ($\epsilon = 10^{-6}$).

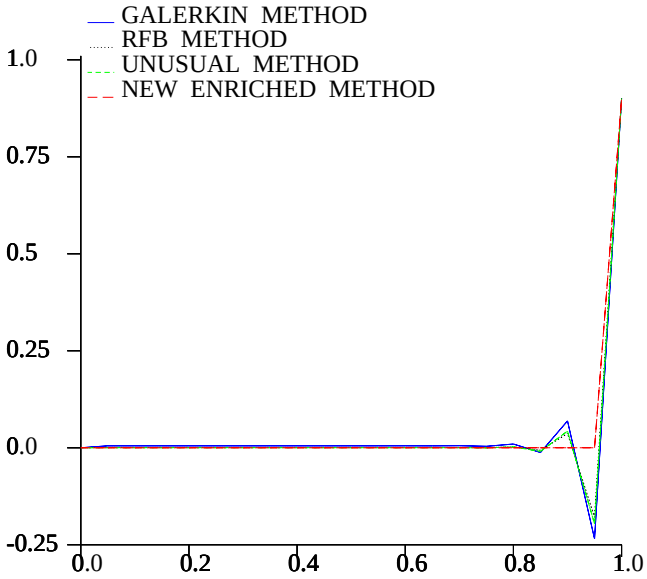

FIGURE 13. Profile of solutions at $y = 0.05$ ($\epsilon = 10^{-6}$).

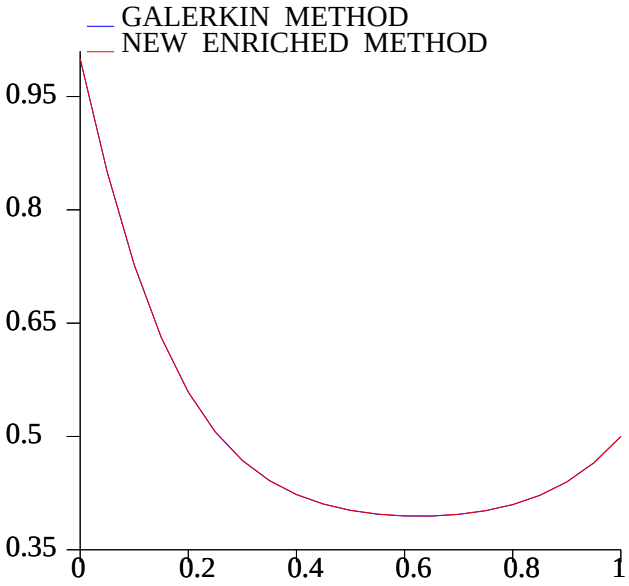

FIGURE 14. Profile of solutions at $y = 0.5$ ($\epsilon = 1$).

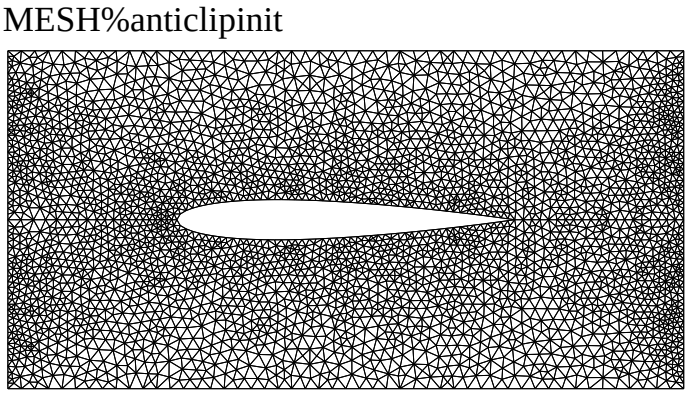

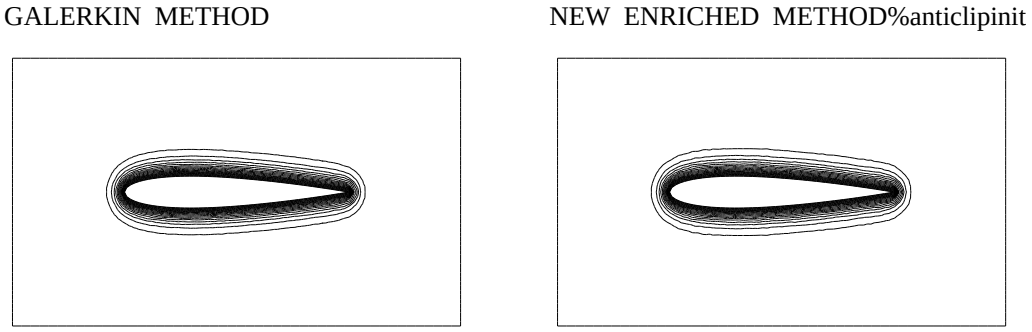

FIGURE 15. Isovalues of the solutions by Galerkin Method and by enriched method. Here $\epsilon = 10^{-2}$.

GALERKIN METHOD%anticlipinit

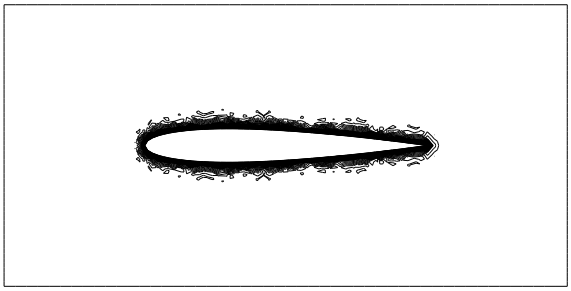

UNUSUAL METHOD%anticlipinit

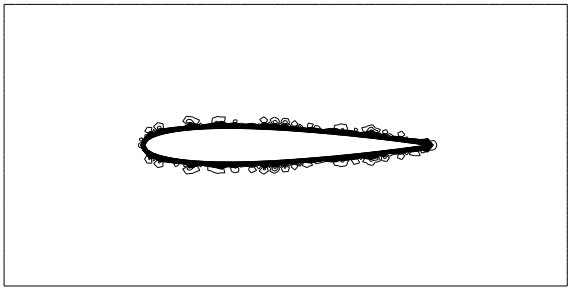

NEW ENRICHED METHOD%anticlipinit

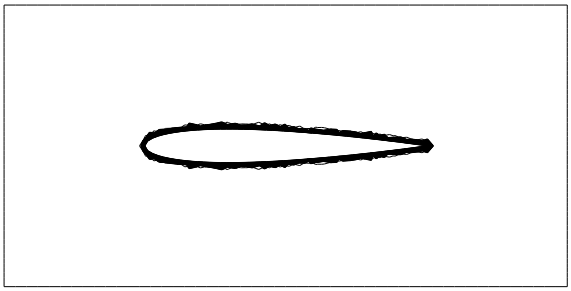

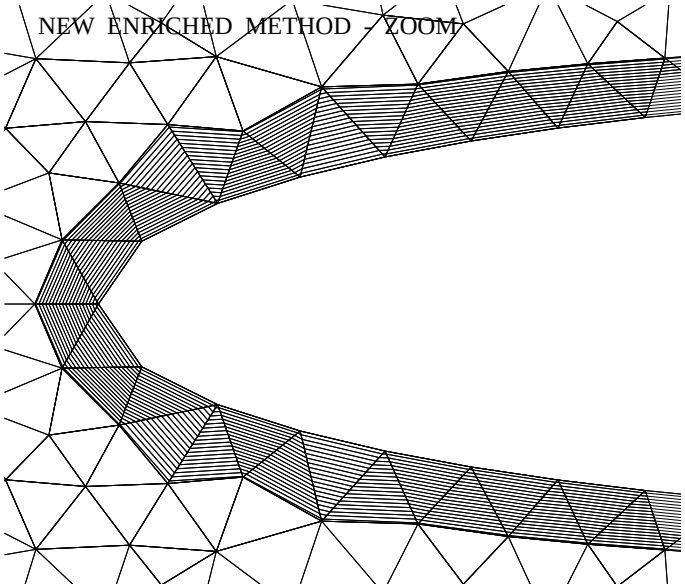

FIGURE 17. The new method captures the boundary layer accurately. Zoom of isovalues ($\epsilon = 10^{-6}$).

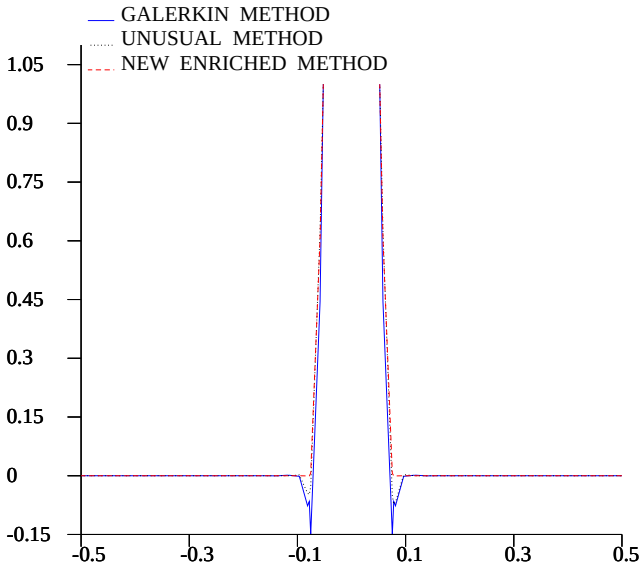

FIGURE 18. Profile of solutions at $x = 0.5$ ($\epsilon = 10^{-6}$).

CHAPTER 5

Modeling PDEs in domains with Rough Boundaries

We are interested in PDEs defined in domains where at least part of the boundary is rugous. The goal is to avoid the expensive discretization of the rough domain, and replace the original PDE by another, in a domain that is easier to discretize. Asymptotic Expansions play a key role here, motivating the development of models, and helping in deriving error estimates.

5.1. Asymptotic Expansion Definition

Let $\Omega^\epsilon \subset \mathbb{R}^2$ be the domain depicted in figure 1. It is basically a square with sides of length one, where the bottom is rugged.

The bottom of Ω^ϵ, containing the wrinkles, is described by $\boldsymbol{\psi}^\epsilon(x_1) = (x_1, \epsilon\psi_r(\epsilon^{-1}x_1))$, where $x_1 \in [0,1]$. The function $\psi_r : \mathbb{R} \to \mathbb{R}$ is independent of ϵ, Lipschitz-continuous with $\psi_r(0) = 0$, and periodic of period 1. Without loss of generality, we can assume $\|\psi_r\|_{L^\infty(\mathbb{R})} = 1$.

We now consider the problem

$$\begin{aligned} -\Delta u^\epsilon &= f \quad \text{in } \Omega^\epsilon, \\ u^\epsilon &= 0 \quad \text{on } \partial\Omega^\epsilon. \end{aligned} \tag{5.1.1}$$

It is clear that the solution $u\epsilon$ depends in a nontrivial way on the small parameter ϵ. It is our goal to make clear how is this dependence, and how this can be used to develop models for (5.1.1). We shall search for a formal asymptotic expansion in the general form,

$$u^\epsilon \sim u^0 + \epsilon v^1(\epsilon) + \epsilon\Psi^1(\epsilon) + \epsilon^2 v^2(\epsilon) + \epsilon^2\Psi^2(\epsilon) + \cdots, \tag{5.1.2}$$

where the $\Psi^i(\epsilon)$ are boundary correctors. The terms $v^i(\epsilon)$, and $\Psi^i(\epsilon)$ depend on ϵ, as the notation indicates. Although this appears strange at first sight, it actually renders the

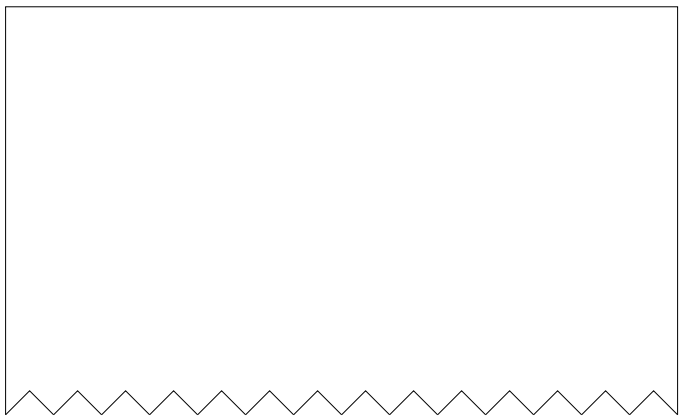

FIGURE 1. Description of the domain Ω^ϵ.

development of the expansion easier. At a second stage, it is possible to reorder (5.1.2) as a formal power series where all the terms are independent of ϵ.

Our procedure to find out the terms in the expansion has a "domain decomposition flavor", and uses the following result.

LEMA 5.1.1. Let Ω be a Lipschitz bounded domain of $\mathbb{R}^2$ and Γ an interface that divide Ω into two sub-domains Ω^- and Ω^+. Assume that e satisfies $e = 0$ on $\partial\Omega^-\backslash\Gamma \cup \partial\Omega^+\backslash\Gamma$. Then there exists a constant c such that

$$\|e\|_{H^1(\Omega^-)} + \|e\|_{H^1(\Omega^+)} \leq c\big(\|\Delta e\|_{0,\Omega^-} + \|\Delta e\|_{0,\Omega^+} + \|[e]\|_{\frac{1}{2},\Gamma} + \|[\partial e/\partial n]\|_{-\frac{1}{2},\Gamma}\big) \tag{5.1.3}$$

where $[\cdot]$ represent the jump function over Γ. The constant c is independent of Ω^-.

PROOF. We first define

$$e^- = e|_{\Omega^-}\,, \qquad e^+ = e|_{\Omega^+}\,.$$

It follows from Green's identity that

$$\int_{\Omega^-} |\nabla e^-|^2\, d\mathbf{x} = -\int_{\Omega^-} e^-\,\Delta e^-\, d\mathbf{x} - \int_\Gamma e^- \frac{\partial e^-}{\partial n^+}\, d\Gamma,$$
$$\int_{\Omega^+} |\nabla e^+|^2\, d\mathbf{x} = -\int_{\Omega^+} e^+\,\Delta e^+\, d\mathbf{x} + \int_\Gamma e^+ \frac{\partial e^+}{\partial n^+}\, d\Gamma,$$

where n^+ indicates the outward normal vector with respect to Ω^+. Combining both identities, and adding and subtracting $\int_\Gamma e^-\partial e^+/\partial n^+\, d\Gamma$, we gather that

$$\begin{aligned}
&|e^-|^2_{H^1(\Omega^-)} + |e^+|^2_{H^1(\Omega^+)} \\
&= -\int_{\Omega^-} e^-\,\Delta e^-\, d\mathbf{x} - \int_{\Omega^-} e^+\,\Delta e^+\, d\mathbf{x} + \int_\Gamma e^-\left(\frac{\partial e^+}{\partial n^+} - \frac{\partial e^-}{\partial n^+}\right) d\Gamma + \int_\Gamma (e^+ - e^-)\frac{\partial e^+}{\partial n^+}\, d\Gamma \\
&\leq \|e^-\|_{L^2(\Omega^-)}\|\Delta e^-\|_{L^2(\Omega^-)} + \|e^+\|_{L^2(\Omega^+)}\|\Delta e^+\|_{L^2(\Omega^+)} \\
&\quad + \|e^-\|_{H^{1/2}(\Gamma)}\|[\frac{\partial e}{\partial n}]\|_{H^{-1/2}(\Gamma)} + \|[e]\|_{H^{1/2}(\Gamma)}\|\frac{\partial e}{\partial n}^+\|_{H^{-1/2}(\Gamma)} \\
&\leq (\|\Delta e^-\|_{L^2(\Omega^-)} + \|\Delta e^+\|_{L^2(\Omega^+)})\|e\|_{L^2(\Omega)} \\
&\quad + \|e^-\|_{H^1(\Omega^-)}\|[\frac{\partial e}{\partial n}]\|_{H^{-1/2}(\Gamma)} + \|[e]\|_{H^{1/2}(\Gamma)}\|e^+\|_{H^1(\Omega^+)}.
\end{aligned}$$

To obtain the inequalities above, we used Cauchy–Schwartz and trace inequalities, and the duality between $H^{-1/2}(\Gamma)$ and $H^{1/2}(\Gamma)$. The lemma follows now from an application of the Poincaré inequality. □

We define now sub-domains of Ω^ϵ, one "close" to the rugosity, the other one far from it. See figure 2. Let $\delta = c_0\epsilon$, where $c_0 > 1$. Let

$$\Omega_s = \{\,\mathbf{x} = (x_1, x_2) \in \Omega^\epsilon : x_2 > \delta\,\}, \quad \Omega_r^\epsilon = \{\,\mathbf{x} = (x_1, x_2) \in \Omega^\epsilon : x_2 < \delta\,\},$$
$$\Gamma = \{\,\mathbf{x} = (x_1, x_2) \in \Omega^\epsilon : x_2 = \delta\,\}.$$

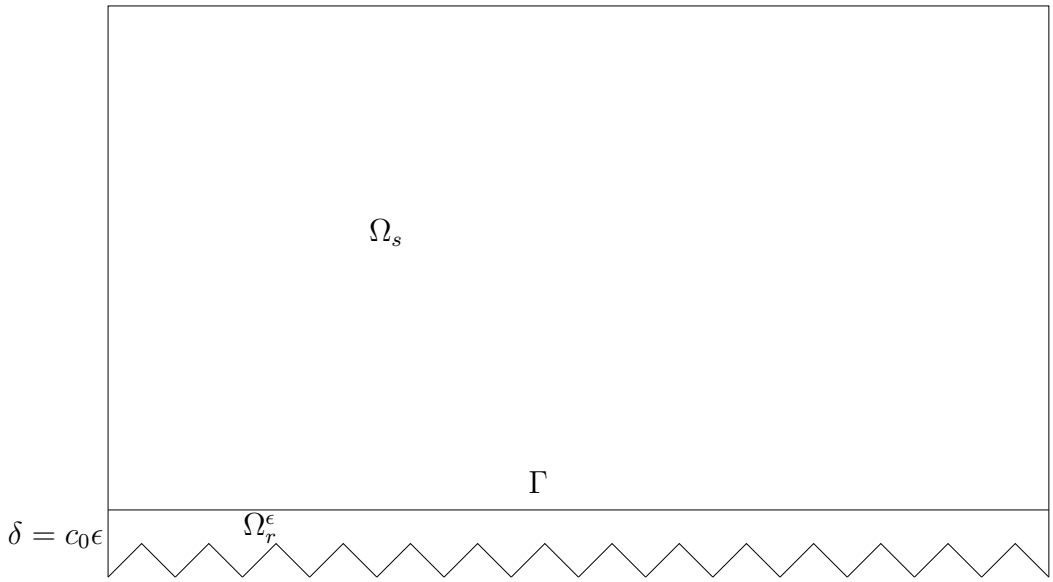

FIGURE 2. Domain decomposition

It is natural to define the first term of the asymptotics such that

$$\begin{aligned} -\Delta u^0 &= f \quad \text{in } \Omega_s, \\ u^0 = 0 \quad \text{on } \partial\Omega_s, &\qquad u^0 = 0 \quad \text{on } \Omega_r^\epsilon. \end{aligned} \tag{5.1.4}$$

Applying Lemma 5.1.1 with $e = u^\epsilon - u^0$, we see that the source of error is the x_2-derivative jump $[\partial_{x_2} u^0]$:

$$\|e\|_{H^1(\Omega_r^\epsilon)} + \|e\|_{H^1(\Omega_s)} \leq c\|\partial_{x_2} u^0\|_{H^{-1/2}(\Gamma)}.$$

We next remedy this. Let $\phi^0(x_1) = \partial_{x_2} u^0(x_1, \delta)$, i.e., ϕ^0 is the restriction of $\partial_{x_2} u^0$ on Γ, and χ_r^ϵ be the characteristic function of the set Ω_r^ϵ, i.e.,

$$\chi_r^\epsilon(\mathbf{x}) = \begin{cases} 1 & \text{if } \mathbf{x} \in \Omega_r^\epsilon, \\ 0 & \text{otherwise.} \end{cases}$$

We add then the function $-\chi_r^\epsilon(\mathbf{x}) x_2 \phi^0(x_1)$ to the asymptotic expansion, to correct the jump of the x_2-derivative. Since the zero Dirichlet boundary condition at Γ_r^ϵ is not satisfied, we add a corrector to the asymptotics: $\Psi^1(\epsilon) - \chi_r^\epsilon Z^1(\epsilon)$. The boundary corrector $\Psi^1(\epsilon)$ is such that

$$-\Delta \Psi^1(\epsilon) = -\chi_r^\epsilon \Delta(\epsilon^{-1} x_2 \phi^0 + Z^1(\epsilon)) \quad \text{in } \Omega^\epsilon, \tag{5.1.5}$$

$$\Psi^1(\epsilon) = \epsilon^{-1} x_2 \phi^0 + Z^1(\epsilon) \quad \text{on } \Gamma_r^\epsilon. \tag{5.1.6}$$

The introduction of $Z^1(\epsilon)$ is necessary to guarantee an exponential decay of $\Psi^1(\epsilon)$ to zero in the x_2-direction. Both $\Psi^1(\epsilon)$ and $Z^1(\epsilon)$ depend on ϵ, and the are not even well-defined yet.

In fact, we shall set, in general, $\Psi^i(\epsilon)$ and $Z^i(\epsilon)$ as formal expansions in ϵ,

(5.1.7)
$$\Psi^i(\epsilon)(\mathbf{x}) \sim \psi^0(\epsilon^{-1}\mathbf{x})\phi^{i-1}(x_1) + \epsilon\psi^1(\epsilon^{-1}\mathbf{x})\partial_{x_1}\phi^{i-1}(x_1) + \epsilon^2\psi^2(\epsilon^{-1}\mathbf{x})\partial_{x_1x_1}\phi^{i-1}(x_1) + \cdots,$$

(5.1.8)
$$Z^i(\epsilon)(\mathbf{x}) \sim z^0\phi^{i-1}(x_1) + \epsilon z^1\partial_{x_1}\phi^{i-1}(x_1) + \epsilon^2 z^2\partial_{x_1x_1}\phi^{i-1}(x_1) + \cdots.$$

In the above, ψ^i is periodic with period ϵ^{-1} in the x_1 direction, and z^i are ϵ-independent constants that depend on the geometry of the wrinkles only. We postpone the precise definition of the terms for now.

So, with the error function $e = u^\epsilon - \big[u^0 - \chi_r^\epsilon x_2\phi^0 - \epsilon\chi_r^\epsilon Z^1(\epsilon) + \epsilon\Psi^1(\epsilon)\big]$, we have

$$\|e\|_{1,\Omega_r^\epsilon} + \|e\|_{1,\Omega_s} \le \epsilon\|Z^1(\epsilon) + c_0\phi^0\|_{\frac12,\Gamma}.$$

We continue to define the terms of the expansion. Set

(5.1.9)
$$\begin{gathered} -\Delta u^1 = 0 \quad \text{in } \Omega_s, \\ u^1 = -(c_0+z^0)\phi^0 \quad \text{on } \Gamma, \qquad u^1 = 0 \quad \text{on } \partial\Omega_s\backslash\Gamma, \qquad u^1 = 0 \quad \text{on } \Omega_r^\epsilon. \end{gathered}$$

So, if $e = u^\epsilon - \big[u^0 - x_2\chi_r^\epsilon\phi^0 - \epsilon Z^1(\epsilon)\chi_r^\epsilon + \epsilon\Psi^1(\epsilon) + \epsilon u^1\big]$, then

$$\|e\|_{1,\Omega_r^\epsilon} + \|e\|_{1,\Omega_s} \le \epsilon\|\partial_{x_2}u^1\|_{-\frac12,\Gamma} + \epsilon^2\|z^1\partial_{x_1}\phi^0 + \epsilon z^2\partial_{x_1x_1}\phi^0 + \cdots\|_{\frac12,\Gamma}.$$

We define $\phi^1 = \partial_{x_2}u^1|_\Gamma$, and add $-\epsilon\chi_r^\epsilon x_2\phi^1 + \epsilon^2\Psi^2(\epsilon) - \epsilon^2\chi_r^\epsilon Z^2(\epsilon)$ to the expansion, where

$$\begin{gathered} -\Delta\,\Psi^2(\epsilon) = -\chi_r^\epsilon\,\Delta(\epsilon^{-1}x_2\phi^1 + Z^2(\epsilon)) \quad \text{in } \Omega^\epsilon, \\ \Psi^2(\epsilon) = \epsilon^{-1}x_2\phi^1 + Z^2(\epsilon) \quad \text{on } \Gamma_r^\epsilon. \end{gathered}$$

So far,

$$e = u^\epsilon - \big[u^0 - x_2\chi_r^\epsilon\phi^0 - \epsilon Z^1(\epsilon)\chi_r^\epsilon + \epsilon\Psi^1(\epsilon) + \epsilon u^1 - \epsilon x_2\chi_r^\epsilon\phi^1 + \epsilon^2\Psi^2(\epsilon) - \epsilon^2\chi_r^\epsilon Z^2(\epsilon)\big],$$

and

$$\|e\|_{1,\Omega_r^\epsilon} + \|e\|_{1,\Omega_s} \le \epsilon^2\|Z^2(\epsilon) + c_0\phi^1 + z^1\partial_{x_1}\phi^0 + \epsilon z^2\partial_{x_1x_1}\phi^0 + \cdots\|_{\frac12,\Gamma}.$$

We proceed one more step by defining $\phi^2 = \partial_{x_2}u^2|_\Gamma$, and adding

$$\epsilon^2u^2 - \epsilon^2x_2\chi_r^\epsilon\partial_{x_2}u^2 + \epsilon^3\Psi^3(\epsilon) - \epsilon^3\chi_r^\epsilon Z^3(\epsilon)$$

to the expansion, where

(5.1.10)
$$\begin{gathered} -\Delta u^2 = 0 \quad \text{in } \Omega_s, \\ u^2 = -(c_0+z^0)\phi^1 + z^1\partial_{x_1}\phi^0 \quad \text{on } \Gamma, \qquad u^2 = 0 \quad \text{on } \partial\Omega_s\backslash\Gamma, \qquad u^2 = 0 \quad \text{on } \Omega_r^\epsilon, \end{gathered}$$

and

(5.1.11)
$$\begin{gathered} -\Delta\,\Psi^3(\epsilon) = -\chi_r^\epsilon\,\Delta(\epsilon^{-1}x_2\phi^2 + Z^3(\epsilon)) \quad \text{in } \Omega^\epsilon, \\ \Psi^3(\epsilon) = \epsilon^{-1}x_2\phi^2 + Z^3(\epsilon) \quad \text{on } \Gamma_r^\epsilon. \end{gathered}$$

The asymptotic error is now

$$\begin{aligned} e = u^\epsilon - \big[u^0 - x_2\chi_r^\epsilon\phi^0 + \epsilon\Psi^1(\epsilon) - \epsilon\chi_r^\epsilon Z^1(\epsilon) + \epsilon u^1 - \epsilon x_2\chi_r^\epsilon\phi^1 + \epsilon^2\Psi^2(\epsilon) - \epsilon^2\chi_r^\epsilon Z^2(\epsilon) \\ + \epsilon^2u^2 - \epsilon^2x_2\chi_r^\epsilon\partial_{x_2}u^2 + \epsilon^3\Psi^3(\epsilon) - \epsilon^3\chi_r^\epsilon Z^3(\epsilon)\big], \end{aligned}$$

and

$$\|e\|_{1,\Omega_r^\epsilon} + \|e\|_{1,\Omega_s} \le \epsilon^3\|z^2\partial_{x_1x_1}\phi^0 + z^1\partial_{x_1}\phi^1 + z^0\phi^2 + \epsilon\cdots\|_{\frac12,\Gamma}.$$

The expansion pattern should be clear by now, and the successive terms are defined in similar manner.

5.2. The boundary Corrector problem

We now analise the boundary corrector problem in more details. Consider the problem of finding Ψ, and Z such that

$$-\Delta\,\Psi = -\chi_r^\epsilon\,\Delta(\epsilon^{-1}x_2\phi + Z) \quad \text{in } \Omega^\epsilon, \tag{5.2.1}$$

$$\Psi = \epsilon^{-1}x_2\phi + Z \quad \text{on } \Gamma_r^\epsilon. \tag{5.2.2}$$

Here, while ϕ is a given function of x_1 only, Z is unknown a priori, and it is introduced to guarantee that Ψ decays exponentially to zero in the x_2 direction. The solutions Ψ and Z will depend on ϵ in a nontrivial way, so we assume that formally

$$\Psi \sim \Psi^0 + \epsilon\Psi^1 + \epsilon^2\Psi^2 + \cdots, \quad Z \sim Z^0 + \epsilon Z^1 + \epsilon^2 Z^2 + \cdots, \tag{5.2.3}$$

The functions involved in (5.2.1), (5.2.2) are not periodic in general. Nevertheless, we try to make use of the periodicity of the wrinkles and recast the corrector problem as a sequence of problems in periodic domains. Furthermore, motivated by the "rapidly" variations of the wrinkles, we make use of the stretched coordinates

$$\hat{\mathbf{x}} = (\hat{x}_1, \hat{x}_2) = (\epsilon^{-1}x_1, \epsilon^{-1}x_2),$$

and assume that a first approximation for Ψ and Z is given by

$$\Psi^0(\mathbf{x}) = \psi^0(\hat{\mathbf{x}})\phi(x_1), \quad Z^0(x_1) = z^0\phi(x_1), \tag{5.2.4}$$

where ψ^0 is $\hat{x}_1$-periodic, z^0 is a constant, and both Ψ^0 and z^0 are to be determined.

Observaçãо. At this stage, there are no good arguments indicating that z^0 is only a constant, but notice that the simpler Z^0 is, the better. And we will show, *a posteriori*, that the form we are assuming for Z^0 suffices to make Ψ^0 exponentially decaying.

It follows from a straightforward computation that the laplacian of a function in the form $u(\hat{x}_1, \hat{x}_2)v(x_1)$ is

$$-(\partial_{11} + \partial_{22})(uv) = -\epsilon^{-2}\big(\partial_{\hat{x}_2\hat{x}_2}u + \partial_{\hat{x}_1\hat{x}_1}u\big)v - 2\epsilon^{-1}\partial_{\hat{x}_1}uv' - uv''. \tag{5.2.5}$$

Hence,

$$\begin{aligned} -\Delta(\psi^0\phi) &= -\epsilon^{-2}\big(\partial_{\hat{x}_2\hat{x}_2}\psi^0 + \partial_{\hat{x}_1\hat{x}_1}\psi^0\big)\phi - 2\epsilon^{-1}\partial_{\hat{x}_1}\psi^0\phi' - \psi^0\phi'', \\ -\Delta(\hat{x}_2\phi) &= -\hat{x}_2\phi'', \qquad -\Delta(z^0\phi) = -z^0\phi''. \end{aligned} \tag{5.2.6}$$

Based on (5.2.1), (5.2.3), (5.2.4), and (5.2.6), and formally equating the same powers of ϵ, we gather that ψ^0 is harmonic. The boundary condition over the wrinkles comes from (5.2.2), (5.2.3), and (5.2.4). The final problem determining the function ψ^0 and the constant z^0 is then

$$\begin{gathered} \partial_{\hat{x}_1\hat{x}_1}\psi^0 + \partial_{\hat{x}_2\hat{x}_2}\psi^0 = 0 \quad \text{in } \Omega_r, \qquad \psi^0 = \hat{x}_2 + z^0 \quad \text{on } \Gamma_r^-, \\ \psi^0 \text{ is } \hat{x}_1\text{-periodic}, \qquad \lim_{\hat{x}_2\to\infty}\psi^0 = 0. \end{gathered}$$

The domain Ω_r occupies the semi-infinite region limited by straight lateral boundaries at $\hat{x}_1 = 0$ and $\hat{x}_1 = 1$, and by the lower boundary $\Gamma_r^- = \{\,(\hat{x}_1, \psi_r(\hat{x}_1)) : \hat{x}_1 \in (0,1)\,\}$.

Hence we have that

$$-\Delta[(\psi^0 - \chi_r^\epsilon \hat{x}_2 + \chi_r^\epsilon z^0)\phi] = -2\epsilon^{-1}\partial_{\hat{x}_1}\psi^0\phi' - \psi^0\phi'' + \chi_r^\epsilon \hat{x}_2\phi'' - \chi_r^\epsilon z^0\phi'' \quad \text{in } \Omega^\epsilon,$$
$$\psi^0 - \hat{x}_2 + z^0 = 0 \quad \text{on } \Gamma_r^\epsilon.$$

We set then $\Psi^1 = \psi^1\phi'$, $Z^1 = z^1\phi'$ where

$$-[\partial_{\hat{x}_2\hat{x}_2}\psi^1 + \partial_{\hat{x}_1\hat{x}_1}\psi^1] = 2\partial_{\hat{x}_1}\psi^0 \quad \text{in } \Omega_r, \qquad \psi^1 = z^1 \quad \text{on } \Gamma_r^-.$$

Hence,

$$-\Delta[(\psi^0 - \chi_r^\epsilon \hat{x}_2 + \chi_r^\epsilon z^0)\phi + \epsilon(\psi^1 + \chi_r^\epsilon z^1)\phi'] = -\psi^0\phi'' + \chi_r^\epsilon \hat{x}_2\phi'' - \chi_r^\epsilon z^0\phi'' - 2\partial_{\hat{x}_1}\psi^1\phi'' - \epsilon\psi^1\phi''' - \epsilon\chi_r^\epsilon z^1\phi''' \quad \text{in } \Omega^\epsilon,$$
$$(\psi^0 - \chi_r^\epsilon \hat{x}_2 + \chi_r^\epsilon z^0)\phi + \epsilon(\psi^1 + \chi_r^\epsilon z^1)\phi' = 0 \quad \text{on } \Gamma_r^\epsilon.$$

Now, $\Psi^2 = \psi^2\phi''$, and $Z^2 = z^2\phi''$ where

$$-[\partial_{\hat{x}_2\hat{x}_2}\psi^2 + \partial_{\hat{x}_1\hat{x}_1}\psi^2] = \psi^0 - \chi_r\hat{x}_2 + \chi_r z^0 + 2\partial_{\hat{x}_1}\psi^1 \quad \text{in } \Omega_r, \qquad \psi^2 = z^2 \quad \text{on } \Gamma_r^-,$$

where $\chi_r(\hat{x}_2) = 1$ if $\hat{x}_2 \le c_0$, and $\chi_r(\hat{x}_2) = 0$ otherwise. It is easy to see that the right hand sides of the equations become more involved as we proceed. The crucial point is to note that in the above cases, the equations did not involve ϕ or their derivatives.

We finally conclude that

$$\Psi(\epsilon) \sim \psi^0\phi + \epsilon\psi^1\phi' + \epsilon^2\psi^2\phi'' + \cdots, \qquad Z(\epsilon) \sim z^0\phi + \epsilon z^1\phi' + \epsilon^2 z^2\phi'' + \cdots. \tag{5.2.7}$$

5.3. Derivation of wall-laws

Our goal is to approximate u^ϵ using finite elements (or finite differences), without having to discretize the rough boundary. One first step would be to try to approximate u^ϵ in Ω_s only, since this is a smooth domain. We consider the series

$$u^0 + \epsilon\psi^0\phi^0 + \epsilon u^1.$$

The functions u^0, u^1 are defined by (5.1.4), (5.1.9), and ψ^0 is defined in the previous section. We would like to approximate u^ϵ by the above sum, but without solving all the problems that define each term. Heuristically, we consider only the functions that actually have influence in the interior of the domain, i.e.,

$$u \approx u^0 + \epsilon u^1.$$

Hence, over Γ, $u \approx u^0 + \epsilon u^1 = -\epsilon(c_0 + z^0)\phi^0$, and $\partial_{x_2}u \approx \phi^0 + \epsilon\phi^1$, so

$$u + \epsilon(c_0 + z^0)\partial_{x_2}u \approx \epsilon^2(c_0 + z^0)\phi^1,$$

and this amount can be small enough for certain applications.

So we define $\bar{u}$ approximating u^ϵ in Ω_s by

$$-\Delta\,\bar{u} = f \quad \text{in } \Omega_s,$$
$$\bar{u} + \epsilon(c_0 + z^0)\partial_{x_2}\bar{u} = 0 \quad \text{on } \Gamma, \qquad \bar{u} = 0 \quad \text{on } \partial\Omega_s\backslash\Gamma. \tag{5.3.1}$$

The error estimates follow by developing asymptotic expansions for $\bar{u}$. In fact, it is easy to see that

$$\bar{u} \sim \bar{u}^0 + \epsilon\bar{u}^1 + \epsilon^2\bar{u}^2 + \cdots,$$

TABLE 1. Relative error convergence rates for order 0 model.

quantity	$L^2(\Omega_s)$ error	$L^2(\mathring{\Omega}_s)$ norm error
u	$O(\epsilon)$	$O(\epsilon)$
∇u	$O(\epsilon^{1/2})$	$O(\epsilon)$

TABLE 2. Relative error convergence rates for order 1 model.

quantity	$L^2(\Omega_s)$ error	$L^2(\mathring{\Omega}_s)$ norm error
u	$O(\epsilon^2)$	$O(\epsilon^2)$
∇u	$O(\epsilon^{1/2})$	$O(\epsilon^2)$

where

$$\begin{aligned} -\Delta \bar{u}^i &= \delta_{i,0} f \quad \text{in } \Omega_s, \\ \bar{u}^i = -(c_0 + z^0)\partial_{x_2} \bar{u}^{i-1} \quad &\text{on } \Gamma, \qquad \bar{u}^i = 0 \quad \text{on } \partial\Omega_s \backslash \Gamma. \end{aligned} \tag{5.3.2}$$

Also,

$$\left\| \bar{u} - \sum_{i=0}^{n} \epsilon^i \bar{u}^i \right\|_{H^k(\Omega_s)} \leq c\epsilon^{n+1}. \tag{5.3.3}$$

The modeling error estimates are then as follows.

$$\begin{aligned} \|u^\epsilon - \bar{u}\|_{H^1(\Omega_s)} &\leq \|u^\epsilon - u^0 - \epsilon u^1\|_{H^1(\Omega_s)} + \|\bar{u} - \bar{u}^0 - \epsilon \bar{u}^1\|_{H^1(\Omega_s)} \\ &\leq \|u^\epsilon - u^0 - \epsilon u^1 - \epsilon \psi^0 \phi^0\|_{H^1(\Omega_s)} + \epsilon \|\psi^0 \phi^0\|_{H^1(\Omega_s)} + c\epsilon^2 \leq c\epsilon^{1/2}, \end{aligned}$$

where in the first inequality we used the triangle inequality, and the identities $u^0 = \bar{u}^0$ and $u^1 = \bar{u}^1$.

In a similar fashion, we can consider other norms, for instance

$$\|u^\epsilon - \bar{u}\|_{L^2(\Omega_s)} \leq c\epsilon^2,$$

Another important measure is how well our model approximates the exact solution in the interior of the domain, i.e., consider $\mathring{\Omega}_s \subset \Omega_s$ such that $\overline{\mathring{\Omega}}_s \cap \overline{\Gamma} = \emptyset$. Hence

$$\|u^\epsilon - \bar{u}\|_{L^2(\Omega_s)} + \|u^\epsilon - \bar{u}\|_{H^k(\mathring{\Omega}_s)} \leq c\epsilon^2.$$

This improved convergence is due to the fact that the boundary layer has no influence far from the wrinkles.

We also compare in tables 1 and 2 the approximability properties of our model and a simple minded model, which approximates u^ϵ by u^0 only. We call such model as "order zero model," and our model as "order one model." Note the improved convergence rate for most of the norms, with the exception of the H^1 norm. This is due to the fact that neither approaches captures the boundary layer exactly.

CHAPTER 6

Homogeneização de equações elíticas em uma dimensão

Neste capítulo, investigamos o processo de homogeneização em uma dimensão, enfatizando aspectos teóricos e numéricos. Apresentamos na Seção 6.1 uma equação simples mas que carrega em si várias das dificuldades presentes em problemas mais sofisticados. A seguir discutimos três alternativas de modelagem para a equação em discussão: homogeneização, elementos finitos clássicos, e elementos finitos multiescala. Procuramos nestas seções mostrar e vantagens e desvantagens de cada técnica e apresentamos vários exemplos numéricos. Finalmente concluímos mostrando uma outra dificuldade presente quando o problema "perde coercividade".

6.1. Um modelo

Para descrever as propriedades qualitativas e dificuldades relacionadas com problemas que apresentam caráter oscilatório, consideramos o seguinte modelo unidimensional:

$$\begin{aligned} -\frac{d}{dx}\left(a(x/\epsilon)\frac{du^\epsilon}{dx}(x)\right) &= f(x) \quad \text{em } (0,1), \\ u^\epsilon(0) = u^\epsilon(1) &= 0. \end{aligned} \tag{6.1.1}$$

onde $a(\cdot)$ é suave e periódica com período 1, e $\beta \geq a(x) \geq \alpha > 0$, para α, β reais. Estamos interessados somente no caso em que $\epsilon \leq 1$, portanto assumiremos também esta desigualdade.

Neste caso unidimensional, é fácil obter uma solução analítica para (6.1.1):

$$u^\epsilon(x) = -\int_0^x \left(\frac{1}{a(\xi/\epsilon)}\int_0^\xi f(t)\,dt + c_0\right) d\xi, \qquad c_0 = \frac{1}{\int_0^1 a(\xi/\epsilon)\,d\xi}\int_0^1 \left(\frac{1}{a(\xi/\epsilon)}\int_0^\xi f(t)\,dt\right) d\xi.$$

Nos nossos exemplos, consideraremos

$$f(x) = 1, \qquad a(x) = \frac{1}{2}(\beta-\alpha)(1+\sin(2\pi x)) + \alpha, \qquad \alpha = \frac{1}{2}, \qquad \beta = \frac{5}{2}. \tag{6.1.2}$$

Seja a seguinte sequência de problemas, onde $\epsilon = 1/4$, $\epsilon = 1/8$, e $\epsilon = 1/16$, e veja as figuras 1, 2 e 3. É fácil notar neste exemplo que crescem as oscilações de $a(\cdot/\epsilon)$ quando $\epsilon \to 0$.

Em dimensões maiores, é extremamente difícil obter soluções analíticas. Motivados por esta dificuldade, investigaremos agora como encontrar soluções aproximadas para (6.1.1).

Uma possibilidade explorada na Seção 6.2 é o uso de *técnicas de homogeneização*. Como vimos, a idéia básica apoia-se no fato de que, quando $\epsilon \to 0$, a solução exata converge uma função chamada de *solução homogeneizada*. Espera-se então que para valores de ϵ pequenos, a aproximação pela solução homogeneizada seja boa o suficiente.

Outra possibilidade é o discretizar o problema usando *elementos finitos*. Esta escolha de método numérico deve-se tanto à aplicabilidade do método em diversos problemas de

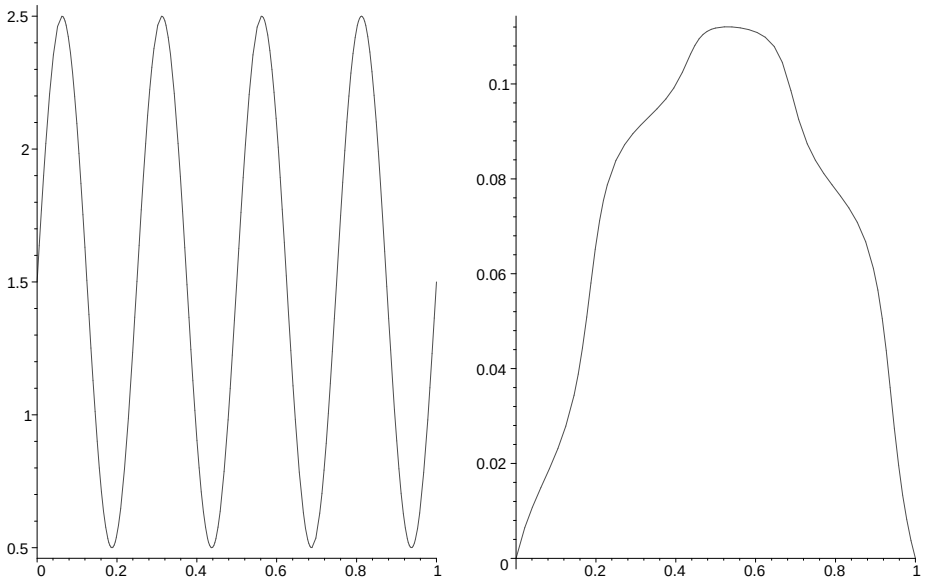

FIG. 1. Gráficos de $a(\cdot/\epsilon)$ e da solução exata para $\epsilon = 1/4$.

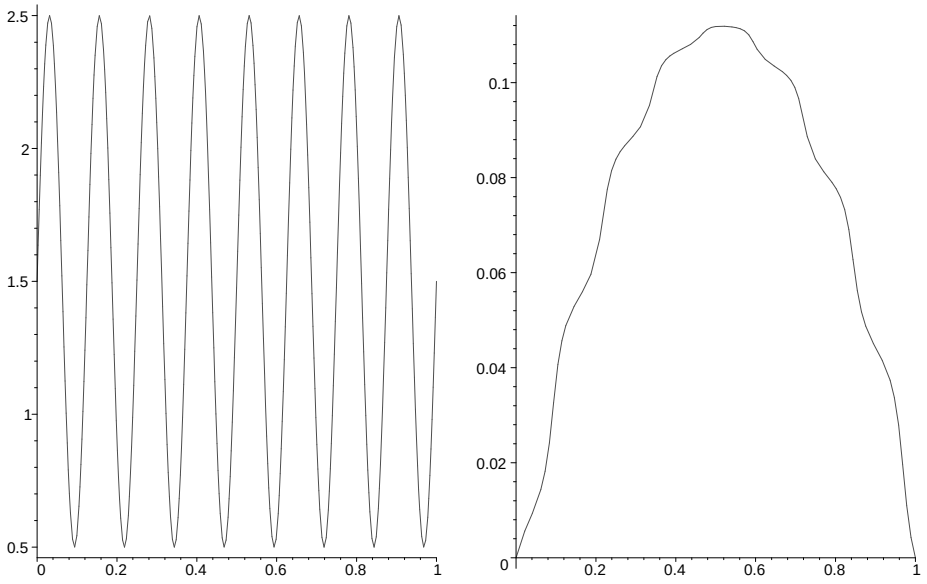

FIG. 2. Gráficos de $a(\cdot/\epsilon)$ e da solução exata para $\epsilon = 1/8$.

interesse, como também a facilidade em desenvolver uma análise de erro que ressalte eventuais dificuldades numéricas. Estas questões são analisadas na Seção 6.3.

Uma outra opção baseada em pesquisa recente [**34, 35**] é o uso de *elementos finitos multiescala*. Nesta técnica, descrita na Seção 6.4, funções de base que resolvem o problema *localmente* são utilizadas para gerar um espaço de elementos finitos, e automaticamente levam informações da pequena escala para a grande escala, num processo de *homogeneização numérica*.

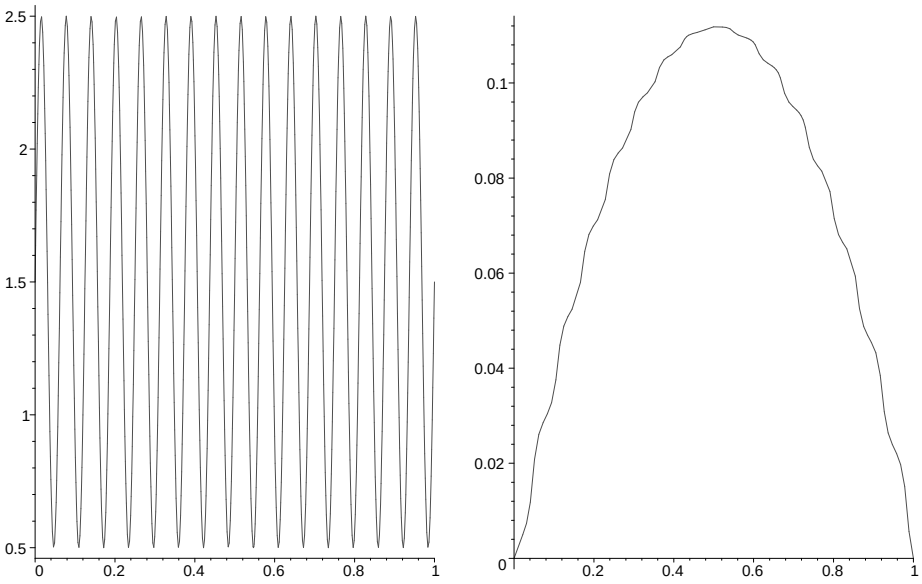

FIG. 3. Gráficos de $a(\cdot/\epsilon)$ e da solução exata para $\epsilon = 1/16$.

6.2. Solução homogeneizada

Seja u^ϵ solução de (6.1.1). É possível então mostrar que u^ϵ converge para u^0, onde

$$
\begin{aligned}
-\frac{1}{\mathcal{M}(1/a)}\frac{d^2}{dx^2}u^0 &= f(x) \quad \text{em } (0,1),\\
u^0(0) &= u^0(1) = 0,
\end{aligned}
\tag{6.2.1}
$$

e

$$\mathcal{M}(1/a) = \int_0^1 \frac{1}{a(x)}\,dx.$$

Em uma dimensão, é fácil calcular u^0 analiticamente:

$$u^0(x) = \mathcal{M}(1/a)\left[-\int_0^x\int_0^\xi f(t)\,dt\,d\xi + x\int_0^1\int_0^\xi f(t)\,dt\,d\xi\right].$$

A convergência ocorre usando norma do espaço $L^2(0,1)$. Este espaço é composto por funções $v : (0,1) \to \mathbb{R}$ "quadrado integráveis", i.e.,

$$L^2(0,1) = \{v \,:\, v \text{ é função real definida em } (0,1) \text{ e } v^2 \text{ é integrável}\}.$$

Neste espaço definimos a norma

$$\|v\|_{L^2(0,1)} = \left(\int_0^1 [v(x)]^2\,dx\right)^{1/2}.$$

OBSERVAÇÃO. Acima, e no restante deste texto, o adjetivo "integrável" quer dizer na verdade *integrável no sentido de Lebesgue*, uma idéia um pouco mais abrangente que a de integração no sentido de Riemann. Entretanto, é suficiente neste texto ter a intuição de funções integráveis como sendo Riemann integráveis.

O seguinte resultado de convergência justifica o uso da solução homogeneizada [**48**].

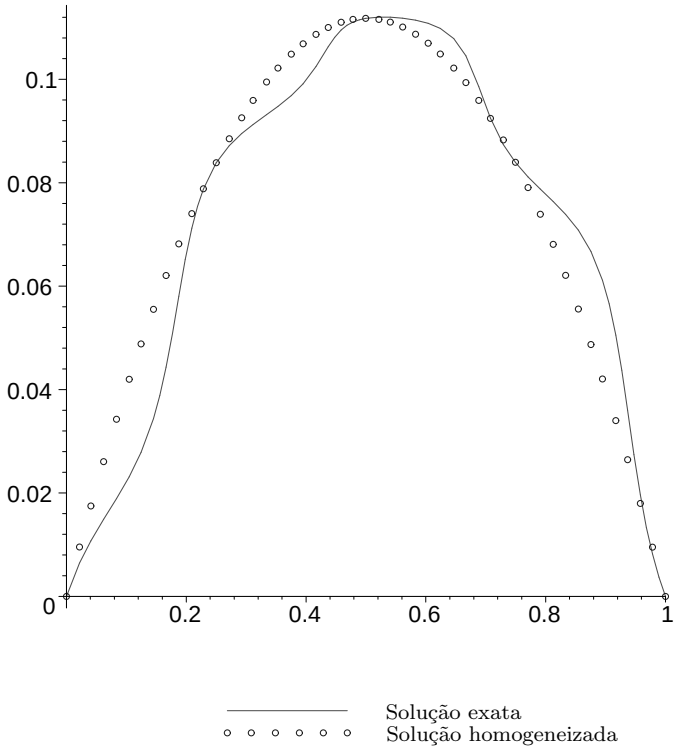

FIG. 4. Comparação entre as soluções exatas e homogeneizada para $\epsilon = 1/4$.

TEOREMA 6.2.1. *Seja $f \in L^2(0,1)$, e seja u^ϵ solução de* (6.1.1). *Então existe uma constante c independente de ϵ, f,α, β tal que*

$$\|u^\epsilon - u^0\|_{L^2(0,1)} \leq c\frac{\epsilon}{\alpha}\|f\|_{L^2(0,1)}.$$

Comparamos agora como a solução homogeneizada se comporta, assumindo (6.1.2). Considere a seguinte sequência of exemplos, onde $\epsilon = 1/4$, $\epsilon = 1/8$, e $\epsilon = 1/16$, e veja as Figuras 4, 5 e 6. Pode-se notar que quando $\epsilon \to 0$, a solução homogeneizada u^0 torna-se uma boa aproximação para a solução exata u^ϵ.

Apesar de serem extremamente úteis em várias aplicações, as técnicas de homogeneização apresentam algumas limitações. Por exemplo, sua aplicabilidade está limitada a valores de ϵ pequenos, como fica aparente na figura 4. Outras dificuldades surgem em casos mais gerais, por exemplo quando $a(\cdot)$ é não periódico.

6.3. Aproximação por Elementos Finitos

O primeiro passo para apresentar o método é reescrever (6.1.1) na sua *forma fraca*. Se multiplicarmos a equação por uma função v suficientemente suave e que se anule em $x = 0$ e $x = 1$ e integrarmos por partes, temos que

$$\int_0^1 \left(a(x/\epsilon)\frac{du^\epsilon}{dx}(x)\frac{dv}{dx}(x) \right) dx = \int_0^1 f(x)v(x)\,dx. \tag{6.3.1}$$

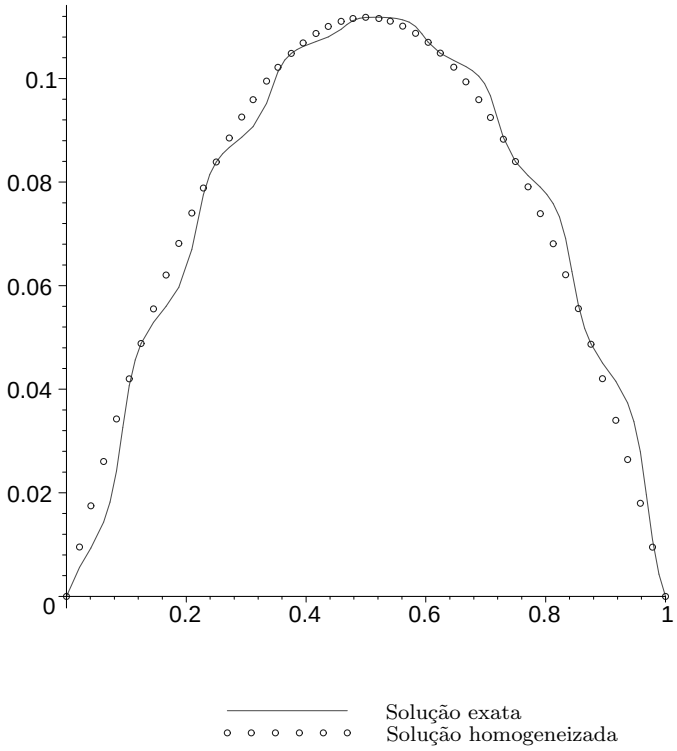

FIG. 5. Comparação entre as soluções exatas e homogeneizada para $\epsilon = 1/8$.

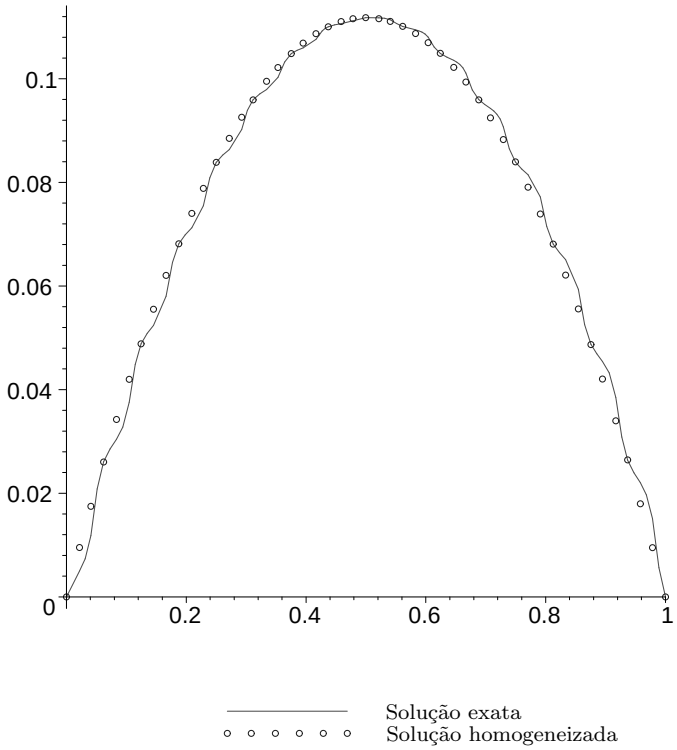

FIG. 6. Comparação entre as soluções exatas e homogeneizada para $\epsilon = 1/16$.

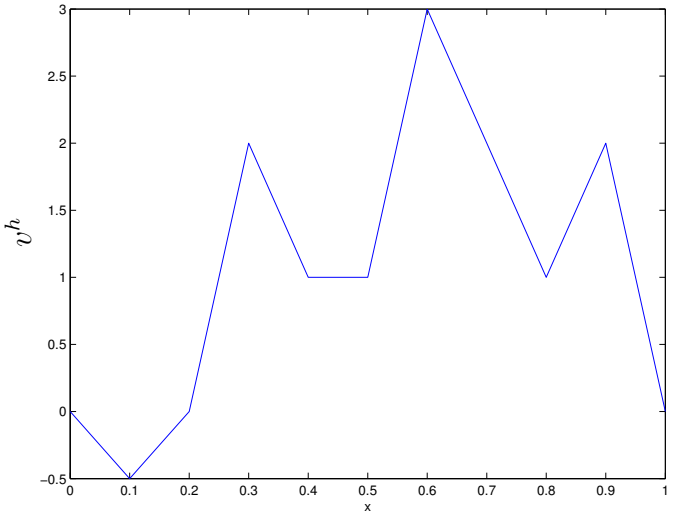

FIG. 7. Exemplo de função linear por partes

Note que se u^ϵ é solução de (6.1.1), então a identidade acima vale para todo v suficientemente suave.

É possível também inverter a ordem desse raciocínio, i.e., gostaríamos de buscar uma função u^ϵ que satisfizesse (6.3.1) para toda v suficientemente suave, e depois poderíamos mostrar que também resolve (6.1.1). Para tal, buscaremos a solução num espaço de funções que sejam contínuas, que tenham derivadas (no sentido fraco), e que se anulem em $x = 0$ e $x = 1$. Além disso, exigiremos que essas funções e suas derivadas sejam quadrado integráveis, i.e., podemos integrar tanto v^2 como $(v')^2$. Chamaremos esse espaço de

$$H_0^1(0,1) = \{v \in C[0,1] \,:\, v(0) = v(1) = 0; \quad v^2 \text{ e } (v')^2 \text{ são integráveis}\},$$

e introduzimos a norma

$$\|v\|_{H^1(0,1)} = \left(\int_0^1 \left\{ [v(x)]^2 + \left[\frac{dv}{dx}(x) \right]^2 \right\} dx \right)^{1/2}.$$

Como exemplo de funções que estão em $H_0^1(0,1)$, temos a importante classe de funções suaves por partes, como por exemplo a função mostrada na figura 7. Note que a função v^h lá representada é contínua, se anula em $x = 0$ e $x = 1$, e além disso só deixa de ser suave num número finito de pontos.

O importante no momento é que é possível provar que existe uma função $u^\epsilon \in H_0^1(0,1)$ satisfazendo (6.3.1) para todo $v \in H_0^1(0,1)$. Além disso, no caso de f ser suave, esta solução também resolve (6.1.1). Ou seja, essas duas formulações são equivalentes.

6.3.1. Discretização por Elementos Finitos. A idéia do método de elementos finitos é escolher um subespaço de $H_0^1(0,1)$ e buscar funções que satisfaçam (6.3.1) dentro desse subespaço. Nós primeiro discretizamos o domínio $(0,1)$ em elementos finitos definindo os nós $0 = x_0 < x_1 < \cdots < x_{N+1} = 1$, onde $x_j = jh$, e $h = 1/(N+1)$ é o parâmetro de malha. A seguir, definimos o espaço de dimensão finita $V_0^h \subset H_0^1(0,1)$, onde

$$V_0^h = \left\{ v^h \in H_0^1(0,1) \,:\, v^h \text{ é linear em } (x_{j-1}, x_j) \text{ for } j = 1, \ldots, N+1 \right\}.$$

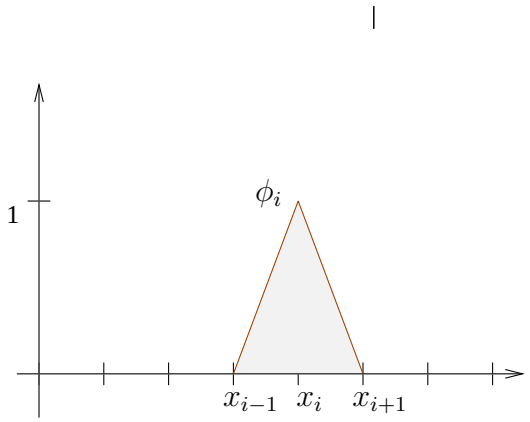

FIG. 8. Uma função da base do espaço de elementos finitos

Chamamos V_0^h de espaço de funções lineares por partes. Uma função de V_0^h típica é representada na figura 7. A aproximação por elementos finitos de u^ϵ é $u^h \in V_0^h$ tal que

$$\int_0^1 \left(a(x/\epsilon) \frac{du^h}{dx}(x) \frac{dv^h}{dx}(x) \right) dx = \int_0^1 f(x) v^h(x)\, dx \quad \text{para todo } v^h \in V_0^h. \tag{6.3.2}$$

OBSERVAÇÃO. Note que u^h também depende de ϵ, apesar desta dependência não estar explicitada na notação.

Observe que uma função em V_0^h pode ser caracterizada de forma única pelos valores que assume nos nós x_1, x_2, etc. Em vista disto, podemos introduzir uma *base* no espaço V_0^h. Seja $\phi_i \in V_0^h$ tal que

$$\phi_i(x_j) = \begin{cases} 1 & \text{se } i = j, \\ 0 & \text{se } i \neq j, \end{cases}$$

para $j = 1, \ldots, N$. Uma função de base típica está representada na figura 8. Temos então $V_0^h = \text{span}\,\{\phi_1, \ldots, \phi_N\}$.

Finalmente, se $u^h(x) = \sum_{i=1}^N u_i \phi_i(x)$, então reescrevemos (6.3.2) como

$$\sum_{i=1}^N u_i \int_0^1 \left(a(x/\epsilon) \frac{d\phi_i}{dx}(x) \frac{d\phi_j}{dx}(x) \right) dx = \int_0^1 f(x) \phi_j(x)\, dx \quad \text{para } j = 1, \ldots, N. \tag{6.3.3}$$

Note que $u_j = u^h(x_j)$ é o valor de u^h no nó x_j.

O método de elementos finitos para (6.1.1) consiste então em achar $\mathbf{u} = (u_1, \ldots, u_N)^T \in \mathbb{R}^N$ tal que

$$\mathbf{M}\mathbf{u} = \mathbf{f},$$

onde a matriz $\mathbf{M} = (M_{i,j}) \in \mathbb{R}^{N \times N}$ e o vetor $\mathbf{f} = (f_1, \ldots, f_N)^T \in \mathbb{R}^N$ são dados por

$$M_{i,j} = \int_0^1 \left(a(x/\epsilon) \frac{d\phi_i}{dx}(x) \frac{d\phi_j}{dx}(x) \right) dx, \qquad f_j = \int_0^1 f(x) \phi_j(x)\, dx.$$

As aproximações numéricas para (6.1.1), onde a é dada por (6.1.2) apresentam resultados variados. Para $\epsilon = 1/4$ e $h = 1/32$, o método de elementos finitos aproxima razoavelmente bem a solução exata, como mostra a figura 9. Entretanto, a aproximação se deteriora quando

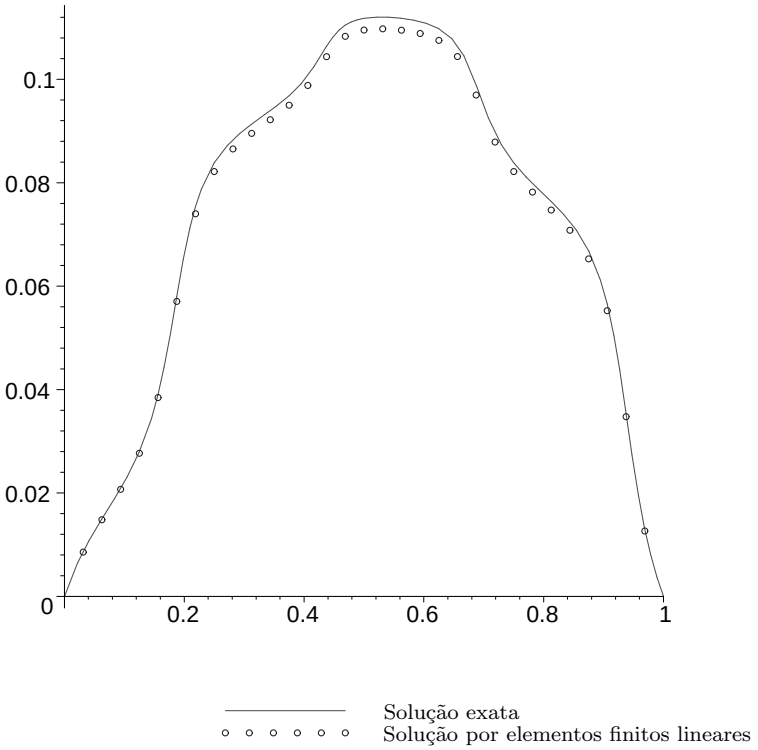

FIG. 9. Gráficos de u^ϵ e de sua aproximação por elementos finitos, com $\epsilon = 1/4$ e $h = 1/32$.

ϵ se torna menor. Veja os gráficos para $h = 1/32$, mas $\epsilon = 1/8$ na figura 10, e $\epsilon = 1/16$ na figura 11.

A aproximação melhora se refinarmos a malha. Por exemplo, tomando o caso $\epsilon = 1/8$, mas com $h = 1/64$, temos uma melhoria na aproximação, como mostra a figura 12.

O ponto que queremos ressaltar é que o método de elementos finitos converge, mas *a taxa de convergência depende de* ϵ. Isto pode ser um problema em dimensões maiores, quando o uso de malhas refinadas torna-se caro computacionalmente.

6.3.2. O que dá errado? A fim de entender melhor porque o método de elementos finitos clássico não funciona bem, desenvolvemos uma análise de erro para esse problema. Aqui e no restante deste capítulo, c denota uma constante universal, independente de ϵ, h, f, α e β. Quando queremos indicar uma constante que pode depender de α ou β, mas não de ϵ, h ou f, utilizamos a letra maiúscula C.

Para facilitar a notação, definimos as formas bilineares

$$b(u,v) = \int_0^1 \left(a(x/\epsilon) \frac{du^\epsilon}{dx}(x) \frac{dv}{dx}(x) \right) dx, \qquad (f,v) = \int_0^1 f(x)v(x)\,dx.$$

Temos então que a solução exata $u^\epsilon \in H_0^1(0,1)$ e sua aproximação por elementos finitos $u^h \in V_0^h$ satisfazem

$$b(u^\epsilon, v) = (f,v) \quad \text{para todo } v \in H_0^1(0,1), \qquad b(u^h, v^h) = (f, v^h) \quad \text{para todo } v^h \in V_0^h.$$

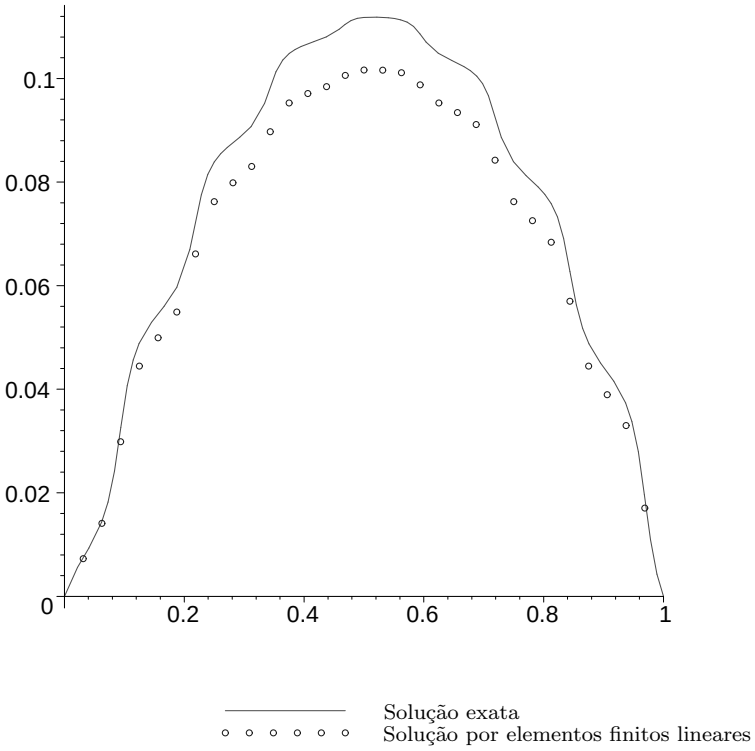

FIG. 10. Gráficos de u^ϵ e de sua aproximação por elementos finitos, com $\epsilon = 1/8$ e $h = 1/32$.

Logo

$$b(u^\epsilon - u^h, v^h) = 0 \quad \text{para todo } v^h \in V_0^h.$$

Na nossa análise, usamos o fato que $\beta \geq a(x) \geq \alpha > 0$. Começamos a investigar a continuidade da forma bilinear $b(\cdot, \cdot)$. Segue-se de sua definição que

$$b(u, v) \leq \beta \|u\|_{H^1(0,1)} \|v\|_{H^1(0,1)} \quad \text{para todo } u, v \in H_0^1(0,1). \tag{6.3.4}$$

A seguir, estimamos a coercividade:

$$b(v, v) \geq \alpha \int_0^1 \left(\frac{dv}{dx}\right)^2 dx \geq c\alpha \|v\|^2_{H^1(0,1)} \quad \text{para todo } v \in H_0^1(0,1), \tag{6.3.5}$$

onde usamos a desigualdade de Poincaré

$$\int_0^1 \left(\frac{dv}{dx}(x)\right)^2 dx \geq c \int_0^1 \left[\big(v(x)\big)^2 + \left(\frac{dv}{dx}(x)\right)^2\right] dx$$

no último passo.

Podemos agora obter estimativas de erro. Usando (6.3.5), e depois (6.3.4), conlcuímos que

$$\begin{aligned} \|u^\epsilon - u^h\|^2_{H^1(0,1)} &\leq \frac{c}{\alpha} b(u^\epsilon - u^h, u^\epsilon - u^h) = \frac{c}{\alpha} b(u^\epsilon - u^h, u^\epsilon - v^h) \\ &\leq c\frac{\beta}{\alpha} \|u^\epsilon - u^h\|_{H^1(0,1)} \|u^\epsilon - v^h\|_{H^1(0,1)} \quad \text{para todo } v^h \in V_0^h. \end{aligned} \tag{6.3.6}$$

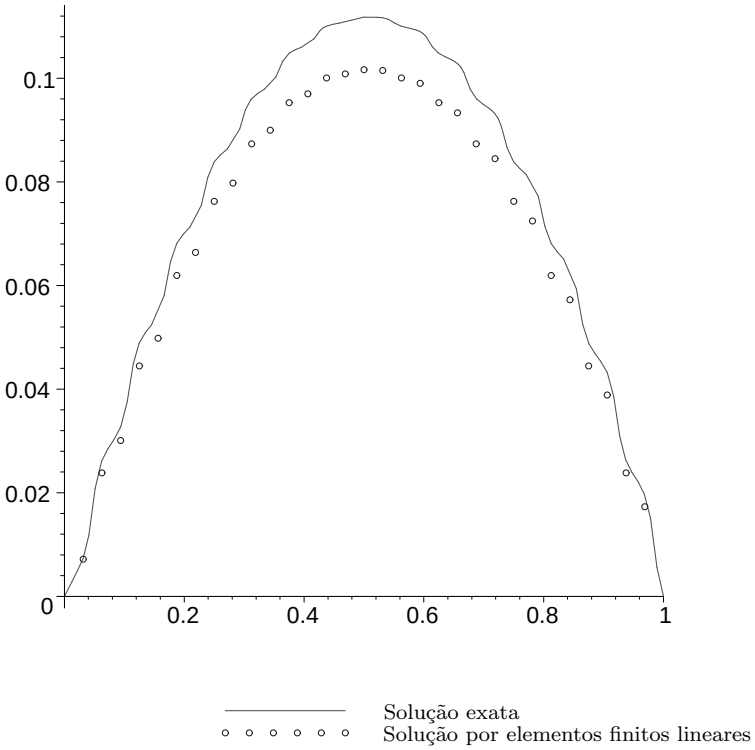

FIG. 11. Gráficos de u^ϵ e de sua aproximação por elementos finitos, com $\epsilon = 1/16$ e $h = 1/32$.

Mostramos assim o Lema de Cea.

LEMA 6.3.1 (Lema de Cea). Sejam u^ϵ e u^h soluções de (6.1.1) e (6.3.2). Então existe uma constante universal c tal que

$$\|u^\epsilon - u^h\|_{H^1(0,1)} \leq c\frac{\beta}{\alpha}\|u^\epsilon - v^h\|_{H^1(0,1)} \quad \text{para todo } v^h \in V_0^h.$$

A seguir, usando estimativas clássicas de interpolação, temos que

$$\|u^\epsilon - I^h u^\epsilon\|_{H^1(0,1)} \leq ch|u^\epsilon|_{H^2(0,1)}, \tag{6.3.7}$$

onde $I^h u^\epsilon = \sum_{j=1}^N u^\epsilon(x_j)\phi_j$ é o interpolador de u^ϵ em V_0^h, e

$$|v|_{H^2(0,1)} = \left(\int_0^1 \left[\frac{d^2v}{dx^2}(x)\right]^2 dx\right)^{1/2}.$$

Fazendo $v^h = I^h u^\epsilon$ em (6.3.6), concluímos que

$$\|u^\epsilon - u^h\|_{H^1(0,1)} \leq c\frac{\beta}{\alpha}h|u^\epsilon|_{H^2(0,1)}.$$

Obtemos finalmente o teorema a seguir usando a estimativa

$$|u^\epsilon|_{H^2(0,1)} \leq \frac{c\beta}{\alpha^2\epsilon}\|f\|_{L^2(0,1)}, \tag{6.3.8}$$

onde assumimos $|a'(x)| \leq c\beta$.

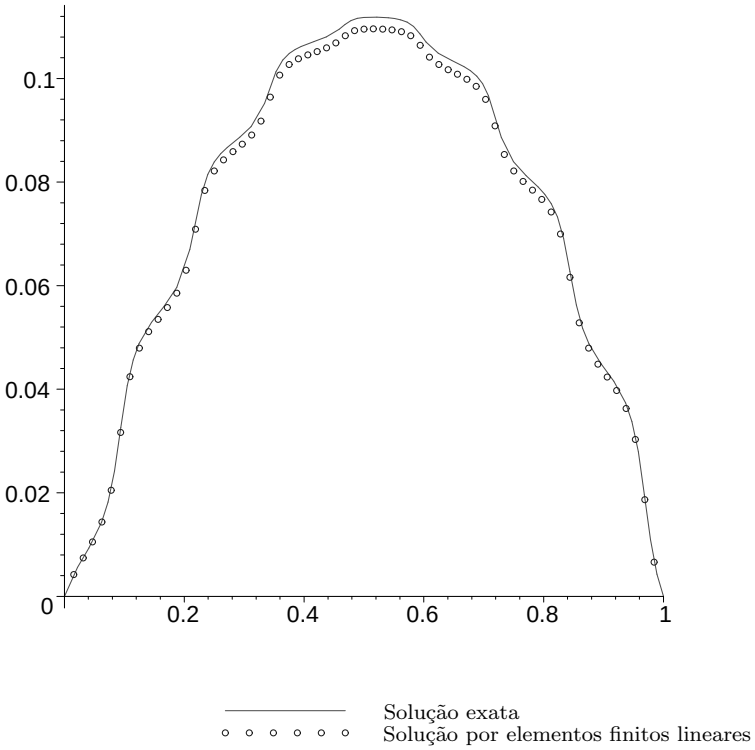

FIG. 12. Gráficos de u^ϵ e de sua aproximação por elementos finitos, com $\epsilon = 1/8$ e $h = 1/64$.

TEOREMA 6.3.2. *Seja $f \in L^2(0,1)$, e seja u^ϵ solução de* (6.1.1). *Então existe uma constante c independente de ϵ, f,α, β tal que*

$$\|u^\epsilon - u^h\|_{H^1(0,1)} \leq c\frac{\beta^2}{\alpha^3}\frac{h}{\epsilon}\|f\|_{L^2(0,1)}. \tag{6.3.9}$$

Paramos por um momento agora para interpretar a estimativa obtida. Antes de mais nada, *o método converge quando $h \to 0$*. De fato, para ϵ fixo, o erro vai a zero que o tamanho da malha vai a zero. O problema é que a convergência em h não é uniforme em ϵ.

Logo, para ϵ pequeno, a menos que a malha seja muito refinada ($h \ll \epsilon$), a estimativa (6.3.9) indica que o erro na norma $H^1(0,1)$ é grande. Isto faz com que o método de elementos finitos tradicional sejam quase inúteis para este tipo de problema, e explica os maus resultados das figuras 10 e 11.

6.4. Elementos Finitos Multiescala

Mais recentemente, Tom Hou e seus colaboradores [**34, 35**] propuseram uma nova forma de aproximação numérica para EDPs em duas dimensões com coeficientes oscilatórios. A idéia básica é mudar as funções de base do espaço de elementos finitos. Ao invés de usar funções lineares por partes, a técnica de *elementos finitos multiescala* usa funções que resolvem localmente (em cada elemento) a equação em questão.

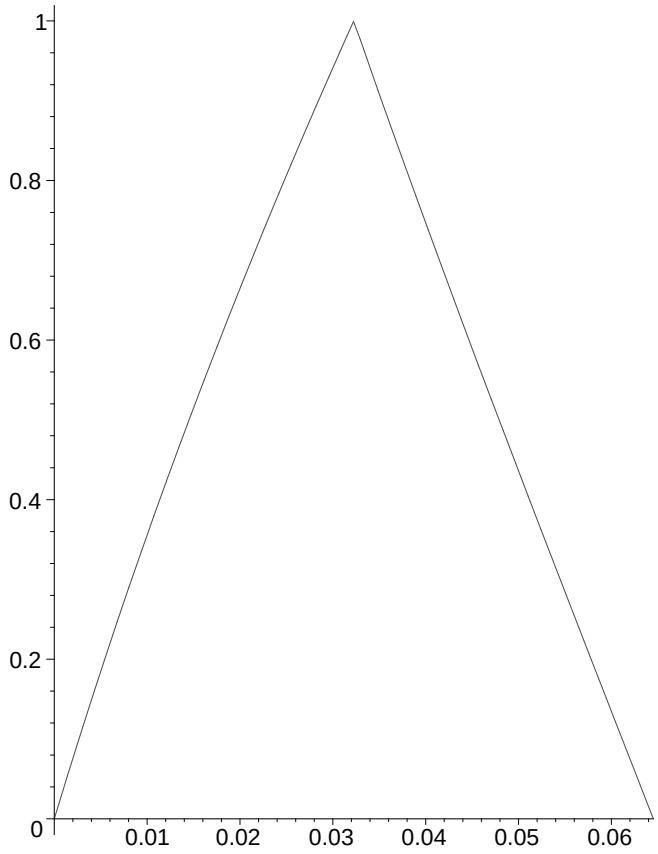

FIG. 13. Gráficos de ψ_1 com $\epsilon = 1/4$ e $h = 1/32$.

Apresentamos aqui as idéias no caso unidimensional. Em quase todos os aspectos, incluindo a análise de erro, a extensão para duas dimensões é natural. Comentamos ao fim desta seção alguns pontos onde esta generalização não é trivial.

Nós começamos a definir o método construindo as funções de base. Seja ψ_i tal que

$$-\frac{d}{dx}\left(a(x/\epsilon)\frac{d\psi_i}{dx}(x)\right) = 0 \quad \text{em } \cup_{j=1}^{N+1}(x_{j-1}, x_j), \qquad \psi_i(x_j) = \begin{cases} 1 & \text{se } i = j, \\ 0 & \text{se } i \neq j, \end{cases} \tag{6.4.1}$$

para $i = 1, \ldots, N$. Definimos então o espaço de elementos finitos multiescala como sendo

$$V_0^{h,\epsilon} = \text{span}\,\{\psi_1, \ldots, \psi_N\}.$$

Uma função de base típica é apresentada na figura 13 para $\epsilon = 1/4$ e $h = 1/32$. Note que a função se parece muito com a função de base do método de elementos finitos usual. Isto se explica pois neste caso o parâmetro de malha h é bem menor do que ϵ, e a função de base tradicional ainda funciona bem, vide figura 9. No caso oposto, quando ϵ é bem menor que h, temos que a função de base tem caráter oscilatório, como é mostrado na figura 14, para $\epsilon = 1/128$ e $h = 1/32$.

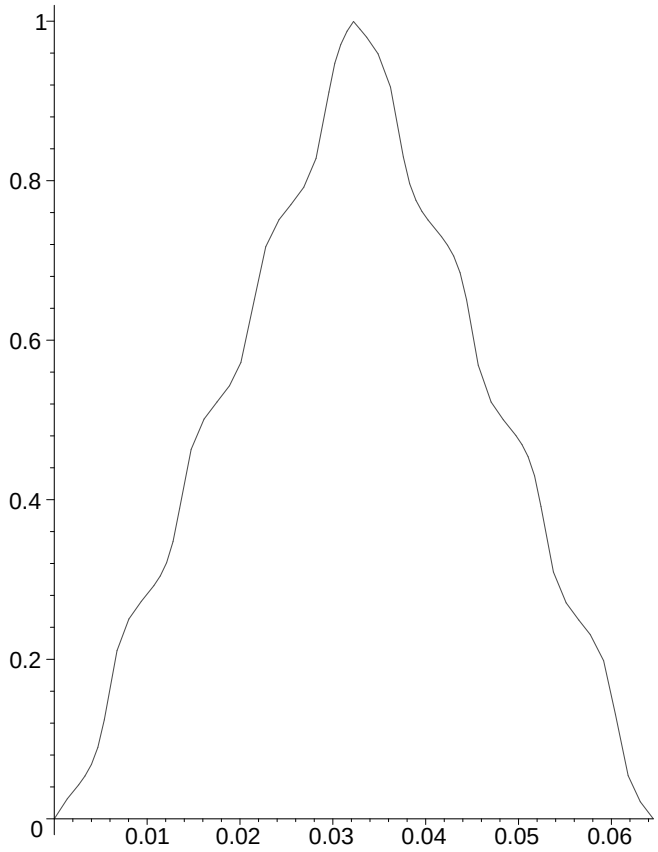

FIG. 14. Gráficos de ψ_1 com $\epsilon = 1/128$ e $h = 1/32$.

Usando o espaço acima definido, o método de elementos finitos multiescala busca $u^{h,\epsilon} \in V_0^{h,\epsilon}$ tal que

$$\int_0^1 \left(a(x/\epsilon) \frac{du^{h,\epsilon}}{dx}(x) \frac{dv^{h,\epsilon}}{dx}(x) \right) dx = \int_0^1 f(x) v^{h,\epsilon}(x)\, dx \quad \text{para todo } v^{h,\epsilon} \in V_0^{h,\epsilon}. \tag{6.4.2}$$

Matricialmente, temos que se $u^{h,\epsilon}(x) = \sum_{i=1}^N u_i^\epsilon \psi_i(x)$, então $\mathbf{u}^\epsilon = (u_1^\epsilon, \ldots, u_N^\epsilon)^T \in \mathbb{R}^N$ é tal que

$$\mathbf{M}^\epsilon \mathbf{u}^\epsilon = \mathbf{f}^\epsilon,$$

onde a matriz $\mathbf{M}^\epsilon = (M_{i,j}^\epsilon) \in \mathbb{R}^{N \times N}$ e o vetor $\mathbf{f}^\epsilon = (f_1^\epsilon, \ldots, f_N^\epsilon)^T \in \mathbb{R}^N$ são dados por

$$M_{i,j}^\epsilon = \int_0^1 \left(a(x/\epsilon) \frac{d\psi_i}{dx}(x) \frac{d\psi_j}{dx}(x) \right) dx, \qquad f_j^\epsilon = \int_0^1 f(x) \psi_j(x)\, dx.$$

Testando então a aproximação para $\epsilon = 1/16$ e $h = 1/10$, vemos na figura 15 que a solução aproximada pelo método de elementos finitos multiescala interpola a solução exata nos nós. Isto não é uma coincidência, é apenas uma característica em uma dimensão de métodos de elementos finitos que utilizam funções que são soluções locais da própria EDP que estão aproximando. Em dimensões maiores essa propriedade é (infelizmente) perdida.

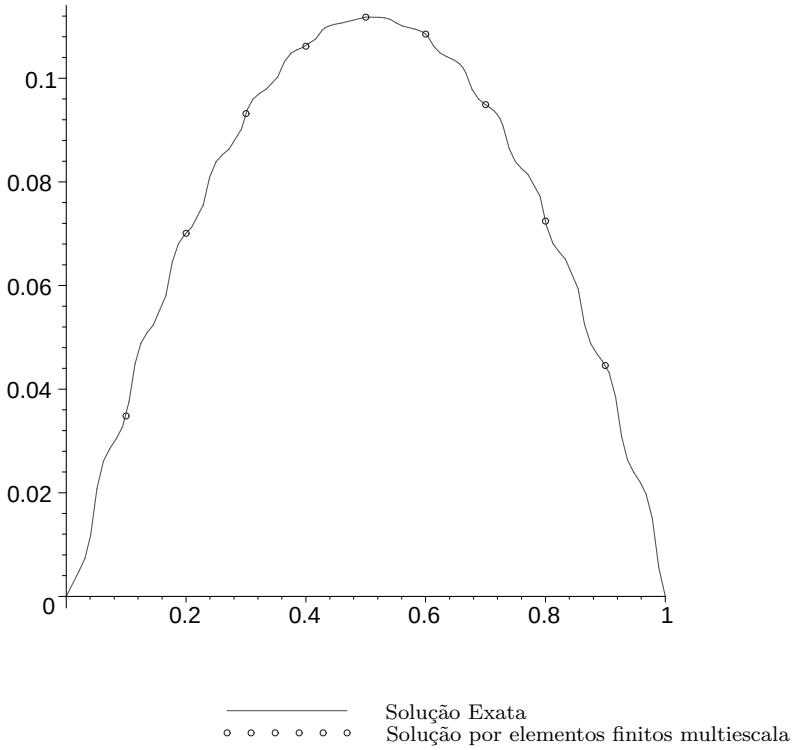

FIG. 15. Gráficos de u^ϵ e de sua aproximação por elementos finitos multiescala, com $\epsilon = 1/16$ e $h = 1/10$.

6.4.1. Análise de erro. A análise de erro desenvolvida em [**35**] baseia-se no Lema de Cea, como feito na subseção 6.3.2.

LEMA 6.4.1 (Lema de Cea). Sejam u^ϵ e $u^{h,\epsilon}$ soluções de (6.1.1) e (6.4.2). Então existe uma constante universal c tal que

$$\|u^\epsilon - u^{h,\epsilon}\|_{H^1(0,1)} \leq c\frac{\beta}{\alpha}\|u^\epsilon - v^{h,\epsilon}\|_{H^1(0,1)} \quad \text{para todo } v^{h,\epsilon} \in V_0^{h,\epsilon}.$$

No método de elementos finitos clássico, encontramos uma função em V_0^h que "aproximasse bem" u^ϵ e estimamos o erro de aproximação. No caso, a função em V_0^h era o interpolador de u^ϵ. Utilizando o Lema de Cea (Lema 6.3.1) obtivemos a estimativa final.

Similarmente, o desafio agora é achar uma aproximação para u^ϵ no espaço multiescala $V_0^{h,\epsilon}$. A análise divide-se em dois casos distintos, dependendo se a malha é refinada o suficiente ou não, em relação a ϵ.

Caso I: $h \ll \epsilon$**.** Neste caso em que assumimos a malha suficientemente refinada, obtemos a seguinte resultado de convergência, que , a menos de constantes, é o mesmo que o do Teorema 6.3.2. Ou seja, para malhas refinadas, *o método multiescala funciona tão bem quanto o método tradicional*.

TEOREMA 6.4.2. *Seja $f \in L^2(0,1)$, e seja u^ϵ solução de (6.1.1). Então existe uma constante c independente de ϵ, f,α, β tal que*

$$\|u^\epsilon - u^{h,\epsilon}\|_{H^1(0,1)} \leq c\frac{\beta^3}{\alpha^4}\frac{h}{\epsilon}\|f\|_{L^2(0,1)}.$$

O teorema acima segue facilmente do Lema de Cea (Lema 6.4.1) e do seguinte resultado de interpolação [**35**].

LEMA 6.4.3. Seja u^ϵ solução de (6.1.1), e seja $I^{h,\epsilon}u^\epsilon = \sum_{j=1}^N u^\epsilon(x_j)\psi_j$ interpolador de u^ϵ em $V_0^{h,\epsilon}$. Então existe uma constante c tal que

$$\|u^\epsilon - I^{h,\epsilon}u^\epsilon\|_{H^1(0,1)} \leq c\frac{\beta^2}{\alpha^3}\frac{h}{\epsilon}\|f\|^2_{L^2(0,1)}, \|f\|_{L^2(0,1)}.$$

A constante C pode depender de α e β, mas é independente de ϵ e f.

DEMONSTRAÇÃO. Seja $u_l = I^h u^\epsilon$ interpolador de u^ϵ em V_0^h. Então a teoria clássica de interpolação nos diz que

$$\|u^\epsilon - u_l\|_{H^1(x_{j-1},x_j)} \leq ch|u^\epsilon|_{H^2(x_{j-1},x_j)}. \tag{6.4.3}$$

Como a desigualdade triangular nos dá

$$\|u^\epsilon - I^{h,\epsilon}u^\epsilon\|_{H^1(x_{j-1},x_j)} \leq \|u^\epsilon - u_l\|_{H^1(0,1)} + \|u_l - I^{h,\epsilon}u^\epsilon\|_{H^1(0,1)}, \tag{6.4.4}$$

temos então "somente" que estimar $\|u_l - I^{h,\epsilon}u^\epsilon\|_{H^1(0,1)}$. Note que

$$\begin{aligned}
\alpha|u_l - I^{h,\epsilon}u^\epsilon|^2_{H^1(x_{j-1},x_j)} &\leq \int_{x_{j-1}}^{x_j} \frac{d}{dx}(u_l - I^{h,\epsilon}u^\epsilon)a(x/\epsilon)\frac{d}{dx}(u_l - I^{h,\epsilon}u^\epsilon)\,dx \\
&= -\int_{x_{j-1}}^{x_j} (u_l - I^{h,\epsilon}u^\epsilon)\frac{d}{dx}\left[a(x/\epsilon)\frac{d}{dx}(u_l - I^{h,\epsilon}u^\epsilon)\right]dx \\
&= -\int_{x_{j-1}}^{x_j} (u_l - I^{h,\epsilon}u^\epsilon)\frac{d}{dx}\left[a(x/\epsilon)\frac{d}{dx}u_l\right]dx \\
&= -\int_{x_{j-1}}^{x_j} (u_l - I^{h,\epsilon}u^\epsilon)\left\{\frac{d}{dx}\left[a(x/\epsilon)\frac{d}{dx}(u_l - u^\epsilon)\right] - f\right\}dx \\
&= \int_{x_{j-1}}^{x_j} \frac{d}{dx}(u_l - I^{h,\epsilon}u^\epsilon)a(x/\epsilon)\frac{d}{dx}(u_l - u^\epsilon)\,dx + \int_{x_{j-1}}^{x_j}(u_l - I^{h,\epsilon}u^\epsilon)f\,dx \\
&\leq \beta|u_l - I^{h,\epsilon}u^\epsilon|_{H^1(x_{j-1},x_j)}|u_l - u^\epsilon|_{H^1(x_{j-1},x_j)} + \|u_l - I^{h,\epsilon}u^\epsilon\|_{L^2(x_{j-1},x_j)}\|f\|_{L^2(x_{j-1},x_j)}.
\end{aligned}$$

Mas a desigualdade de Poincaré nos dá que $\|v\|_{L^2(x_{j-1},x_j)} \leq ch|v|_{H^1(x_{j-1},x_j)}$ para todo $v \in H_0^1(x_{j-1},x_j)$, e então

$$\alpha|u_l - I^{h,\epsilon}u^\epsilon|^2_{H^1(x_{j-1},x_j)} \leq ch|u_l - I^{h,\epsilon}u^\epsilon|_{H^1(x_{j-1},x_j)}(\beta|u^\epsilon|_{H^2(x_{j-1},x_j)} + \|f\|_{L^2(x_{j-1},x_j)}).$$

Logo,

$$|u_l - I^{h,\epsilon}u^\epsilon|_{H^1(x_{j-1},x_j)} \leq c\frac{h}{\alpha}(\beta|u^\epsilon|_{H^2(x_{j-1},x_j)} + \|f\|_{L^2(x_{j-1},x_j)}).$$

De (6.4.4) e (6.4.3) temos

$$\|u^\epsilon - I^{h,\epsilon}u^\epsilon\|_{H^1(x_{j-1},x_j)} \leq ch\left(1 + \frac{\beta}{\alpha}\right)|u^\epsilon|_{H^2(x_{j-1},x_j)} + c\frac{h}{\alpha}\|f\|_{L^2(x_{j-1},x_j)}.$$

Para encontrar uma estimativa global, basta somar a desigualdade acima em todos os elementos:

$$\|u^\epsilon - I^{h,\epsilon}u^\epsilon\|^2_{H^1(0,1)} \leq ch^2 \sum_{j=1}^{N} \left[\left(1+\frac{\beta}{\alpha}\right)^2 |u^\epsilon|^2_{H^2(x_{j-1},x_j)} + \frac{1}{\alpha^2}\|f\|^2_{L^2(x_{j-1},x_j)} \right]$$
$$= ch^2 \left[\left(1+\frac{\beta}{\alpha}\right)^2 |u^\epsilon|^2_{H^2(0,1)} + \frac{1}{\alpha^2}\|f\|^2_{L^2(0,1)} \right] \leq c\frac{\beta^4}{\alpha^6}\frac{h^2}{\epsilon^2}\|f\|^2_{L^2(0,1)},$$

onde usamos a estimativa de regularidade (6.3.8), e c é uma constante universal. Tirando raízes dos dois lados da equação obtemos o resultado. □

Caso II: $\epsilon \ll h$. Mesmo quando ϵ é pequeno em relação à malha, e o método de elementos finitos lineares não funciona a contento, os elementos finitos multiescala aproximam bem a soluçãoexata. Abaixo apresentamos uma estimativa de erro.

Teorema 6.4.4. *Seja $f \in L^2(0,1)$, e seja u^ϵ solução de* (6.1.1). *Então existe uma constante C independente de ϵ e f tal que*

$$\|u^\epsilon - u^{h,\epsilon}\|_{H^1(0,1)} \leq C(\epsilon h^{-1/2} + h)\|f\|_{L^2(0,1)}.$$

Para estimar o erro de aproximação do presente método, temos que encontrar uma função em $V_0^{h,\epsilon}$ que aproxime u^ϵ para então aplicar o Lema de Cea (Lema 6.4.1). Nosso candidato é u_I, interpolador de u^0 em $V_0^{h,\epsilon}$. Note que no **Caso I** (quando $h \ll \epsilon$), tomamos como candidato o interpolador de u^ϵ, diferentemente do que fazemos agora.

Para entender porque este o método multiescala funciona bem quando $\epsilon \ll h$, é necessário usar uma melhor aproximação assintótica (inclusive com estimativas de erro) de u^ϵ. Isto é possível se calcularmos os primeiros termos da expansão assintótica. De fato, seja u^0 como acima e χ solução de

$$\begin{aligned} -\frac{d}{dy}\left(a(y)\frac{d\chi}{dy}(y)\right) &= \frac{da}{dy}(y) \quad \text{em } (0,1), \\ \chi \text{ periódica com período 1}, \qquad & \int_0^1 H(y)\,dy = 0. \end{aligned} \tag{6.4.5}$$

Além disso, seja

$$u^1(x) = -H(x/\epsilon)\frac{du^0}{dx}(x). \tag{6.4.6}$$

e θ tal que

$$\begin{aligned} -\frac{d}{dx}\left(a(x/\epsilon)\frac{d\theta}{dx}(x)\right) &= 0 \quad \text{em } (0,1), \\ \theta(0) = u^1(0), \quad & \theta(1) = u^1(1). \end{aligned} \tag{6.4.7}$$

Temos então o seguinte resultado [**48**].

TEOREMA 6.4.5. *Assuma que $f \in L^2(0,1)$, e seja u^ϵ solução de (6.1.1). Sejam u^0, u^1 e θ definidos por (6.2.1), (6.4.6) e (6.4.7) respectivamente. Então existe uma constante C independente de f e de ϵ tal que*

$$\|u^\epsilon - u^0 - \epsilon u^1 + \epsilon\theta\|_{H^1(0,1)} \leq C\epsilon\|u^0\|_{H^2(0,1)}.$$

Hou et al. [**35**] notaram que a expansão acima vale tanto para a solução exata como para os elementos da base de elementos finitos multiescala. Logo, para $i = 1, \ldots, N$ a função ψ_i pode ser aproximada por

$$\psi_i^0 + \epsilon\psi_i^1 - \epsilon\theta_i,$$

onde

$$-\frac{d^2}{dx^2}\psi_i^0 = 0 \quad \text{em } \cup_{j=1}^{N+1}(x_{j-1}, x_j), \qquad \psi_i(x_j) = \begin{cases} 1 & \text{se } i = j, \\ 0 & \text{se } i \neq j, \end{cases}$$

e $\psi_i^1 = H(x/\epsilon)d\psi_i^0/dx$. Finalmente

$$-\frac{d}{dx}\left(a(x/\epsilon)\frac{d\theta_i}{dx}(x)\right) = 0 \quad \text{em } \cup_{j=1}^{N+1}(x_{j-1}, x_j), \qquad \theta_i(x_j) = \psi_i^1(x_j).$$

OBSERVAÇÃO. Note que no caso unidimensional, ψ_i^0 nada mais é que a função de base linear por partes ϕ_i.

Como acima, u_I pode ser aproximado por $u_I^0 + \epsilon u_I^1 - \epsilon\theta_I$, onde $u_I^0 = \sum_{i=1}^N u^0(x_i)\psi_i^0$, e $u_I^1 = H(x/\epsilon)du_I^0/dx$. Além disso,

$$-\frac{d}{dx}\left(a(x/\epsilon)\frac{d\theta_I}{dx}(x)\right) = 0 \quad \text{em } \cup_{j=1}^{N+1}(x_{j-1}, x_j), \qquad \theta_I(x_j) = u_I^1(x_j).$$

Temos então que

$$\begin{aligned}(6.4.8)\quad \|u^\epsilon - u_I\|_{H^1(0,1)} \leq{}& \|u^\epsilon - u^0 - \epsilon u^1 + \epsilon\theta\|_{H^1(0,1)} + \|u^0 - u_I^0\|_{H^1(0,1)} + \epsilon\|u^1 - u_I^1\|_{H^1(0,1)} \\ &+ \epsilon\|\theta\|_{H^1(0,1)} + \epsilon\|\theta_I\|_{H^1(0,1)} + \|u_I - u_I^0 - \epsilon u_I^1 + \epsilon\theta_I\|_{H^1(0,1)}\end{aligned}$$

A desigualdade

$$\|u^\epsilon - u^0 - u^1 + \epsilon\theta\|_{H^1(0,1)} \leq C\epsilon\|u^0\|_{H^2(0,1)} \tag{6.4.9}$$

é apresentada no Teorema 6.4.5. Já

$$\|u_I - u_I^0 - u_I^1 + \epsilon\theta_I\|_{H^1(0,1)} \leq C\epsilon\|u^0\|_{H^2(0,1)} \tag{6.4.10}$$

baseia-se no Teorema 6.4.5 e na estimativa $\|u_I^0\|_{H^2(x_{j-1},x_j)} \leq C\|u^0\|_{H^2(x_{j-1},x_j)}$ (ver os detalhes em [**35**]). Para obter

$$\|u^0 - u_I^0\|_{H^1(0,1)} \leq Ch\|u^0\|_{H^2(0,1)}, \tag{6.4.11}$$

basta observar que u_I^0 é a interpolação de u^0 por funções lineares por partes.

A seguir, usamos

$$\begin{aligned}\|u^1 - u_I^1\|_{H^1(x_{j-1},x_j)} = \left\|H(\cdot/\epsilon)\frac{d(u^0 - u_I^0)}{dx}\right\|_{H^1(x_{j-1},x_j)} &\leq \epsilon^{-1}\left\|\frac{dH}{dx}\right\|_{L^\infty(0,1)}\|u^0 - u_I^0\|_{H^1(x_{j-1},x_j)} \\ &+ \|H\|_{L^\infty(0,1)}\|u^0 - u_I^0\|_{H^2(x_{j-1},x_j)} \leq C\epsilon^{-1}\|u^0 - u_I^0\|_{H^1(x_{j-1},x_j)} + C\|u^0\|_{H^2(x_{j-1},x_j)}.\end{aligned}$$

Somando o quadrado da desigualdade acima entre $j = 1$ e $j = N + 1$ temos

$$\|u^1 - u_I^1\|_{H^1(0,1)} \leq C(\epsilon^{-1}h + 1)\|u^0\|_{H^2(0,1)}. \tag{6.4.12}$$

Finalmente temos

$$\|\theta\|_{H^1(0,1)} \leq C(|u^1(0)| + |u^1(1)|) \leq C\|H\|_{L^\infty(0,1)}\left(\left|\frac{du^0}{dx}(0)\right| + \left|\frac{du^0}{dx}(1)\right|\right) \leq C\|u^0\|_{H^2(0,1)}, \tag{6.4.13}$$

e

$$\|\theta_I\|^2_{H^1(x_{j-1},x_j)} \leq Ch^{-1}(|u_I^1(x_{j-1})|+|u_I^1(x_j)|)^2 \leq Ch^{-1}\|H\|^2_{L^\infty(0,1)}\left(\left|\frac{du_I^0}{dx}(x_{j-1})\right|+\left|\frac{du_I^0}{dx}(x_j)\right|\right)^2$$
$$\leq Ch^{-1}\|u^0\|^2_{H^2(x_{j-1},x_j)}.$$

Somando a desigualdade acima entre $j = 1$ e $j = N + 1$, concluímos que

$$\|\theta_I\|_{H^1(0,1)} \leq Ch^{-1/2}\|u^0\|_{H^2(0,1)}. \tag{6.4.14}$$

Demonstração. (do Teorema 6.4.4) Para obtermos a estimativa, basta juntar o resultado do Lema 6.4.1 e as desigualdades (6.4.8)–(6.4.14), e o resultado de regularidade (6.3.8). □

Observação. O resultado do Teorema 6.4.4 é melhor que o demonstrado em [**48**], onde a taxa de convergência alegada é

$$\|u^\epsilon - u^{h,\epsilon}\|_{H^1(0,1)} \leq C_1 h\|f\|_{L^2(0,1)} + C_2(\epsilon/h)^{1/2}.$$

A diferença aparece nas estimativas de θ e θ_I, que é diferente em uma ou duas dimensões.

6.4.2. Outros Comentários. Uma importante diferença entre uma e duas dimensões na técnica de elementos multiescala é que no caso bidimensional não é claro que condições de contorno deve-se impor nas arestas na definição das funções de base ψ_i, ver equação (6.4.1). Em uma dimensão este problema não existe, já que não existe aresta.

Uma primeira idéia no caso de elementos poligonais seria impor ψ_i linear nas arestas. Nos artigos [**34, 35**] surge a interessante proposta de que as funções de base também deveriam satisfazer uma "restrição unidimensional" do operador diferencial que define a EDP, ao longo das arestas. Esta proposta é *ad hoc*, assim como a definição do que é uma restrição unidimensional de um operador bidimensional, mas parece funcionar bem numericamente. A demonstração de convergência em [**35**] foi feita assumindo que as funções de base são lineares nas arestas.

Ainda mais recentemente, Giancarlo Sangalli aplicou a idéia de *Residual Free Bubbles* em problemas com coeficientes oscilatórios também com excelentes resultados [**53**]. A idéia básica de Sangalli é também fazer com que o método numérico automaticamente leve em conta as oscilações presentes no problema, e guarda forte similaridades com o método presente neste capítulo. Ver [**36**] onde o método de Residual Free Bubbles é brevemente descrito.

6.5. Uma dificuldade extra

Um outro problema que pode surgir quando tratamos de modelagem de meio heterogêneos, é a perda de coercividade. De fato, se α é muito pequeno em (6.1.1), o problema torna-se mais difícil de ser tratado. Consideramos aqui o exemplo dado por (6.1.2) mas com $\alpha = 0.01$, e $\epsilon = 1/8$. Na figura 16 mostramos o gráfico de $a(\cdot/\epsilon)$ e u^ϵ.

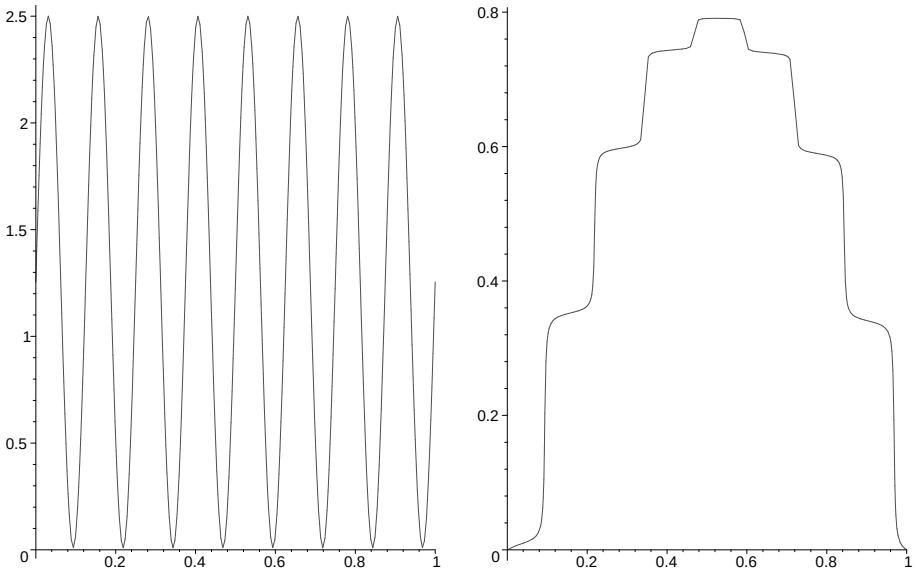

FIG. 16. Gráficos de $a(\cdot/\epsilon)$ e da solução exata para $\epsilon = 1/8$.

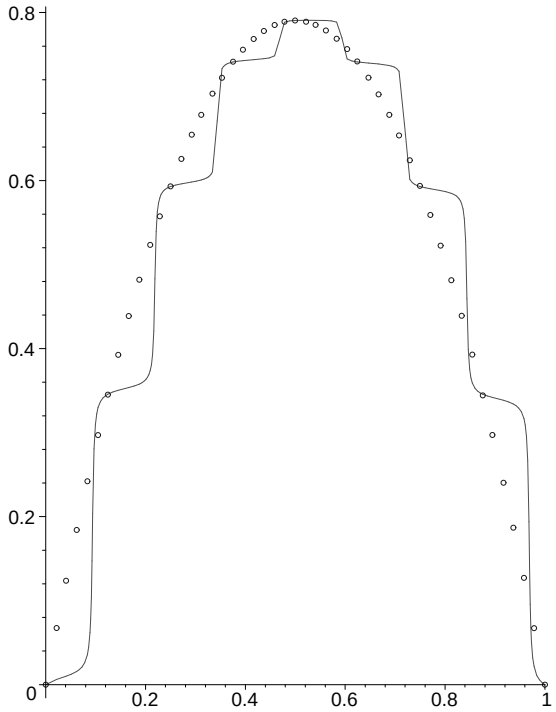

FIG. 17. Comparação entre as soluções exatas e homogeneizadas para $\epsilon = 1/8$.

Mesmo para ϵ pequeno a aproximação pela solução homogeneizada já não é satisfatória. Comparando-se as figuras 5 e 17, percebe-se a deterioração da aproximação no último caso, como já era previsto pelo Teorema 6.2.1.

Esta deterioração é ainda mais aparente se utilizarmos elementos finitos lineares, como mostram as figuras 12 e 18. Note que, desta vez, a origem da dificuldade não é a magnitude

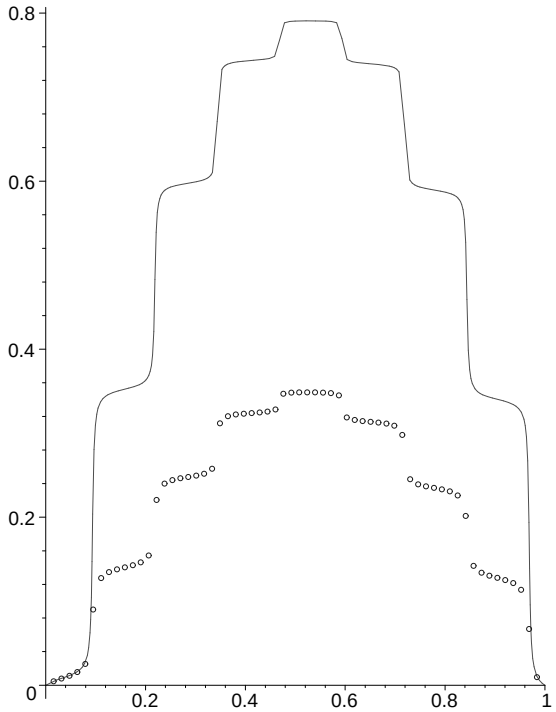

FIG. 18. Gráficos de u^ϵ e de sua aproximação por elementos finitos, com $\epsilon = 1/8$ e $h = 1/64$.

de ϵ, mas sim a de α. De fato, mesmo para ϵ relativamente grande, a aproximação por elementos finitos falha. Na figura 19 apresentamos um exemplo numérico para $\epsilon = 1/2$ e $h = 1/64$. Mais uma vez esta piora era indicada por estimativas de erro. No Teorema 6.3.2, a constante é proporcional a α^{-3}.

Finalmente, por manter a característica de interpolar a solução exata em uma dimensão, o método de elementos finitos multiescala não se degrada mesmo com α pequeno, como pode ser visto na figura 20.

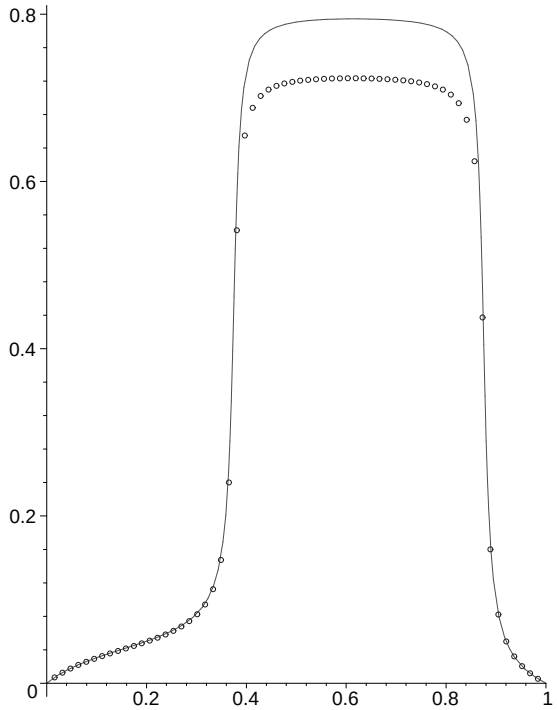

FIG. 19. Gráficos de u^ϵ e de sua aproximação por elementos finitos, com $\epsilon = 1/2$ e $h = 1/64$.

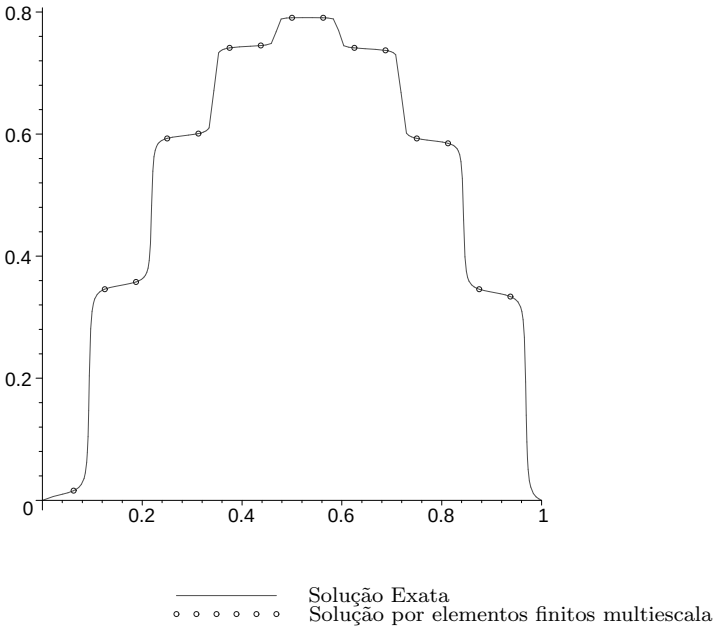

FIG. 20. Gráficos de u^ϵ e de sua aproximação por elementos finitos multiescala, com $\epsilon = 1/8$ e $h = 1/16$.

Bibliography

[1] S. M. Alessandrini, Some two–dimensional plate models: derivation, asymptotic properties, and numerical approximation, *Ph.D. Dissertation, Rutgers University*, 1991.

[2] S.M. Alessandrini, D.N. Arnold, R.S. Falk, A.L. Madureira, Derivation and Justification of Plate Models by Variational Methods, *Centre de Recherches Mathematiques, CRM Proceedings and Lecture Notes*, 1999.

[3] D.N. Arnold and R.S. Falk, Asymptotic Analysis of the Boundary Layer for the Reissner–Mindlin Plate Model, *SIAM J. Math. Anal.*, 27:486-514, 1996

[4] D.N. Arnold and R.S. Falk, Edge effects in the Reissner-Mindlin plate theory,*Analytic and Computational Models of Shells*, (A. K. Noor, T. Belytschko, and J. C. Simo, eds.), A.S.M.E. 71-90, 1989

[5] I. Babuška and M. Suri, The optimal convergence rate of the p-version of the finite element method, *SIAM J. Numer. Anal.*, Vol. 24, 4:750–776, 1987

[6] I. Babuška and L. Li, Hierarchical modelling of plates, *Computers and Structures*, Vol. 40, 419–430, 1991

[7] I. Babuška and L. Li, The problem of plate modeling: Theoretical and computational results, *Comput. Methods Appl. Mech. Engrg.*, Vol. 100, 249–273, 1992

[8] C. Baiocchi, F. Brezzi, and L. P. Franca, *Virtual bubbles and the Galerkin-least-squares method*, Comput. Meth. Appl. Mech. Engrg, (1993), pp. 125–141.

[9] C. Bernardi and Y. Maday, Spectral Methods, *Handbook of Numerical Analysis*, (P. G. Ciarlet and J. L. Lions, eds.), Elsevier Science, Vol. V, 1997

[10] F. Brezzi, L.P. Franca, T.J.R. Hughes, and A. Russo, Stabilization Techniques and Subgrid Scales Capturing, *The State of the Art in Numerical Analysis*, (I.S. Duff and G.A. Watson, eds.), IMA Conference Series, Oxford University Press, 63:391-406, 1996

[11] F. Brezzi, M. O. Bristeau, L. P. Franca, M. Mallet, and G. Rogé, *A relationship between stabilized finite element methods and the Galerkin method with bubble functions*, Comput. Meth. Appl. Mech. Engrg., 96 (1992), pp. 117–129.

[12] F. Brezzi, L. P. Franca, T. J. R. Hughes, and A. Russo, $b = \int g$, Comput. Meth. Appl. Mech. Engrg., 145 (1997), pp. 329–339.

[13] F. Brezzi, L.P. Franca, and A. Russo, Further Considerations on Residual-Free Bubbles for Advective-Diffusive Equations, *Computer Methods in Applied Mechanics and Engineering*, 166:25-33, 1998

[14] F. Brezzi and A. Russo, *Choosing bubbles for advection-diffusion problems*, Math. Models Methods Appl. Sci., 4 (1994), pp. 571–587.

[15] A.N. Brooks and T.J.R. Hughes, Streamline Upwind/Petrov–Galerkin Formulations for Convection Dominated Flows with Particular Emphasis on the Incompressible Navier–Stokes Equations,*Computer Method in Applied Mechanics and Engineering*, 32:199-259, 1982

[16] C. Chen Asymptotic Convergence Rates for the Kirchhoff Plate Model *Ph.D. Dissertation, The Pennsylvania State University*, 1995.

[17] P. G. Ciarlet, Mathematical Elasticity, volume II: Theory of Plates, Studies in mathematics and its applications *Elsevier Science B. V.*, Vol. 27 1997.

[18] Doina Cioranescu e Patrizia Donato An introduction to Homogenization, Oxford Lecture Series in mathematics and its Applications, Vol. 17 1999

[19] M. Dauge and I. Gruais, Asymptotics of arbitrary order for a thin elastic clamped plate, I: Optimal error estimates,*Asymptotic Analysis*, Vol. 13, 167-197, 1996

[20] M. Dauge, I. Gruais, A. Rössle, The influence of lateral boundary conditions on the asymptotics in thin elastic plates I: Clamped and simply supported plates,*Institut de Recherche Mathématique de Rennes*, Vol. 97–28, 1997

[21] M. Dorr, The approximation theory for the p-version of the finite element method,*SIAM J. Numer. Anal.*, Vol. 21, 6:1180–1207, 1984

[22] M. Dorr, The approximation of solutions of elliptic boundary-value problems via the p-version of the finite element method,*SIAM J. Numer. Anal.*, Vol. 23, 1:58–77, 1986

[23] Kenneth Eriksson, Some error estimates for the p-version of the finite element method,*SIAM J. Numer. Anal.*, Vol. 23, 2:403–411, 1986

[24] L. P. Franca and E. G. Dutra do Carmo, *The Galerkin gradient least-squares method*, Comput. Meth. Appl. Mech. Engrg., 74 (1989), pp. 41–54.

[25] L. P. Franca, C. Farhat, A. P. Macedo, and M. Lesoinne, *Residual-free bubbles for the Helmholtz equation*, Internat. J. Numer. Methods Engrg., 40 (1997), pp. 4003–4009.

[26] L. Franca, A. Madureira, L. Tobiska, and F. Valentin, *Convergence analysis of a multiscale finite element method for singularly perturbed problems*, preprint, (2003).

[27] L. Franca, A. Madureira, and F. Valentin, *Towards multiscale functions : enriching finite element spaces with local but not bubble-like functions*, Comput. Meth. Appl. Mech. Engrg., (accepted).

[28] L. P. Franca and A. Russo, *Approximation of the Stokes problem by residual-free macro bubbles*, East-West J. Numer. Math., 4 (1996), pp. 265–278.

[29] ——, *Deriving upwinding, mass lumping and selective reduced integration by residual-free bubbles*, Appl. Math. Lett., 9 (1996), pp. 83–88.

[30] L.P. Franca and A. Russo, Mass Lumping Emanating from Residual Free Bubbles, *Computer Methods in Applied Mechanics and Engineering*, 142:353-360, 1997

[31] L.P. Franca and A. Russo, Unlocking with Residual Free Bubbles, *Computer Methods in Applied Mechanics and Engineering*, 142:361-364, 1997

[32] I. Harari and T. J. R. Hughes, *Stabilized finite elements methods for steady advection-diffusion with production*, Comput. Meth. Appl. Mech. Engrg., (1994), pp. 165–191.

[33] C. O. Horgan and J. K. Knowles, Recent Developments Concerning Saint-Venant's Priciple,*Advances in Applied Mechanics*, Vol. 23, 169-189, 1983

[34] T.Y. Hou and X.H. Wu, A multiscale finite element method for elliptic problems in composite materials and porous media,*JCP*, 134:169-189, 1997

[35] T.Y. Hou, X.H. Wu and Z. Cai, Convergence of a multiscale finite element method for elliptic problems with rapidly oscillating coefficients,*Math. Comp.*, Vol. 68, 227:913–943, 1999

[36] T. Hou, Numerical Aproximation to Multiscale Solutions in PDEs, *Frontiers in numerical analysis : Durham 2002*, (James F. Blowey, Alan W. Craig, Tony Shardlow, eds.), Springer, 241–302, 2003

[37] T.J.R. Hughes, A Simple Scheme for Developing 'Upwind' Finite Elements,*International Journal for Numerical Methods in Engineering*, 12:1359-1365, 1978

[38] T.J.R. Hughes, The finite element method: Linear static and dynamic finite element analysis, *Prentice-Hall, Englewood Cliffs*, 1987.

[39] C. Johnson, Numerical Solutions of Partial Differential Equations by the Finite Element Method *Cambridge University Press*, 1987.

[40] K. H. Lo, R. M. Christensen and E. M. Wu, A high-Order Theory of Plate Deformation, *J. Appl. Mech.*, Vol. 46, 663–676, 1977

[41] R. B. Kellogg, Notes on piecewise smooth elliptic boundary value problems, *Institute for Physical Science and Technology*, Technical Note BN-1137, College Park, Md., 1992

[42] A.L. Madureira, Asymptotics and Hierarchical Modeling of Thin Domains, *Ph.D. Dissertation, The Pennsylvania State University*, 1999.

[43] W. G. Mazja and S. A. Nazarow and B. A. Plamenewski, Asymptotische Theorie Ellipscher Randwertaufgaben in Singulär gestörten Gebieten I, *Akademie Verlag*, 1991.

[44] D. S. Mitrinović and J. E. Pečarić and A. M. Fink, Inequalities Involving Functions and their Integrals and Derivatives, *Kluwer Academic Publishers*, 1991.

[45] B. Miara, Optimal Spectral Approximation in Linearized Plate Theory, Mathematics and its applications, *Applicable Analysis*, Vol. 31, No. 291–307, 1989

[46] J.M. Melenk and C. Schwab, Analytic Regularity for a Singularly Perturbed Problem, *SIAM J. Math. Anal.*, Vol. 30, No. 2:379-400, 1999

[47] D. Morgenstern Herleitung der plattentheorie aus der dreidimensionalen Elastizitats-theorie, *Arch. for Rational Mech. and Anal.*, Vol. 4, 145–152, 1959

[48] S. Moskow, M. Vogelius, First order corrections to the homogenized eigenvalues of a periodic composite medium. A convergence proof, *Proceedings of the Royal Society of Edinburgh*, 127A:1263–1299, 1997

[49] O. Ovaskainen, J. Pitkäranta, An energy method approach to the problem of elastic strip, *SIAM J. Appl. Math.*, Vol. 58, No. 3:999–1021, 1998

[50] J.-C. Paumier, A. Raoult, Asymptotic consistency of the polynomial approximation in the linearized plate theory application to the Reissner-Mindlin model,*Centre National de la reserche Scientifique*, Rapport Technique, 1996

[51] H.-G. Roos, M. Stynes, L.Tobiska, Numerical Methods for Singularly Perturbed Differential Equations, *Springer Series in Computational Methematics 24*, 1996.

[52] Andreas Rössle, Manfred Bischoff, Wolfang Wendland, Ekkehard Ramm, On the mathematical foundation of the $(1, 1, 2)$-plate model,*Sonderforschungsbereich Vol 404, Universität Stuttgart*, preprint, 1997

[53] G. Sangalli, Capturing small scales in elliptic problems using a Residual-Free Bubbles Finite Element Method,*Multiscale Modeling and Simulation: A SIAM Interdisciplinary Journal*, Vol. 1, No. 3:485-503, 2003

[54] C. Schwab, Hierarchic modelling in mechanics, *Wavelets, Multilevel Methods and Elliptic PDEs*, (M. Ainsworth, J. Levesley, W.A. Light and M. Marletta, eds.), Oxford University Press, 85–160, 1997

[55] M. Vogelius and I. Babuška, On a dimensional reduction method. I. The optimal Selection of basis functions, *Mathematics of computation*, Vol. 37, No. 155:31–46, 1981

[56] M. Vogelius and I. Babuška, On a dimensional reduction method. II. Some approximation-theoretic results, *Mathematics of computation*, Vol. 37, No. 155:47–68, 1981

[57] M. Vogelius and I. Babuška, On a dimensional reduction method. III. A posteriori error estimation and an adaptive approach, *Mathematics of computation*, Vol. 37, No. 156:361–384, 1981